ISTANBUL TECHNICAL UNIVERSITY ★ GRADUATE SCHOOL

EQUIVALENT LINEAR AND NONLINEAR SITE RESPONSE ANALYSIS, STUDY CASE FOR BANDA ACEH, INDONESIA

M.Sc. THESIS

Amelia FITRI

Department of Civil Engineering

Soil Mechanics and Geotechnical Engineering Programme

AUGUST 2022

ISTANBUL TECHNICAL UNIVERSITY ★ GRADUATE SCHOOL

EQUIVALENT LINEAR AND NONLINEAR SITE RESPONSE ANALYSIS, STUDY CASE FOR BANDA ACEH, INDONESIA

M.Sc. THESIS

Amelia FITRI
(501161321)

Department of Civil Engineering

Soil Mechanics and Geotechnical Engineering Programme

Thesis Advisor: Prof. Dr. Musaffa Ayşen LAV

AUGUST 2022

ISTANBUL TEKNİK ÜNİVERSİTESİ ★ LİSANSÜSTÜ EĞİTİM ENSTİTÜSÜ

YEREL ZEMİN KOŞULLARININ SİSMİK ETKİLER ALTINDA EŞDEĞER DOĞRUSAL VE DOĞRUSAL OLMAYAN ANALİZİ, BANDA ACEH, ENDONEZYA İÇİN BİR ÇALISMA

YÜKSEK LİSANS TEZİ

Amelia FITRI
(501161321)

İnşaat Mühendisliği Anabilim Dalı

Zemin Mekaniği ve Geoteknik Mühendisliği Programı

Tez Danışmanı: Prof. Dr. Musaffa Ayşen LAV

AĞUSTOS 2022

Amelia Fitri, a M.Sc student of İTU Graduate School student ID 501161321, successfully defended the thesis/dissertation entitled "EQUIVALENT LINEAR AND NONLINEAR SITE RESPONSE ANALYSIS, STUDY CASE FOR BANDA ACEH, INDONESIA", which she prepared after fulfilling the requirements specified in the associated legislations, before the jury whose signatures are below.

Thesis Advisor :	**Prof. Dr. Musaffa Ayşen LAV** İstanbul Technical University	....
Jury Members :	**Prof. Dr. Ayşe EDİNÇLİLER** Boğaziçi Üniversitesi	....
	Asst. Prof. Dr. Berrak TEYMÜR İstanbul Technical University	....

Date of Submission : 20 July 2022
Date of Defense : 18 August 2022

To my parents,

FOREWORD

The opportunity to study Master's Science Degree at Istanbul Technical University is one of the most important and valuable parts of my life. I want to express my deepest gratitude to all people who assist and encourage me during the years I have spent studying here.

I feel extremely grateful for my adviser Professor Musaffa Ayşen LAV. She supported and encouraged me during my research.

I give thanks to YTB for providing funds during my master's science education and also appreciate the assistance of members working at the Soil Mechanics Laboratory of Syiah Kuala University in Aceh, Indonesia that provided the data used in this study.

Finally, my special thanks to all my family and friends, without their encouragement and support, I couldn't finish my thesis.

August 2022

Amelia FITRI
(Civil Engineer)

TABLE OF CONTENTS

Page

FOREWORD .... **ix**
TABLE OF CONTENTS .... **xi**
ABBREVIATIONS .... **xiii**
SYMBOLS .... **xv**
LIST OF TABLES .... **xvii**
LIST OF FIGURES .... **xix**
SUMMARY .... **xxiii**
ÖZET .... **xxv**
1. INTRODUCTION **1**
2. EARTHQUAKE AND ITS HAZARD **3**
2.1 Seismicity Condition in Banda Aceh 3
2.2 Earthquake-induced Hazards in Banda Aceh 6
2.2.1 Ground shaking 6
2.2.2 Structural hazards 8
2.2.3 Liquefaction 13
2.2.4 Landslide 14
2.2.5 Retaining structure 15
2.2.6 Lifeline hazard 16
2.2.7 Tsunamis and seiches 17
2.2.8 Fault rupture hazard 19
2.2.9 Coastal subsidence 21
3. SEISMIC HAZARD ANALYSIS **25**
3.1 Deterministic Seismic Hazard Analysis 25
3.2 Probabilistic Seismic Hazard Analysis 26
3.3 Banda Aceh Probabilistic Seismic Hazard Analysis 28
4. DEVELOPMENT OF UNIFORM HAZARD GROUND MOTION RESPONSE SPECTRA **37**
4.1 Earthquake Input Ground Motion 37
4.1.1 Sumatra-Andaman earthquake 37
4.1.2 Characteristic of the earthquake 38
4.1.3 Fault surface rupture 39
4.1.4 Earthquake effects on Banda Aceh 39
4.2 Site Characterization of Banda Aceh 40
4.3 Soil Dynamic Properties 40
4.4 Method of One-Dimensional Site Response Analysis 41
4.4.1 Linear analysis 41
4.4.2 Equivalent linear analysis 43
4.4.3 Nonlinear analysis 45
4.5 Seismic Code for Soil and Earthquake Design 47
5. CASE STUDY: EQUIVALENT LINEAR AND NONLINEAR SITE RESPONSE ANALYSIS OF BANDA ACEH **49**
5.1 In-situ Soil TestingTesting 50

5.2 Equivalent Linear Analysis Using Deepsoil 54
5.3 Nonlinear Analysis Using Deepsoil 61
5.4 Comparison Between ELA and NLA 67
5.5 Liquefaction Analysis Practical Application of This Study 68
6. CONCLUSIONS AND RECOMMENDATIONS 75
REFERENCES 77
APPENDICES 81
APPENDIX A 82
CURRICULUM VITAE 111

ABBREVIATIONS

CPT	**:** Cone Penetration Test
CQ/H	**:** General Quadratic/Hyperbolic
CRR	**:** Cyclic Resistance Ratio
CSR	**:** Cyclic Stress Ratio
EL	**:** Equivalent Linear
FC	**:** Fines Content
FS	**:** Factor of Safety
GWT	**:** Ground Water Table
MSF	**:** Magnitude Scaling Factor
NL	**:** Nonlinear
OCR	**:** Over Consolidation Ratio
PGA	**:** Peak Ground Analysis
PI	**:** Plasticity Index
SDOF	**:** Single Degree of Freedom System
SNI	**:** Standar National Indonesia (Indonesian National Standard Code)
SPT	**:** Standard Penetration Test

SYMBOLS

C_E	:	Hammer energy ratio correction
C_N	:	Overburden pressure correction
C_R	:	Rod length correction factor
C_B	:	Borehole diameter correction factor
C_S	:	Correction factor for using a split spoon for liners
E_s	:	Elasticity modulus
$F(\omega)$	:	Transfer function
G	:	Shear modulus
g	:	Gravity acceleration
K_σ	:	Overburden correction factor
M	:	Earthquake magnitude
N_m	:	SPT blow count measured
$N_{(60)}$	:	SPT blow number (corrected)
$(N_1)_{60cs}$	:	SPT blow number (corrected) clean sand
PI	:	Plasticity index
q_c	:	CPT cone bearing
r_d	:	Stress reduction coefficient
R_γ	:	Ratio of the effective shear strain to maximum shear strain
T_s	:	Fundamental period of soil
V_s	:	Shear wave velocity
α_{max}	:	Maximum ground acceleration
σ_v	:	Vertical total stress
σ'_v	:	Vertical total stress effective
μ	:	Poisson ratio
ξ	:	Damping ratio
ρ	:	Mass density (of soil)
γ_{eff}	:	Effective shear strain
γ_{max}	:	Maximum shear strain
ω_o	:	Fundamental frequency of soil

LIST OF TABLES

Page

Table 2.1 : Some Significant Earthquakes Affected Banda Aceh Region (BMKG, 2018). **7**
Table 2.1 (continued) : Some Significant Earthquakes Affected Banda Aceh Region (BMKG, 2018)........ **8**
Table 3.1 : Function attenuation for Banda Aceh hazard analysis (A Yahya et al, 2016). **30**
Table 5.1 : Summary of location from soil profile selected for this study........ **50**
Table 5.2 : SPT-1 unit weight information. **50**
Table 5.3 : Correction Factor for N-SPT (Youd et al, 2001). **52**
Table 5.4 : Corrected N-SPT Values for SPT-1. .... **52**
Table 5.5 : Comparison between ELA and NLA in terms of response spectra. **68**
Table 5.6 : Comparison between ELA and NLA in terms of PGA........ **68**
Table 5.7 : Liquefaction evaluation of the SPT-1 soil profiles. **74**
Table 5.7 (continued) : Liquefaction evaluation of the SPT-1 soil profiles. **74**
Table A.1 : Liquefaction evaluation of the SPT-1 soil profiles. **90**
Table A.1 (continued) : Liquefaction evaluation of the SPT-1 soil profiles........ **90**
Table A.2 : Liquefaction evaluation of the SPT-2 soil profiles. **99**
Table A.2 (continued) : Liquefaction evaluation of the SPT-2 soil profiles. **99**
Table A.3 : Liquefaction evaluation of the SPT-2 soil profiles. **108**
Table A.3 (continued) : Liquefaction evaluation of the SPT-2 soil profiles........ **109**

LIST OF FIGURES

Page

Figure 2.1 : Indonesian and the surrounding region's tectonic setting. The country of Indonesia is marked in green. Major plate borders, faults, and plate boundaries are all represented. (Source: Hutchings, S. J., & Mooney, W. D., 2021 referencing the plate velocities with respect to the Sunda plate obtained from the MORVEL velocity model (DeMets et al., 2010). Faults and boundaries are obtained from Moore and Silver (1983), Silver, McCaffrey, and Smith (1983), Silver, Reed, et al. (1983), Widiwijayanti et al. (2004), Besana and Ando (2005), Roosmawati and Harris (2009), Watkinson et al. (2011), Hall (2012), Mukti et al. (2012), Tsutsumi and Perez (2013), Saputra et al. (2014), Cipta et al. (2016), Koulali et al. (2016), Omang et al. (2016), Adhitama et al. (2017), Patria and Hall (2017), Watkinson and Hall (2017), Hall (2018), Nugraha and Hall (2018), Supendi et al. (2018), Valkaniotis et al. (2018), and Irsyam et al. (2020). **4**

Figure 2.2 : Earthquake events occurred in Indonesia from January, 1st 2000 to July, 28th 2020 (a) Event for M ≥4.6 (b) Event for M ≥7.0, source data was taken from USGS (2020). The majority of the earthquake was shallow and low magnitude event with M<6 (Source: Hutchings, S. J., & Mooney, W. D., 2021). **5**

Figure 2.3 : A steel truss bridge deck had been swept away 50 meters by earthquake and tsunami and a temporary Bailey bridge had been installed in its place in Lhoknga, Banda Aceh (Ghobarah et al., 2006). **9**

Figure 2.4 : A Closer look from a wrecked structural steel bridge with a destroyed Lafarge cement plant in Lhoknga, Banda Aceh (Ghobarah et al., 2006). **9**

Figure 2.5 : Department of Finance Building in Banda Aceh, a three-story structure destroyed by 2004 earthquake (Ghobarah et al., 2006). **10**

Figure 2.6 : A flexural hinging at the upper and lower part of structural columns in a mosque located in Banda Aceh (Ghobarah et al., 2006). **10**

Figure 2.7 : A collapsed ground floor of a store in Banda Aceh with second and third floor left intact (Ghobarah et al., 2006). **11**

Figure 2.8 : The Pante Pirak shopping complex in Banda Aceh suffered from strong beam–weak column and beam–column joint failure (Ghobarah et al., 2006). **11**

Figure 2.9 : A four-floor office building in Banda Aceh had a beam–column joint failure caused by the absence of transversal reinforcements (Ghobarah et al., 2006). **12**

Figure 2.10 : Tower of Baiturrahman Grand Mosque damaged by the 2004 seismic event in Banda Aceh (Ghobarah et al., 2006). **12**

Figure 2.11 : Foundation partial settlement of a hotel building because of liquefaction in Banda Aceh (Jalil et al., 2020). **13**

Figure 2.12 : Phenomenon of the foundation settlement of a multi-storey building due to liquefaction in Banda Aceh (Jalil et al., 2020). **14**
Figure 2.13 : Banda Aceh Landslide Susceptibility (Source: https://thinkhazard.org/en/report/73705-indonesia-nangroe-aceh-darussalam-kota-bandaaceh/LS). **15**
Figure 2.14 : Offshore diesel-generating electrical station that was swept inland by tsunami waves, now it is one of monuments to commemorate the devastating event (Source: https://static. trip101.com/paragraph_media/pictures/002/269/764/large/1024px-PLTD_Apung.jpg). **16**
Figure 2.15 : Tsunami height and run-up measurements in Lampuuk, Banda Aceh (Source: https://cmgds.marine.usgs.gov/data/sumatra05/heights.html). **17**
Figure 2.16 : Damage in Banda Aceh after tsunami 2004 (Source: http://ioc3.unesco.org). **18**
Figure 2.17 : The effect of the tsunami in Banda Aceh (source: https://www.sms-tsunami-warning.com/pages/tsunami-sumatra-2004#.Yd8jvdFBzIU).**..18**
Figure 2.18 : Before and after the tsunami, aerial views of Banda Aceh's northern shore (Ghobarah et al., 2008). **19**
Figure 2.19 : Illustration of principal surface hazards due to fault rupture (Bray, 2001). **20**
Figure 2.20: Map of Northern Sumatra Fault (Sugiyanto et al., 2011). **21**
Figure 2.21: Coseismic subsidence induced by the 2004 Sumatra-Andaman seismic event around Lhoknga, Banda Aceh, proven by trees dropped into the surf zone. (Source: https://cmgds.marine.usgs.gov/data/sumatra05/subsidence.html). **22**
Figure 2.22: Uplift event in Simelue Island made coral reef exposed out of the water (Source: https://cmgds.marine.usgs.gov/data/sumatra05/subsidence. html). **22**
Figure 2.23: Coastal subsidence maps from the 2004 Sumatra-Anadaman earthquake (Source: Chlieh et al., 2007). **23**
Figure 3.1 : The steps for calculating DSHA (Source: Kramer, 1996). **26**
Figure 3.2 : The steps for calculating PSHA (Source: Kramer, 1996). **27**
Figure 3.3 : Map of seismicity around Sumatra from compiling catalogues (Source: A Yahya et al, 2016). **28**
Figure 3.4 : Map of model shallow earthquke for Sumatra from Island (Source: A Yahya et al, 2016). **29**
Figure 3.5 : Map of fault mechanism used for PSHA study (Source: A Yahya et al, 2016). **30**
Figure 3.6 : PGA hazard conditions in the bedrock over a period of 2475 years for Banda Aceh and Northern Sumatra region. PGA value was ranged from 0.15g to 1.3g (Source: A Yahya et al, 2016). **31**
Figure 3.7 : Map of hazard conditions SA 0.2 seconds in the bedrock over a period of 2475 years for Banda Aceh and Northern Sumatra region. SA value was ranged from 0.35g to 2.8g (Source: A Yahya et al, 2016). **32**
Figure 3.8 : Map of hazard conditions SA 1 seconds in the bedrock over a period of 2475 years for Banda Aceh and Northern Sumatra region. SA value was ranged from 0.30g to 1.30g (Source: A Yahya et al, 2016). **33**
Figure 3. 9 : Curve hazard conditions in the bedrock PGA Banda Aceh (Source: A Yahya et al, 2016). **34**
Figure 3. 10 : Curve SA 0.2 seconds hazard conditions in the bedrock Banda Aceh (Source: A Yahya et al, 2016). **34**

Figure 3. 11 : Curve SA 1 seconds hazard conditions in the bedrock Banda Aceh (Source: A Yahya et al, 2016). **35**
Figure 4.1 : Illustration of site response analysis (Kramer, 1996). **37**
Figure 4.2 : Map of the epicenter, aftershocks, and area of the major fault rupture for the Sumatra-Andaman Earthquake (Fehr et al., 2004). **38**
Figure 4.3 : A Simulated acceleration and velocity waveforms for Banda Aceh for 2004 Sumatra-Andaman earthquake proposed by Sørensen et al. (2007). **39**
Figure 4.4 : Banda Aceh and surrounding area shear wave velocity (Polom et al., 2008). **40**
Figure 4.5 : The influence of frequency on steady state response for undamped linear elastic layer (Source: Kramer 1996). **42**
Figure 4.6 : The influence of frequency on steady state response for damped linear elastic layer (Source: Kramer 1996). **43**
Figure 4.7 : Two shear strain time histories with identical peak shear strains. For the transient motion of an actual earthquake, the effective shear strain is usually taken as 65% of the peak strain (Source: Kramer, 1996). **44**
Figure 4.8 : Iteration toward strain-compatible shear modulus and damping ratio in equivalent linear analysis (Source: Kramer, 1996). **44**
Figure 4.9 : Extended masing criteria for nonlinear method (a) variation with time; (b) resulting stress-strain behavior (backbone criteria indicated by dashed line (Source: Kramer, 1996). **46**
Figure 4.10 : Indonesian Earthquake Zonation Map (2017). **47**
Figure 5.1 : The location details of the boreholes. **49**
Figure 5.2 : SPT-1 Soil Profile. **51**
Figure 5.3 : The corrected N Value Graph for SPT-1. .... **53**
Figure 5.4 : Shear Wave Velocity for SPT-1. .... **54**
Figure 5.5 : Analysis type definition. **54**
Figure 5.6 : Input soil profile to Deepsoil. **55**
Figure 5.7 : Deepsoil software generating the soil profile definition. **55**
Figure 5.8 : SPT-1 EL earthquake input motion selection. **56**
Figure 5.9 : SPT-1 EL viscous/small strain damping definition. **56**
Figure 5.10 : Analysis control definition. **57**
Figure 5.11 : SPT-1 EL time history plot. **57**
Figure 5.12 : SPT-1 EL stress-strain plot. **58**
Figure 5.13 : SPT-1 EL spectral plot. **58**
Figure 5.14 : SPT-1 EL profile plot. **59**
Figure 5.15 : SPT-1 EL displacement plot. **59**
Figure 5.16 : SPT-1 EL response spectra plot. **60**
Figure 5.17 : SPT-1 EL check convergence. **60**
Figure 5.18 : Analysis type definition for NL SPT-1. .... **61**
Figure 5.19 : NL SPT-1 input soil profile to Deepsoil. **61**
Figure 5.20 : NL SPT-1 Deepsoil software generating the soil profile definition. .. **62**
Figure 5.21 : NL SPT-1 input motion selection. **62**
Figure 5.22 : NL SPT-1 viscous/small strain damping definition. **63**
Figure 5.23 : NL SPT-1 analysis control definition. **63**
Figure 5.24 : NL SPT-1 time history plot. **64**
Figure 5.25 : NL SPT-1 stress-strain plot. **64**
Figure 5.26 : NL SPT-1 spectral plot. **65**
Figure 5.27 : NL SPT-1 profile plot. **65**

Figure 5.28 : SPT-1 NL mobiled strength plot. **66**
Figure 5.29 : NL SPT-1 displacement plot. **66**
Figure 5.30 : NL SPT-1 response spectra plot. **67**
Figure 5.31 : NL SPT-1 check convergence. **67**
Figure 5.32 : Shear stress reduction factor, r_d, ground surface depth, and earthquake magnitude relationship (Source: Idriss and Boulanger, 2014). **70**
Figure 5.33 : Overburden correction factor (K_σ) and vertical effective stress relationship (Source: Idriss and Boulanger, 2014). **71**
Figure 5.34 : Comparison of some magnitude scaling factor (MSF) relationship (Source: Idriss and Boulanger, 2014). **72**
Figure A.1 : Soil Profile for SPT-1. .... **82**
Figure A.2 : Corrected $(N_1)_{60}$ for SPT-1. .... **83**
Figure A.3 : Shear Wave Velocity for SPT-1. .... **83**
Figure A.4 : ELA Response Spectra for SPT-1. .... **84**
Figure A.5 : ELA Peak Ground Acceleration for SPT-1. .... **85**
Figure A.6 : ELA Maximum Strain for SPT-1. .... **85**
Figure A.7 : ELA Maximum Displacement for SPT-1. .... **86**
Figure A.8 : NLA Response Spectra for SPT-1. .... **87**
Figure A.9 : NLA Peak Ground Acceleration for SPT-1. .... **88**
Figure A.10 : NLA Maximum Strain for SPT-1. .... **88**
Figure A.11 : NLA Maximum Displacement for SPT-1. .... **89**
Figure A.12 : Soil profile for SPT-2. .... **91**
Figure A.13 : Corrected $(N_1)_{60}$ for SPT-2. .... **92**
Figure A.14 : Shear wave velocity for SPT-2. .... **92**
Figure A.15 : ELA Response Spectra for SPT-2. .... **93**
Figure A.16 : ELA Peak Ground Acceleration for SPT-2. .... **94**
Figure A.17 : ELA Maximum Strain for SPT-2. .... **94**
Figure A.18 : ELA Maximum Displacement for SPT-2. .... **95**
Figure A.19 : NLA response spectra for SPT-2. .... **96**
Figure A.20 : NLA Peak Ground Acceleration for SPT-2. .... **97**
Figure A.21 : NLA Maximum Strain for SPT-2. .... **97**
Figure A.22 : NLA Maximum Displacement for SPT-2. .... **98**
Figure A.23 : Soil profile for SPT-3. .... **100**
Figure A.24 : Corrected $(N_1)_{60}$ for SPT-3. .... **101**
Figure A.25 : Shear wave velocity for SPT-3. .... **101**
Figure A.26 : ELA Response Spectra for SPT-3. .... **102**
Figure A.27 : ELA Peak Ground Acceleration for SPT-3. .... **103**
Figure A.28 : ELA Maximum Strain for SPT-3. .... **103**
Figure A.29 : ELA Maximum Displacement for SPT-3. .... **104**
Figure A.30 : NLA Response Spectra for SPT-3. .... **105**
Figure A.31 : NLA Peak Ground Acceleration for SPT-3. .... **106**
Figure A.32 : NLA Maximum Strain for SPT-3. .... **106**
Figure A.33 : NLA Maximum Displacement for SPT-3. .... **107**

EQUIVALENT LINEAR AND NONLINEAR SITE RESPONSE ANALYSIS, STUDY CASE FOR BANDA ACEH, INDONESIA

SUMMARY

Earthquake is one of the most devastating natural hazards faced by various countries around the world. Indonesia has a reputation for being one of the world's most seismically active countries. Indonesia is the world's fourth most populous country, with a population of around 270 million people. Indonesia also has more earthquakes than the majority of other nations on earth. Indonesia is surrounded by over 18,000 km long of major tectonic plate boundaries. This is attributed to its geographical location, which is surrounded by three major active tectonic plates: Eurasian, Indo-Australian, and Philippine plates.

Banda Aceh, a city located in the west part of Indonesia, that have experienced the most devastating earthquake in Indonesia. Banda Aceh geographically is located on 05º30′ – 05º35′ N and 95º30′ – 99º16′ E. At least there are 1,271 earthquakes occurred from 1907-2020 with a magnitude > 5 Mw happened around Banda Aceh area. The earthquakes of December 26, 2004 (Mw 9.1) and March 28, 2005 (Mw 8.7) are the two largest subduction earthquakes that have ever been recorded happened in the country. For such an area, better knowledge of seismic ground response is needed to design earthquake-resistant, sustainable, and cost-effective infrastructures.

Both deterministic and probabilistic seismic hazard analyses can be used to objectively assess the seismicity of a particular location. These days, probabilistic seismic hazard analysis is commonly used since it carefully considers uncertainties such as the earthquake's location, time of occurrence, and magnitude. Probabilistic seismic hazard analysis has been used to assess the seismicity of Banda Aceh city. For this purpose, the earthquake catalog of the region was prepared by using the instrumental period data of Badan Meteorologi Klimatologi dan Geofisika (BMKG), Engdahl van der hilst and Bulland (EHB) Bulletin, and United States Geological Survey (USGS). All earthquake magnitudes in the earthquake catalog were converted to the same type of earthquake magnitudes using empirical formulas and the entire earthquake catalog was made homogeneous. Foreshock and aftershock are removed using a Z-Map with the criteria Gardner and Knopoff (1974), the software is also used to calculate b-value and rate recurrence mainshock. The subduction zone and shallow crustal are the seismic source models used. The seismotectonic conditions, local geology, and spatial data are used for basis of the characterization model. Seismic source and shallow earthquake data were modeled after ISC focal mechanism. Meanwhile, for the area that is not incorporated with the focal mechanism, the normal-slip mechanism is assumed to weight at 0.2, the reverse-slip mechanism at 0.4, and the strike-slip mechanism at 0.4. Because there are no specific attenuation functions for Indonesia region, attenuation function derived for other regions and worldwide was used.

A computer software called EZ-Frisk used to perform the seismic hazard on Banda Aceh. PGA and SA in the period spectra 0.2 and 1 second was obtained. PSHA was

carried out on the layer of bedrock with Vs_{30} at 750 m/s. Grid for a 50 km of the fault zone was set to be 0.1° x 0.1° and for 0.5° x 0.5° for the zone outside from the fault zone. The seismic acceleration from each grid was mapped using ArcGIS 9.3 software. The result obtained from the study was a seismic hazard map for Banda Aceh with the 2475 year return period. Based on the results in the form of hazard maps by the tremor in the bedrocks, the value of PGA in Banda Aceh and northern Sumatra ranged from 0.15 to 1.3g, SA 0.2 seconds value ranges from 0.35 to 2.8 g and SA 1 second ranging from 0.3 to 1.3g with the dominant source of the earthquake in the region is the megathrust fault and Sumatra-Andaman fault.

This thesis focuses on understanding a phenomenon better known as site or ground response in which soil layers alter the amplitude, frequency content, and duration of earthquake-induced ground motion. Site Response Analysis is one of the most critical steps in geotechnical earthquake engineering. The amplification of seismic waves due to the geological structure of a particular site has been found to be an important topic for many researchers and civil engineers. The degree of the amplification caused by site conditions depends on the dynamic characteristics of the soil, the characteristics of the base rock motions, the impedance contrast between the soil profile and the base rock and the depth of semi-infinite half space.

The objective of this research is to compare one-dimensional Equivalent Linear (EQL) and Nonlinear (NL) ground response analysis on some selected sites in the Banda Aceh region using Deepsoil software.

Soil profile as several representatives from the region was selected and idealized. Due to the lack of shear wave velocity data, V_s profile was obtained from correlation. The earthquake time history used for this study was 2004 Sumatra-Andaman earthquake. Because the limited digitalized and recorded earthquake acceleration data, earthquake input motion used in this study was taken from simulated one produced by Sørensen et al in 2007. For equivalent linear analysis, the solution type selected is frequency domain. General Quadratic/Hyperbolic Model (GQ/H) model was used. Non-masing hysteretic loading was selected. For nonlinear analysis, the solution type selected is time domain. General Quadratic/Hyperbolic Model (GQ/H) model was used. Masing hysteretic loading was selected.

Maximum strain values from Equivalent Linear (EL) and Nonlinear (NL) analyses showed only a few insignificant diffrences. However, the response spectra from the EL analyses are higher than those of the NL analyses, especially in soft soil. The site response analysis results reveal that the Banda Aceh soil profiles have a tendency to amplify the earthquake motions.

In site response analysis studies, another issue that is as important as the effects of soils on the propagation of earthquake waves is the evaluation of the liquefaction potential of the soil under dynamic loadings. It is stated that the soil deposits with clay content may be evaluated as non-liquefiable. For this study, liquefaction analysis was conducted solely to saturated sand layers. For this study, the simplified method that compares CRR (Cyclic Resistance Ratio) which is the resistance of a soil layer against liquefaction to CSR (Cyclic Stress Ratio) was used to determine the factor of safety (FS) of the given soil. The formulas and table used were based on the method proposed by Idriss and Boulanger (2014). From the liquefaction analysis, the soil profile SPT-1 and SPT-2 are susceptible to liquefaction and SPT-3 sand layer was not liquefied.

YEREL ZEMİN KOŞULLARININ SİSMİK ETKİLER ALTINDA EŞDEĞER DOĞRUSAL VE DOĞRUSAL OLMAYAN ANALİZİ, BANDA ACEH, ENDONEZYA İÇİN BİR ÇALISMA

ÖZET

Depremler, dünyadaki çeşitli ülkelerin karşılaştığı en yıkıcı doğal tehlikelerden biridir. Endonezya, dünyanın sismik olarak en aktif ülkelerinden biri olarak bilinir. 270 milyondan fazla nüfusuyla Endonezya, dünyanın en kalabalık dördüncü yaşamaktadır. Endonezya ayrıca dünyadaki diğer birçok ülkeden daha fazla deprem yaşıyor. Endonezya, 18.000 kilometreden daha fazla tektonik plaka sınırına sahip dünyadaki en aktif tektonik bölgelerden biridir. Dünyanın üç büyük aktif tektonik plakası olan Avrasya Plakası, Hint-Avustralya Plakası ve Filipin Plakası ile çevrili olduğu için konumu nedeniyle depremselliği yüksektir. Bu plakalar, Güneydoğu Asya bölgesinde aktif olarak birbirlerine doğru hareket etmekte ve karmaşık bir plaka sınırları ağı oluşturmaktadır. Batı Endonezya tektonik olarak Sumatra, Java, Bali, Borneo adalarını ve Sulawesi'nin güneybatı kısmını içeren Sunda'nın deprem bölgesinden oluşur. Batı Endonezya'nın aktif tektoniğine, Avustralya plakasının Sumatra ve Java ile yakınsaması hakimdir. Doğu Endonezya tektonik olarak, Banda denizinin altında çarpışan iki plaka var. Daha doğuda, Avustralya plakasının kıtasal kısmı Banda yayı ile çarpışır ve Banda Adası yayı boyunca yaygın deformasyona neden olur. Ayrıca Doğu Endonezya'nın tektoniğini karmaşıklaştıran Avustralya kıtası'da Pasifik okyanus plakası, Yeni Gine adasında yükselme ve geniş çaplı faylanma ile sonuçlanır.

Banda Aceh, Endonezya'nın batı kesiminde yer alan ve Endonezya'daki en yıkıcı depremi yaşamış bir bölgedir. Banda Aceh coğrafi olarak 05º30′ – 05º35′ K ve 95º30′ – 99º16′ D üzerinde yer almaktadır. Banda Aceh şehri ve çevredeki alanlar esas olarak Hint-Avustralya plakasının Avrasya plakasına doğru kuzey-kuzeydoğu yönelimli yakınsaması ile yılda yaklaşık 40-60 mm'lik bir çarpışma oranıyla üretilir. 1907-2020 yılları arasında Banda Aceh bölgesi çevresinde en azından 5 Mw büyüklüğünde meydana gelen 1.271 deprem meydana geldi. 26 Aralık 2004 (Mw 9.1) ve 28 Mart 2005 (Mw 8.7) depremleri, bu ilde meydana gelen en büyük iki dalma-batma bölgesi depremidir. Banda Aceh'teki binaların çoğunluğu bir ve iki katlı yüksek konut ve ticari binalardır. Bu yapılar genellikle mühendislik ürünü değildir ve ahşap veya betonarme betondan yapılmıştır. Bu nedenle Banda Aceh deprem hareketine ve yapısal tehlikeye çok yatkındır. Buna ek olarak, Banda Aceh kalın aluvyon birikintileri üzerinde yer almaktadır. Ayrıca, 26 Aralık 2004'te meydana gelen Sumatra-Andaman depremi, Banda Aceh'in çeşitli yerlerinde sıvılaşmaya ve yanal yayılmaya neden oldu. Banda Aceh'in batı kıyısındaki bölge çoğunlukla kum tabakaları içeriyordu ve sıvılaşmaya daha yatkındı. Okyanus tabanı, büyük 2004 Sumatra-Andaman depremi sırasında fay kopmasının bir sonucu olarak yükseltildi ve şimdiye kadar kaydedilen en felaket tsunami dalgaları dizisine neden oldu. Dalgalar Hint Okyanusu'nu süpürdü. 30 dakikadan kısa bir sürede batı kıyısına karşı üç büyük dalganın patladığı Aceh Eyaleti, hasarın çoğunu aldı. Yüksekliği 4 ila 39 metre arasında değişen tsunami dalgaları,

250'den fazla sahil köyünde olumsuz etkiledi. Bu bölge ve benzer bölgeler için depreme dayanıklı, sürdürülebilir ve uygun maliyetli altyapılar tasarlamak için sismik zemin tepkisi konusunda daha iyi bir bilgi edinilmesi gerekir.

Belirli bir sahanın depremselliği deterministik sismik tehlike analizleri ve olasılıksal sismik tehlike analizleri ile nicel olarak değerlendirilebilir. Depremin yeri, meydana gelme zamanı ve depremin büyüklüğü gibi belirsizlikleri açık ve detaylı bir şekilde ele alması nedeniyle olasılıksal sismik tehlike analizi günümüzde sıklıkla tercih edilmektedir. Banda Aceh tehlike analizi ile ilgili literatür çalışması daha önce A Yahya (2016) tarafından yapılmıştır. Banda Aceh şehrinin depremselliği olasılıksal sismik tehlike analizi ile değerlendirilmiştir. Bu amaçla ilk olarak *Badan Meteorologi Klimatologi dan Geofisika* (BMKG), *Engdahl van der hilst and Bulland* (EHB) *Bulletin,* ve *United States Geological Survey* (USGS) verileri kullanılarak bölgenin aletsel dönem deprem kataloğu hazırlanmıştır. Deprem kataloğundaki tüm deprem büyüklükleri aynı tip deprem büyüklüğüne ampirik formüller kullanılarak dönüştürülmüş ve tüm deprem kataloğu homojen hale getirilmiştir. Öncü depremi ve artçı depremi, Gardner ve Knopoff (1974) kriterlerine sahip bir Z-Map yazılımını kullanılarak kaldırılır, Z-Map yazılımını ayrıca b-değerini hesaplamak ve tekrarlama ana şokunu derecelendirmek için kullanılır. Dalma bölgesi ve sığ kabuklu, kullanılan sismik kaynak modelleridir. Sismotektonik koşullar, yerel jeoloji ve mekansal veriler, karakterizasyon modelinin temeli olarak kullanılır. Sismik kaynak ve sığ deprem verileri ISC odak mekanizmasından sonra modellenmiştir. Bu arada, odak mekanizması ile birleştirilmemiş alan için, normal kayma mekanizmasının 0.2'de, ters kayma mekanizmasının 0.4'te ve grev-kayma mekanizmasının 0.4'te ağırlıkta olduğu varsayılır. Endonezya bölgesi için belirli bir atenüasyon fonksiyonu yoktur, diğer bölgeler için türetilmiş ve dünya çapında zayıflatma fonksiyonu kullanılmıştır.

Banda Aceh'teki sismik tehlikeyi gerçekleştirmek için kullanılan EZ-Frisk adlı bir bilgisayar yazılımı. PGA ve SA periyot spektrumlarında 0.2 ve 1 saniye elde edildi. PSHA ana kaya tabakası üzerinde Vs_{30} ile 750 m/s'de gerçekleştirilmiştir. 50 km'lik bir fay zonu için grid $0{,}1^o$ x $0{,}1^o$ ve fay zonunun dışındaki zon için $0{,}5^o$ x $0{,}5^o$ olarak ayarlandı. Her koordinattan gelen sismik ivmelenme, ArcGIS 9.3 yazılımı kullanılarak haritalandı. Çalışmadan elde edilen sonuç, Banda Aceh ve Kuzey Sumatra için 2475 yıllık geri dönüş süresine sahip bir sismik tehlike haritasıydı. Ana kayalardaki titreme ile tehlike haritaları şeklindeki sonuçlara dayanarak, Banda Aceh'deki PGA değeri 0.15 ila 1.3g, SA 0.2 saniye için değeri 0.35 ila 2.8 g arasında değişmektedir, ve SA 1 saniye icin 0.3 ila 1.3 g arasında değişemektedir. Bölgedeki depremin baskın kaynağı *megathrust* ve Sumatra-Andaman itme fayıdır.

Zemin davraniş analizi, deprem ve jeoteknik mühendisliginde en kritik konusundan biridir. Belirli bir alanın jeolojik yapısı nedeniyle sismik dalgaların çoğalması, birçok araştırmacı ve inşaat mühendisi için önemli bir konu olarak bulunmuştur. Bu tez, zemin tabaklarinin ve yerel koşulların, deprem dalgalarının genlik, frekans içeriğini ve süresini nasıl değiştirdiğini inceleyen zemin davranış analizlerine odaklanmaktadır.

Bu çalışmanın amacı, Deepsoil yazılımını kullanarak, Banda Aceh bölgesine ait olan seçilmiş altı zemin profili üzerinde bir boyutlu Eşdeğer Doğrusal ve Doğrusal Olmayan zemin davranış analizi sonuçlarını karşılaştırmaktadır.

İlk olarak, bölgeden birkaç temsilci olarak zemin profili seçildi ve idealize edildi. Kayma dalgası hızı verilerinin olmaması nedeniyle Vs profili korelasyondan elde edildi. İncelenen bölge için bir deprem kaydı da seçilmiştir. Bu çalışmada kullanılan deprem zaman tarihi 2004 Sumatra-Andaman depremidir. Sınırlı dijitalleştirilmiş ve kaydedilmiş deprem ivme verileri nedeniyle, bu çalışmada kullanılan deprem giriş hareketi, 2007 yılında Sørensen et al tarafından üretilen simüle edilmiş olandan alınmıştır. Analiz daha sonra zemin davranış analizleri gerçekleştirilmiştir. Eşdeğer doğrusal analiz için, seçilen çözüm tipi frekans etki alanıdır. Genel Kuadratik/Hiperbolik Modeli kullanıldı. Non-masing histeretik yükleme seçildi. Doğrusal olmayan analiz için, seçilen çözüm türü zaman etki alanıdır. Genel Kuadratik/Hiperbolik Modeli kullanıldı. Masing histeretik yükleme seçildi.

Eşdeğer Doğrusal ve Doğrusal Olmayan zemin davranış analizlerinden (yer tepki analizlerinden) elde edilen birim kayma şekil değistirme değerleri arasındaki fark oldukça küçük mertebelerdedir. Analiz sonuçlarından bazı zemin tabakalarının dinamik özelliklerinin zemin büyütmesine sebep olduğu, bazı tabakalarda da şekil değistirme enerjisini sonanlendirip etkisini azaltabileceği bilinmektedir. Düşük N-SPT değerlerine sahip zayıf aluvyon zeminler, sönüm özelliklerine ve kayma rijitliği özelliklerine bağlı olarak (sönüm özellikleri sınırlı ise) deprem hareketinin genliklerini arttırabilir. Sıvılaşma analizleri sonuçları, 2004 Sumatra-Andaman depremi için seçilen zemin profillerinin sıvılaşma potansiyeli olduğunu göstermektedir, bu nedenle bazı zemin profillerinin davranış (tepki) analizi sonuçları oldukça düşensizdir.

Saha tepki analizi çalışmalarında toprakların deprem dalgalarının yayılımı üzerindeki etkileri kadar önemli olan bir diğer konu da toprağın dinamik yüklemeler altında sıvılaşma potansiyelinin değerlendirilmesidir. Kil içerikli toprak birikintilerinin sıvılaştırılamaz olarak değerlendirilebileceği belirtilmektedir. Bu çalışma için sıvılaştırma analizi sadece doymuş kum tabakalarına yapılmıştır. Bu çalışma için, verilen toprağın güvenlik faktörünü belirlemek için bir toprak tabakasının sıvılaşmaya karşı direnci olan Döngüsel Direnç Oranını Döngüsel Stres Oranı ile karşılaştıran basitleştirilmiş yöntem kullanılmıştır. Kullanılan formüller ve tablo, Idriss ve Boulanger (2014) tarafından önerilen yönteme dayanıyordu. Sıvılaştırma analizinden, toprak profili SPT-1 ve SPT-2 sıvılaşmaya duyarlıdır ve SPT-3 kum tabakası sıvılaştırılmamıştır.

1. INTRODUCTION

The scope of this study is to inspect Banda Aceh's soil behavior to earthquake excitation. Banda Aceh is a city which is located in the northern part of Sumatra Island, Indonesia. With a population of around 270,321 inhabitants, Banda Aceh is the provincial capital and commercial hub in the province of Aceh. (BPS, 2019). The Sultanate of Aceh was the first Islamic state in Southeast Asia and historically had a bilateral relationship with Ottoman Turks in the past.

Banda Aceh geographically is located on 05º30′ – 05º35′ N and 95º30′ – 99º16′ E, with a total area of approximately 61,36 km². It lies between the two seismically active plates, the Eurasian plate, and the Indo-Australian plate. A series of island arcs or non-volcanic prismatic accretion zones and Bukit Barisan mountains with volcanic tracks in the center resulted from the progression between the Eurasian plate and the Indo-Australian plate. The Great Sumatran Fault divides the island of Sumatra from the Gulf Semangko to Banda Aceh and extended into the sea of Andaman (Rusydy, 2013). These faults made Sumatra Island as the areas prone to strong motion earthquakes, for example ($M \geq 8.0$) 2004 Sumatra-Andaman earthquake, 2005 Nias earthquake, and 2005 Simeulue earthquake. Moreover, according to research done by Yunita et. al. (2018) Banda Aceh was located on thick alluvium soil deposits and thus it was very important to understand how the ground would respond to the earthquake motions to improve design and construction practices. Based on the information presented above, Banda Aceh must adopt a building codes that incorporate seismic loads into consideration while designing structures. Structures are designed primarily based on Seismic Hazard Analysis and Site Response Analysis of the particular location.

The objective of this research is to compare one-dimensional Equivalent Linear (EQL) and Nonlinear (NL) of ground response analysis on the 3 selected sites in Banda Aceh region using Deepsoil software. The data used in this study was obtained from the data collection of Syiah Kuala University, Soil Mechanics Laboratory.

Chapter 2 covers the general background of earthquake hazards in the Banda Aceh region. Meanwhile, chapter 3 discussed the seismic hazard analysis conducted for the Banda Aceh region. Chapter 4 discussed the seismic behavior of the soil under earthquake loading and site response, and the process and analysis results presented in chapter 5. The relevant findings of this study were described in chapter 6, along with recommendations for future research.

2. EARTHQUAKE AND ITS HAZARD IN BANDA ACEH

An earthquake is a natural occurrence in which the ground shakes and moves due to a sudden release of energy in the crustal part and upper mantle of the earth's interior. While smaller earthquakes are often unnoticeable, stronger earthquakes can cause severe ground shaking and pose a serious threat to human lives and property (Kramer, 1996).

The study of earthquakes is compelled by their catastrophic effects, and the fact that earthquakes are inevitable presupposes the study of minimizing their impact. This work provides a major contribution to the latter, which we call engineering seismology.

Seismic hazards, or potential risks caused by earthquakes, can endanger lives and cause financial damage. This segment provides an overview of the most common forms of earthquake hazards that occur in Banda Aceh.

2.1 Seismicity Condition in Banda Aceh

According to USGS (2021), Indonesia and its neighborhoods in the Southeast Asia region are susceptible to earthquakes produced by various seismic sources. Indonesia is obliquely located at the meeting point of the Indo-Australian, Philippine Sea, Caroline, and Sunda plates as shown in Figure 2.1. The sources of seismicity in Indonesia are diverse, various seismic sources are including but are not limited to active megathrusts, crustal faults, and normal and reverse intraslab mechanisms.

In the west part of Indonesia, the primary seismicity sources were the Sunda-Java trench and Indo-Australian plate subducts beneath the Sunda plate. Meanwhile, in eastern Indonesia, plate convergence is divided among numerous microplates, resulting in a zone of deformation marked by arc-continent collision, subduction, strike-slip, thrust, and extensional faulting (Hutchings, S. J., & Mooney, W. D., 2021).

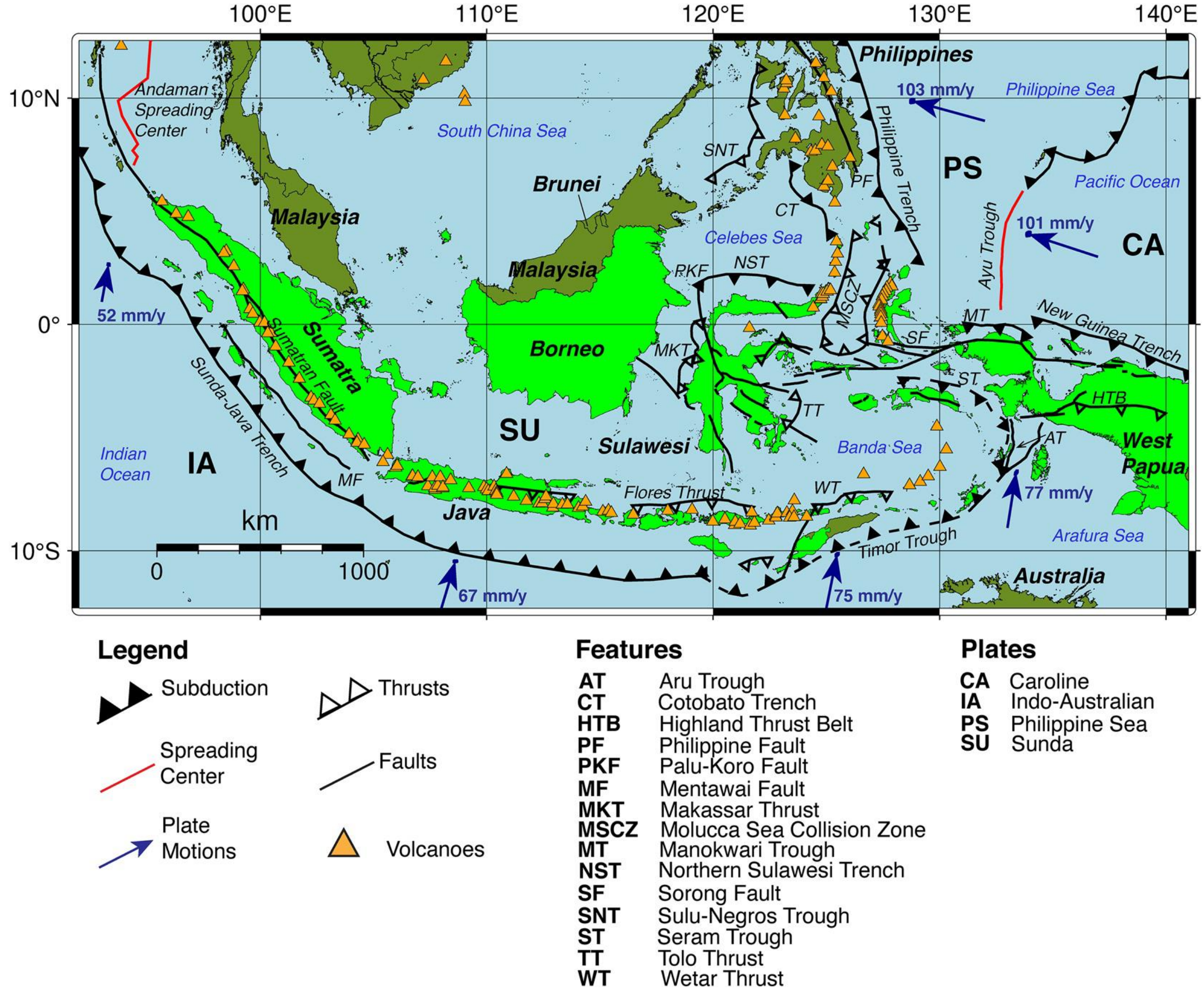

Figure 2.1 : Indonesian and the surrounding region's tectonic setting. The country of Indonesia is marked in green. Major plate borders, faults, and plate boundaries are all represented. (Source: Hutchings, S. J., & Mooney, W. D., 2021 referencing the plate velocities with respect to the Sunda plate obtained from the MORVEL velocity model (DeMets et al., 2010). Faults and boundaries are obtained from Moore and Silver (1983), Silver, McCaffrey, and Smith (1983), Silver, Reed, et al. (1983), Widiwijayanti et al. (2004), Besana and Ando (2005), Roosmawati and Harris (2009), Watkinson et al. (2011), Hall (2012), Mukti et al. (2012), Tsutsumi and Perez (2013), Saputra et al. (2014), Cipta et al. (2016), Koulali et al. (2016), Omang et al. (2016), Adhitama et al. (2017), Patria and Hall (2017), Watkinson and Hall (2017), Hall (2018), Nugraha and Hall (2018), Supendi et al. (2018), Valkaniotis et al. (2018), and Irsyam et al. (2020).

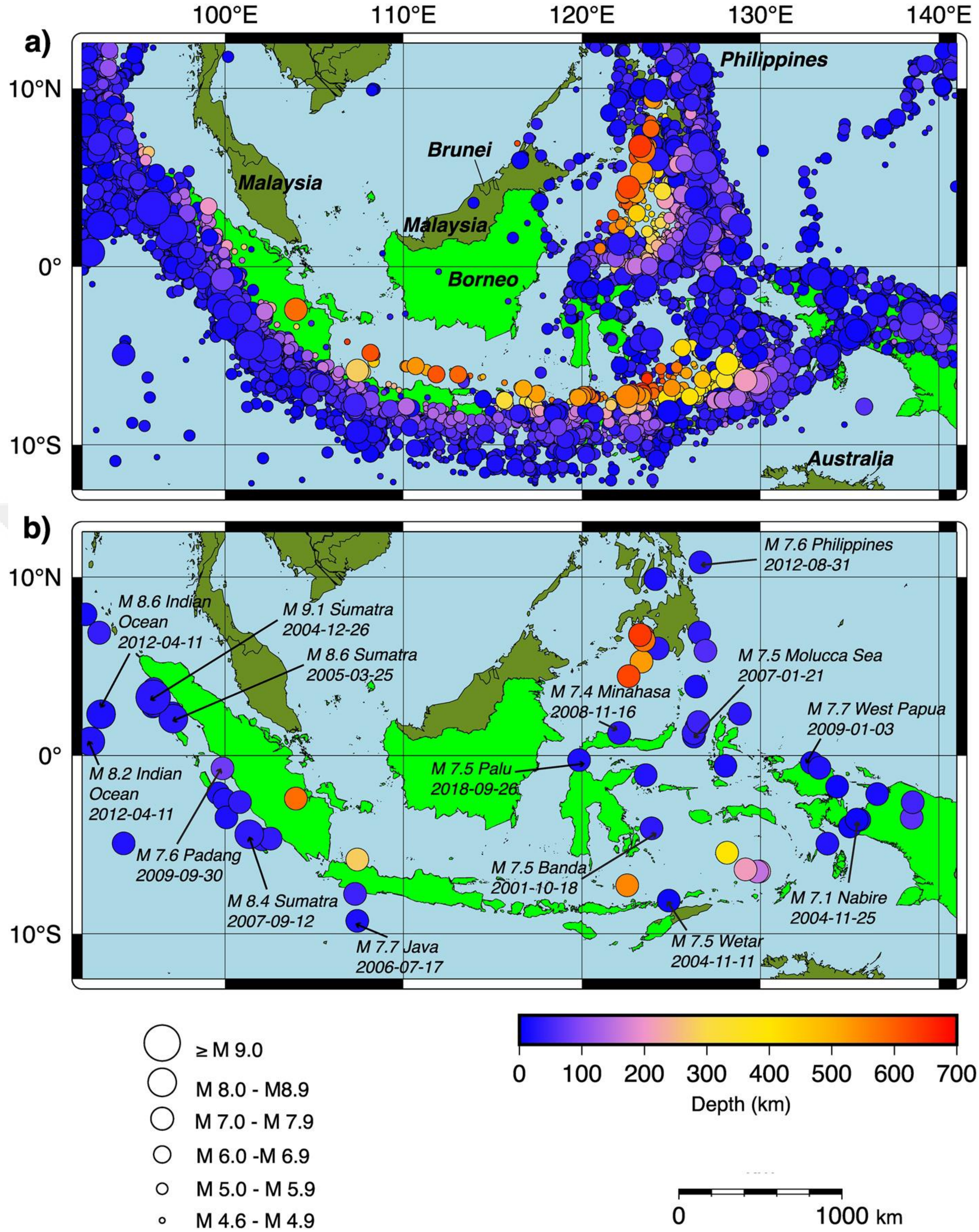

Figure 2.2 : Earthquake events occurred in Indonesia from January, 1st 2000 to July, 28th 2020 (a) Event for M ≥4.6 (b) Event for M ≥7.0, source data was taken from USGS (2020). The majority of earthquake was shallow and low magnitude event with M<6 (Source: Hutchings, S. J., & Mooney, W. D., 2021).

From Figure 2.1 and Figure 2.2 above, it can be concluded that seismic activity in Indonesia mostly occurred near around the plate boundaries. According to Hutchings, S. J., & Mooney, W. D. (2021) averagely, 320 earthquakes with magnitudes ≥5.0 and 3 earthquakes with magnitudes ≥7.0 occurs in Indonesia. Several of the largest instrumentally recorded earthquakes occurred in Indonesia, including five events with magnitudes ≥8.0 since January 2000, the most destructive being the 2004 Mw 9.1 Sumatran-Andaman earthquake which was causing a very devastating catastrophe in Aceh.

2.2 Earthquake-induced Hazards in Banda Aceh

Earthquake-induced hazards or seismic hazards, can endanger lives and cause economic losses. This section is a brief explanation for some types of seismic hazards.

2.2.1 Ground shaking

Ground motion or ground shaking is a primary hazard of earthquake that causes slight or entire subside of structures. Earthquakes induce ground motions, that are the shaking of the ground. Strong ground motions may cause structural damage to dwelling structures, streets, bridges, dams, and other structures. At least there are 1,271 earthquakes occurred from 1907-2020 with a magnitude > 5 Mw happened around Banda Aceh area (USGS, 2020). Some of the significant earthquakes can be seen in Table 2.1.

Stiff low-rise structures escaped with only minor damage. According to the testimony, the ground motion in Banda Aceh was mostly the long period one. This is to be anticipated, considering that the city is 255 kilometers from the epicenter of the great Sumatra-Andaman earthquake and that the area's soft soil contributed to the ground motion's amplification (Ghobarah et al., 2006).

Tabel 2.1 : Some Significant Earthquakes Affected Banda Aceh Region (BMKG, 2018).

Date Proposed	**Fault Source /Mechanism**	**Location**	**Magnitude**	**Duration (minutes)**	**Depth (km)**	**Casualty**
23 August 1936		6.1N 94.7E	- Banda Aceh : VII - VIII			9 dead, 20 injured
02 April 1964		5.9N 95.7E	5.2 Banda Aceh : VII			20-30% structure made from brick damaged
12 April 1967	No tsunami	5.3N 97.3E	6.1		55	
26 December 2004	Undersea megathrust (a rupture along the fault between the Burma Plate and the Indian Plate) earthquake followed by tsunami	Aceh	9.0 – 9.3 (MMI – IX)	8-10	30	165.708 were accounted for as dead. 12.132 as missing. and 703.5 18 as displaced.
28 March 2005	Undersea megathrust with tsunami, subduction is forcing the Indo-Australian Plate to the southwest under the Eurasian Plate's Sunda edge	Nias	8.7	2	30	The total number of dead varied from 150 to 870.
20 Feb 2008		Simeulue	7.3		20	3 dead, 25 injured
07 April 2010	Eathquake with local tsunami (40 cm)	Sinabang	7.6		34	22 injured
09 Mei 2010	Eathquake with local tsunami (20 cm)	Meulaboh	7.2		30	5 injured
20 Feb 2008		Simeulue	7.3		20	3 dead, 25 injured

Tabel 2.1 (continued) : Some Significant Earthquakes Affected Banda Aceh Region (BMKG, 2018).

Date Proposed	**Fault Source /Mechanism**	**Location**	**Magnitude**	**Duration (minutes)**	**Depth (km)**	**Casualty**
13 June 2010		Aceh-Andaman	7.5		21	-
11 April 2012	Eathquake with tsunami (80 cm)	Simeulu	8.4		12.3	5 people dead because of heart attack, 11 injured
21 January 2013		Pidie Jaya 4,82 N 95.95 E	5.9		31.77	1 dead, 10 injured
2 July 2013		Bener Meuriah	6.1		25.6	42 dead, 6 lost, 210 injured
7 December 2016	Strike-slip (Definite fault is unknown, possibly Samalanga-Sipopok Fault)	Pidie Jaya, Aceh	6.4 - Banda Aceh (III – IV - Aceh Jaya : VII - VIII MMI)	0.16-0.25	10	104 dead, 1000 injured
8 February 2018	Land earthquake	Pidie, Aceh	5.1 - Banda Aceh : III MMI - Aceh Jaya : III MMI		10	Small damage (4 houses, 1mosque, 1 health care unit)

2.2.2 Structural hazards

According to a report submitted by Ghobarah et al. (2006) the majority of buildings in Banda Aceh are one and two stories high residential and commercial buildings. These structures are most usually not engineered and are constructed of timber or reinforced concrete. Engineers designed many of the 3-5 story reinforced concrete structures. In most cases, earthquake failure can not be distinguished from the tsunami damage. Collapsed and damaged structures due to the 2004 Sumatra-Andaman strong ground motion included but not limited to dwelling and office buildings, infrastructure, shopping centers, governmental buildings, mosques and various towers, as shown in Figure 2.3 to Figure 2.10.

The earthquake intensity in Banda Aceh was briefly described as difficult to walk or stand during the earthquake, severe damage, and partial or complete collapse of improperly designed or poorly constructed structures. This corresponds to an intensity of VII to VIII on the Modified Mercalli Scale (Ghobarah et al., 2006).

Figure 2.3 : A steel truss bridge deck had been swept away 50 meters by earthquake and tsunami and a temporary Bailey bridge had been installed in its place in Lhoknga, Banda Aceh (Ghobarah et al., 2006).

Figure 2.4 : A Closer look from a wrecked structural steel bridge with a destroyed Lafarge cement plant in Lhoknga, Banda Aceh (Ghobarah et al., 2006).

Figure 2.5 : Department of Finance Building in Banda Aceh, a three-story structure destroyed by 2004 earthquake (Ghobarah et al., 2006).

Figure 2.6 : A flexural hinging at the upper and lower part of structural columns in a mosque located in Banda Aceh (Ghobarah et al., 2006).

Figure 2.7 : A collapsed ground floor of a store in Banda Aceh with the second and third floors left intact (Ghobarah et al., 2006).

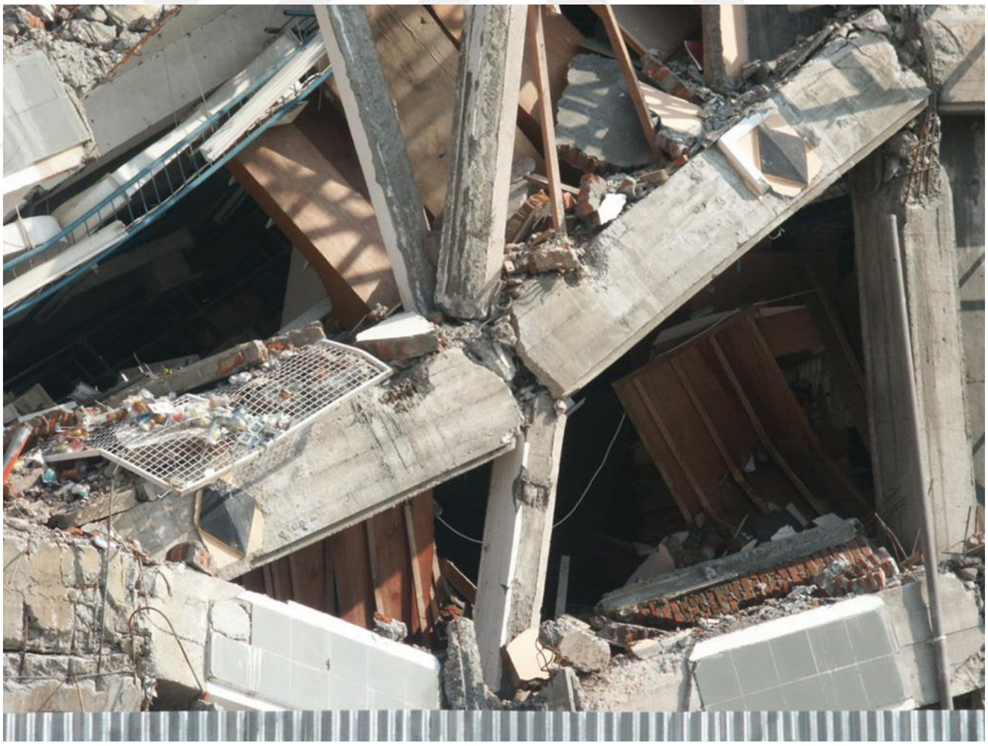

Figure 2.8 : The Pante Pirak shopping complex in Banda Aceh suffered from a strong beam - weak column and beam–column joint failure (Ghobarah et al., 2006).

Figure 2.9 : A four-floor office building in Banda Aceh had a beam–column joint failure caused by the absence of transversal reinforcements (Ghobarah et al., 2006).

Figure 2.10 : Tower of Baiturrahman Grand Mosque damaged by the 2004 seismic event in Banda Aceh (Ghobarah et al., 2006).

2.2.3 Liquefaction

The term liquefaction refers to a situation of soils acting more like a liquid than a solid due to the accumulation of excess pore-water pressure within soils during ground shaking. Liquefaction can cause massive ground displacements, causing damage to buildings and other facilities. Liquefaction is most often located near rivers, bays, and other bodies of water since it commonly occurs in saturated soils (Kramer, 1996).

According to Jalil et al. (2020) Sumatra-Andaman earthquake that occurred on December 26, 2004, caused liquefaction and lateral spreading in various locations in Banda Aceh. The west coast area of Banda Aceh mostly contained sand layers, and was more prone to liquefaction. Figure 2.11 and Figure 2.12 shows the liquefaction with the emergence of the foundation settlement of building and tilt in the Banda Aceh area as an after-effect of the 2004 earthquake.

Figure 2.11 : Foundation partial settlement of a hotel building because of liquefaction in Banda Aceh (Jalil et al., 2020).

Figure 2.12 : Phenomenon of the foundation settlement of a multi-story building due to liquefaction in Banda Aceh (Jalil et al., 2020).

2.2.4 Landslides

Landslides are phenomena in which soils or rocks fall downhill due to gravity. Earthquakes, rainfall, construction activities, and other factors may all trigger landslides. During earthquakes, shear stresses in the slopes' soils/rocks surpass their shear strength, causing the soils or rocks to slide and fall down then bury people, buildings, and property. (Kramer, 1996).

During Sumatra-Andaman earthquake, there is no major landslides observed. According to information obtained from thinkhazard.org (2020) Banda Aceh landslide susceptibility is categorized as very low according to the current data available. However, further research and future observation still needed to confirm this statement.

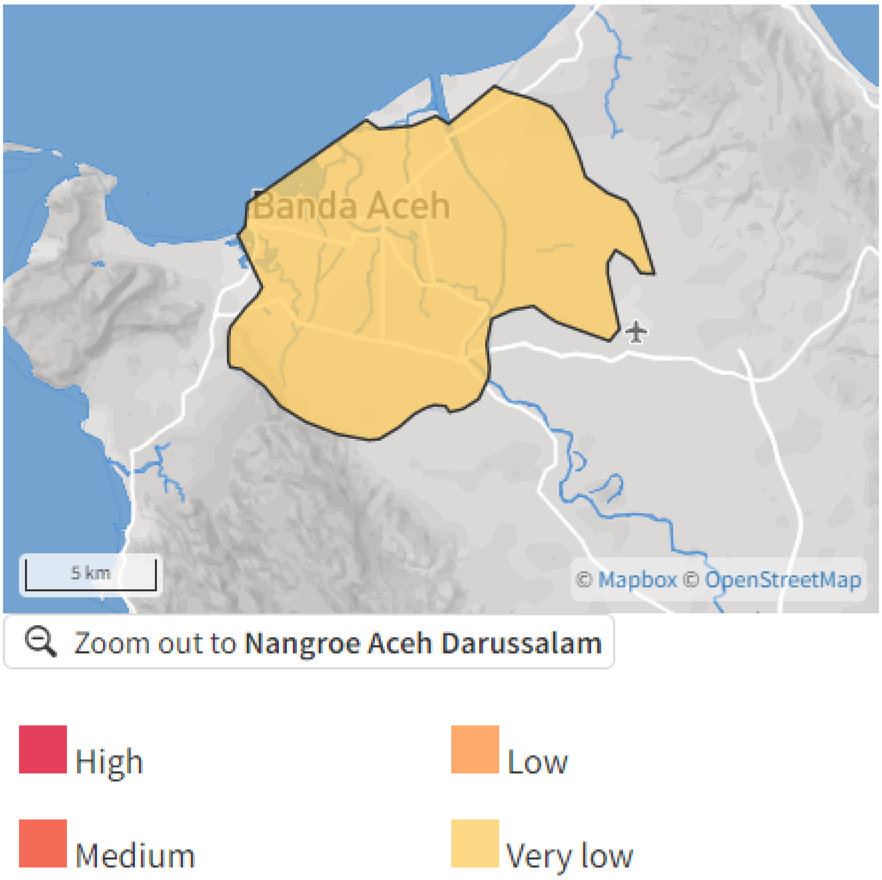

Figure 2.13 : Banda Aceh landslide susceptibility (Source: https://thinkhazard.org/en/report/73705-indonesia-nangroe-aceh-darussalam-kota-bandaaceh/LS).

2.2.5 Retaining structure failures

During earthquakes, quay walls, anchored bulkheads, and other retaining structures are often destroyed. During the 2004 Sumatra-Andaman earthquake, the majority of retaining structure damages occured around the water's edge, such as in ports and harbors.

2.2.6 Lifeline hazards

Failures of lifelines not only have serious economic effects, but they may also have a negative impact on the climate and quality of life in the aftermath of an earthquake. Indonesia's public electric supply is provided by PT PLN, the state-owned electric company. According to an observation made by Cluff (2007) Sumatra-Andaman earthquake and tsunami caused no major structural damage to the well-built electric generating plants in Aceh Province, but most of the above-ground distribution electrical cables were severely damaged by tsunami. Tsunami wave surge in Banda Aceh swept an 11-megawatt diesel-generating station situated on a barge offshore more than 3 kilometers inland (see Figure 2.14), the power plant was not harmed, but as it sped onshore houses and other buildings were destroyed. PT PLN restored the emergency-response customers within 3 days, but most of Banda Aceh inhabitant suffered a blackout for about two weeks.

Figure 2.14 : Offshore diesel-generating electrical station that was swept inland by tsunami waves, now it is one of the monuments to commemorate the devastating event (Source: https://static.trip101.com/paragraph_media/pictures/002/269/764/large/1024px-PLTD_Apung.jpg).

On the west coast of Aceh Province, particularly in Banda Aceh, Pertamina, the state-owned petroleum firm suffered significant damage to fuel depots, where storage facilities were damaged and some fuel was lost. The petroleum storage and distribution complex at Kreung Raya lost half of its above-ground pipework and three of its twelve liquid fuel storage tanks (diesel, high-octane gas, oil, and kerosene). None of the tanks were properly anchored, and the three that were washed away by tsunami waves were only partially full. The nine fully loaded storage tanks were spared. Most above-ground distribution systems, like the electric system, were severely damaged or destroyed by the tsunami (Cluff, 2007).

The ferocity of the tsunamis wreaked havoc on roads and bridges. Hundreds of kilometers Aceh Province's west coast transportation network was swept away. Hundreds of bridges were lifted up by the tsunami waves from its foundation and swept inland, some for more than a kilometer. The massive damage to bridges hampered rescue and relief activities, as the bridges were key connectors to the region's population centers. (Cluff, 2007).

2.2.7 Tsunami and seiche hazards

Tsunami is a long-period sea waves propagated by abrupt vertical seafloor movements, typically generated by a fault rupture during earthquakes. Another type of an earthquake-induced waves that occurs in an enclosed bodies of water is called seiche, usually caused by a long-period seismic waves that match the natural period of oscillation of the water in a lake or reservoir. Seiche may be seen from some distances from the source of a seismic event (Kramer, 1996).

The ocean floor was raised as a result of the fault rupture during the great 2004 Sumatra-Andaman earthquake, resulting in the most catastrophic series of tsunami waves ever recorded. The waves swept across the Indian Ocean, wreaking havoc on 12 countries' coastal populations. Aceh Province, where three massive waves blasted against the western shore in less than 30 minutes, took the brunt of the damage. Tsunami waves ranging in height from 4 to 39 meters (see Figure 2.15) impacted negatively on more than 250 coastal villages (Cluff, 2007). The devastating catastrophe of the event shown in Figure 2.16 to Figure 2.18.

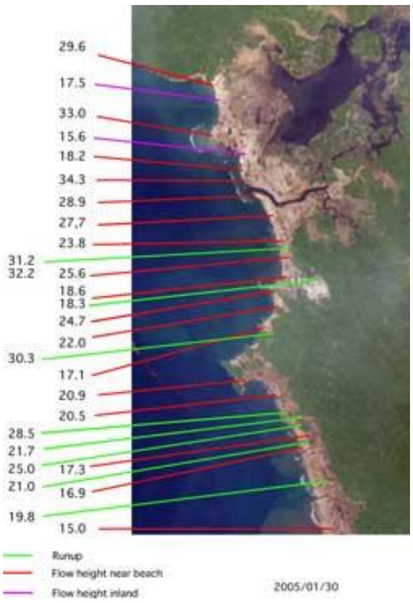

Figure 2.15 : Tsunami height and run-up measurements in Lampuuk, Banda Aceh (Source: https://cmgds.marine.usgs.gov/data/sumatra05/heights.html).

Figure 2.16 : Damage in Banda Aceh after tsunami 2004 (Source: http://ioc3.unesco.org).

Figure 2.17 : The effect of the tsunami in Banda Aceh (source: https://www.sms-tsunami-warning.com/pages/tsunami-sumatra-2004#.Yd8jvdFBzIU).

Figure 2.18 : Before and after the tsunami, aerial views of Banda Aceh's northern shore (Ghobarah et al., 2008).

2.2.8 Fault rupture hazards

Numerous examples of the destructive effects of earthquake surface fault rupture on the built environment have been produced by earthquakes. During the Chi-Chi earthquake in Taiwan in 1999, a surface fault was ruptured along the Chelungpu fault. Due to differential vertical ground motions, this earthquake tore apart houses, thrusted them laterally, and racked them. Similarly, surface ruptures displaced bridges, buildings, and buried lifelines during the 1999 Kocaeli and Duzce earthquakes in Turkey (Bray, 2001). Figure 2.19 shows the principal surficial hazards of earthquake fault rupture.

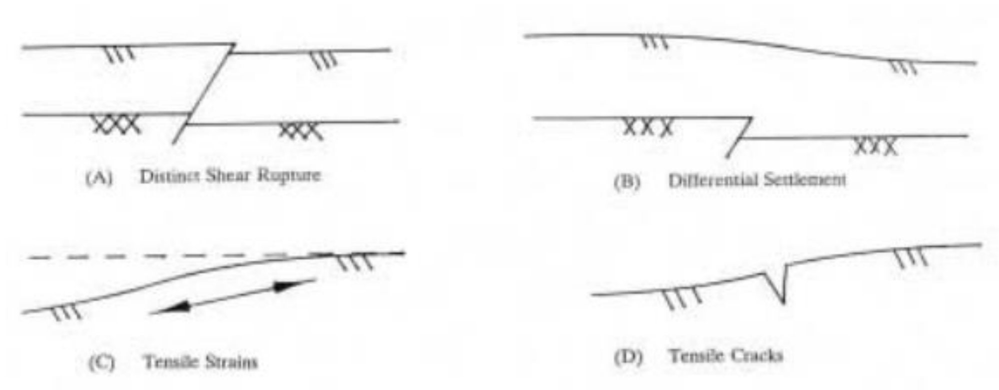

Figure 2.19 : Illustration of principal surface hazards due to fault rupture (Bray, 2001).

Aceh located on three segments of the Sumatra fragment system (see Figure 2.20), namely segment of Aceh, Tripa and Seulimeum. Aceh segment stretched from Central Aceh to Mata Ie and up all the way to Pulau Aceh. Before 1892 this segment had not experienced any earthquake more than 6 Mw. However, in 2013 this segment experienced a stong motion with a magnitude of 6 Mw in Central Aceh and Bener Meriah. Tripa segment experienced earthquakes in 1990 in Gayo Luwes district with magnitude 6.8 Ms and in Southeast Aceh in 1936 with a magnitude of 7.2 Ms. The Seulimeum segment is the active part of the Sumatra fault, which extends from the north part of Aceh. The active route of this segment is marked by high cliffs and split sediment of young volcano on the southwest side of Seulawah Agam volcano then passed the Seulimeum rivulet (Sieh and Natawidjaja, 2000). Earthquakes occurred on this segment in December, 17, 1975 with a magnitude of 6.2 Mw in Krueng Raya (Rusydy, 2013).

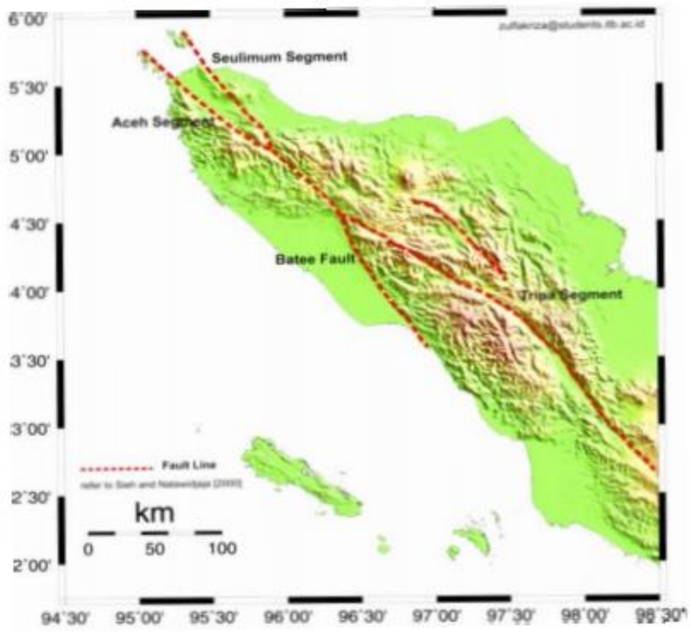

Figure 2.20 : Map of Northern Sumatra Fault (Sugiyanto et al., 2011).

The Sumatra-Andaman earthquake on December 26, 2004, began slowly, with small slip and a sluggish rupture pace for the first 40 to 60 seconds. The rupture then spread north northwest at a pace of about 2.5 kilometers per second, spreading 1200 to 1300 kilometers to Andaman. Along a 600-kilometer stretch of the plate boundary offshore of northwestern Sumatra and the southern Nicobar Islands, peak displacements reached up to 15 meters. Slip was less in the northern 400 to 500 kilometers of the aftershock zone, and some slip may have occurred there on a time scale outside the seismic band (Ammon, C. J., 2005). The rupture happened under the sea generated tsunami.

2.2.9 Coastal subsidence

Earthquakes in coastal areas can cause vertical movement of the land relative to the sea level, whether submerged or uplift displacement. It was observebed by USGS (2006) that in Aceh, the 2004 Sumatra-Andaman earthquake permanently dropped Banda Aceh coastline by up to 1 m (Figure 2.21), and uplifted nearby islands by up to 2 m (Figure 2.22). Maps for the coastal subsidence of Banda Aceh and its surrounding area can be seen in Figure 2.23.

Figure 2.21 : Coseismic subsidence induced by the 2004 Sumatra-Andaman seismic event around Lhoknga, Banda Aceh, proven by trees dropped into the surf zone. (Source: https://cmgds.marine.usgs.gov/data/sumatra05/subsidence.html).

Figure 2.22 : Uplift event in Simelue Island made coral reef exposed out of the water (Source: https://cmgds.marine.usgs.gov/data/sumatra05/subsidence.html).

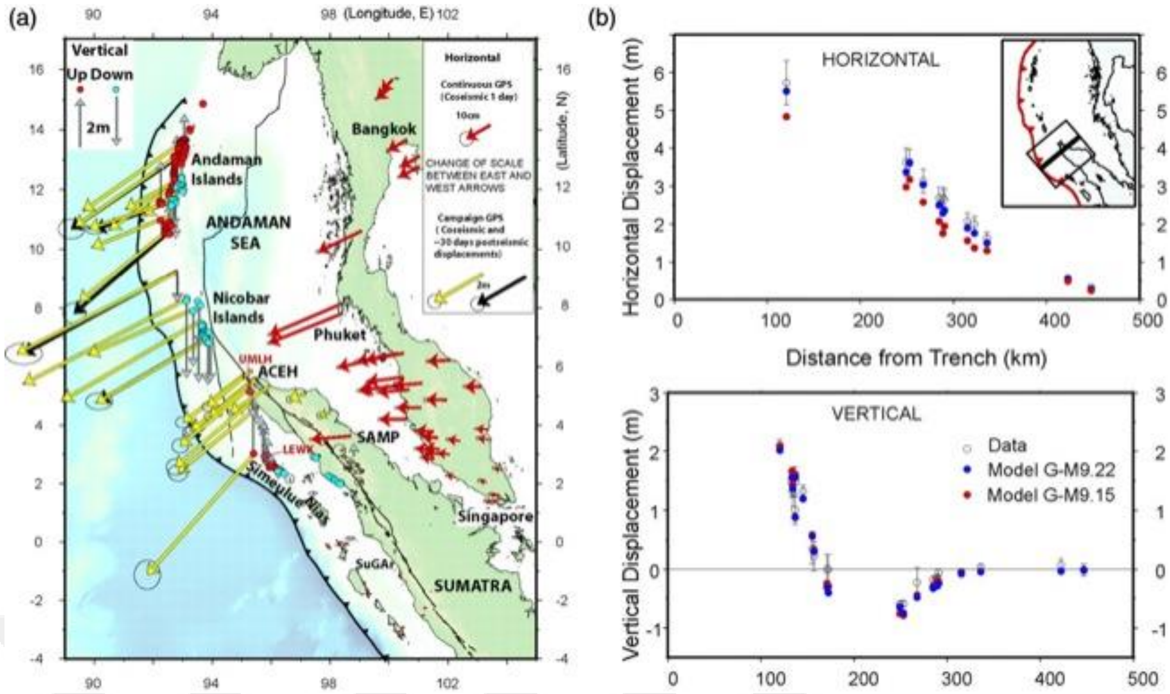

Figure 2.23 : Coastal subsidence maps from the 2004 Sumatra-Anadaman earthquake (Source: Chlieh et al., 2007).

3. SEISMIC HAZARD ANALYSIS

3.1 Deterministic Seismic Hazard Analysis

The use of deterministic seismic hazard analysis (DSHA) is more common in the early years of geotecnical engineering. DSHA entails the creation of a specific seismic scenario on which a ground motion hazard assessment is based. The scenario is based on the occurrence of an earthquake of a certain magnitude at a particular location. Figure 3.1 below shown a scheme for calculating DSHA, the first step is to collect all earthquake sources capable of causing significant ground motion at the location, the earthquake data then must be identified and characterized. The second step is for each source zone, a source-to-site distance parameter is chosen. The shortest distance between the source zone and the site of interest is chosen in most DSHAs. Depending on the distance measure of the predictive relationship used in the next phase, the distance can be stated as an epicentral distance or a hypocentral distance. The third step is to choose the controlling earthquake (usually the earthquake with the strongest ground motion measured). The site's hazard is formally defined, usually in terms of the ground vibrations caused by the controlling earthquake. One or more ground motion parameters derived through predictive relatioship are commonly used to define its properties. Seismic hazard usually translated as peak acceleration, peak velocity, and response spectrum ordinates (Kramer, 1996).

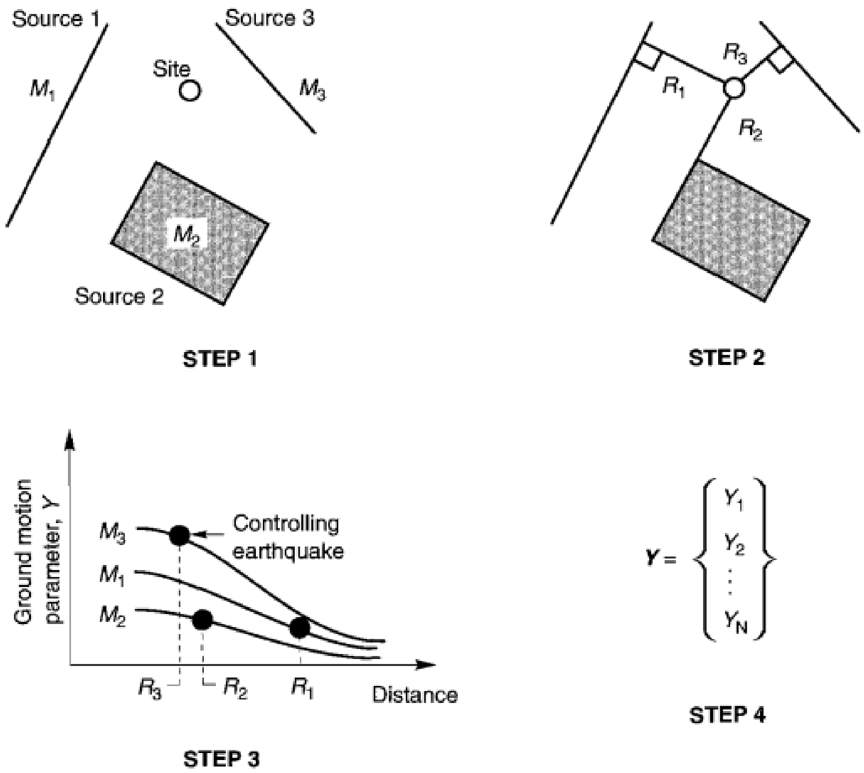

Figure 3.1 : The steps for calculating DSHA (Source: Kramer, 1996).

DSHA provides a convenient approach for assessing worst-case ground motions. It does not, however, provide information on the possibility of the controlling earthquake occurring, the possibility of it occurring where it is assumed to occur, the level of shaking that might be expected over a finite time period (such as the useful lifetime of a specific structure or facility), or the consequences of uncertainties in the various steps required.

3.2 Probabilistic Seismic Hazard Analysis

According to Kramer (1996), Probabilistic Seismic Hazard Analysis was developed in more recent year as a complementary method for DSHA that consider uncertainties in earthquake size, location, and rate of recurrence, as well as variations in ground motion characteristics as a function of earthquake size and location, to be explicitly incorporated in the assessment of seismic risks Kramer, 1996). The PSHA method is developed using procedures and formulas established by Cornell (1968) and Algermisen et al. (1982)

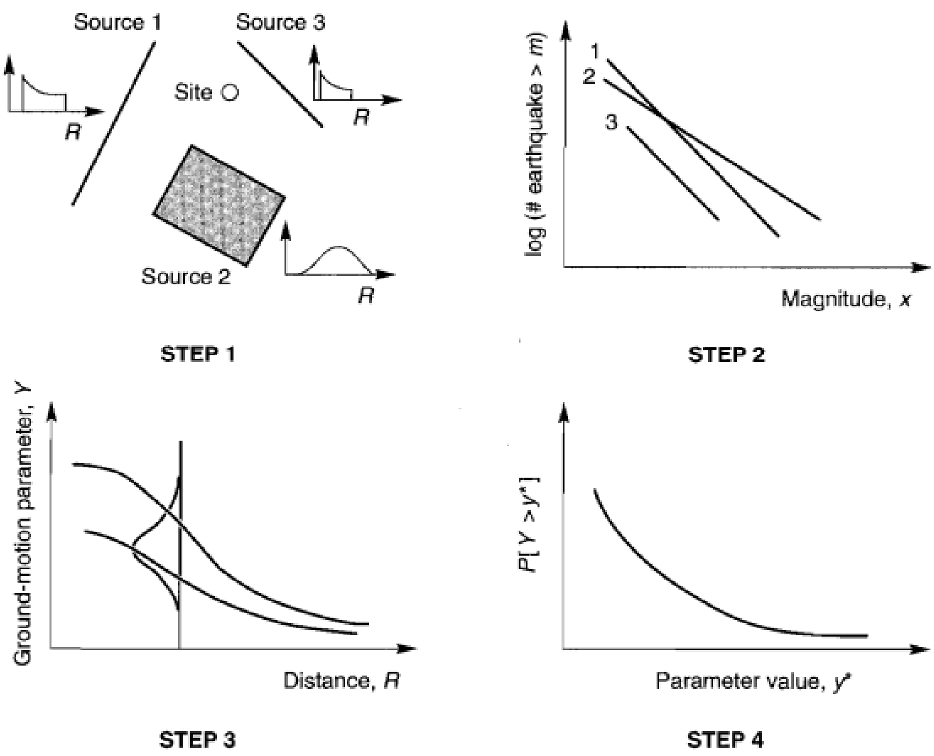

Figure 3.2 : The steps for calculating PSHA (Source: Kramer, 1996).

The stages of calculating PSHA can also be concluded into four steps (Figure 3.2). The first step is same with the DSHA method that is to determining the earthquke catalogue with an exception that it is also necessary to characterize the probability distribution of probable rupture locations inside the source. These distributions are then integrated with the source geometry to produce the source-to-site distance probability distribution. The seismicity or the time distribution of earthquake occurrence, must then be determined. To quantify the seismicity of each source zone, a recurrence relationship is utilized, which specifies the average rate at which an earthquake of a certain size will be exceeded. The largest size earthquake may be accommodated by the recurrence relationship, but it does not limit consideration to the strongest earthquake. Next, the predictive relationships must be used to determine the ground motion produced at the site by earthquakes of any size occurring at any place in each source zone. In a

PSHA, the uncertainty in the prediction relationship is also taken into account. Finally, the uncertainties in earthquake location, earthquake size, and ground motion parameter prediction are combined to obtain the probability that the ground motion parameter will be exceeded during a particular time period.

3.3 Banda Aceh Probabilistic Seismic Hazard Analysis

A study about Banda Aceh Probabilistic Seismic Hazard Analyis was conducted by Yahya et al (2016). Data used in this study are combination of earthquake catalog from Badan Meteorologi Klimatologi dan Geofisika (BMKG), Engdahl van der hilst and Bulland (EHB) Bulletin, and United States Geological Survey (USGS) from 1907 to 2014 with a maximum depth 300 km by 700 km radius of the outermost point of the study area, the earthquake data plot was shown in Figure 3.3 below.

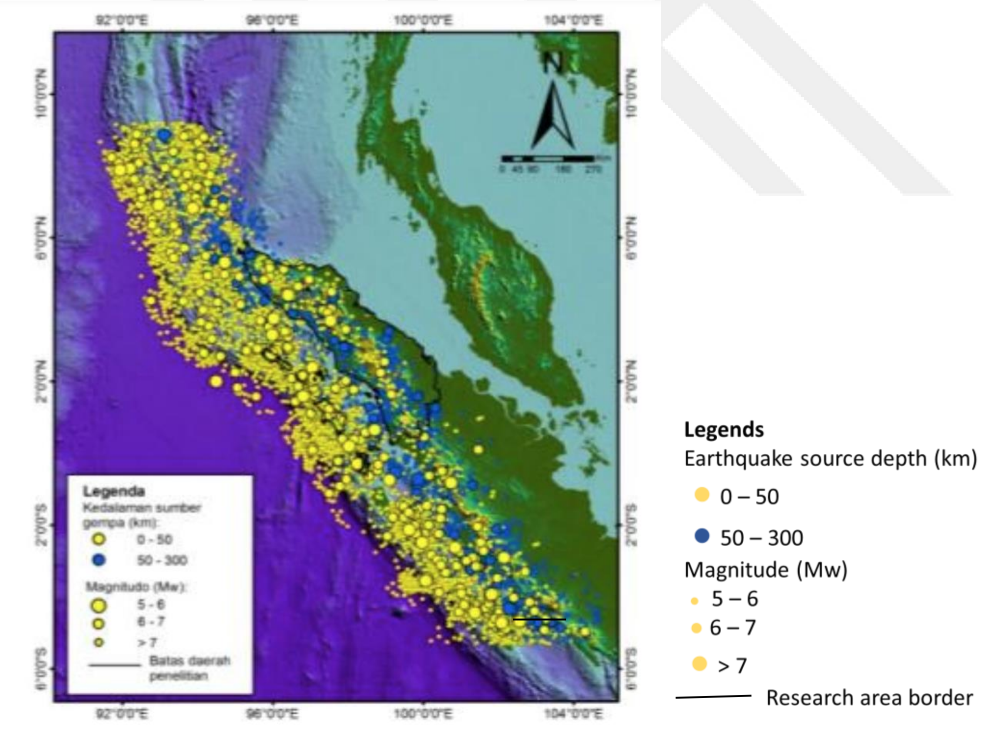

Figure 3.3 : Map of seismicity around Sumatra from compiling catalogues (Source: A Yahya et al, 2016).

In addition the data used focal mechanism of the International seismilogical Center (ISC). Foreshock and aftershock is removed using a Z-Map with the criteria Gardner and Knopoff (1974), the software is also used to calculate b-value and rate reccurence mainshock. The subduction zone and shallow crustal are the seismic source models used. The seismotectonic conditions, local geology, and spatial data are used for basis of the characterization model. Seismic source and shallow earthquake data were modeled after ISC focal mechanism. Meanwhile, for the area that is not incorporated with focal mechanism, the normal-slip mechanism is assumed to weight at 0.2, the reverse-slip mechanism at 0.4, and the strike-slip mechanism at 0.4. The model shallow earthquake is shown in Figure 3.4 below. The fault mechanism used in the study was shown in Figure 3.5.

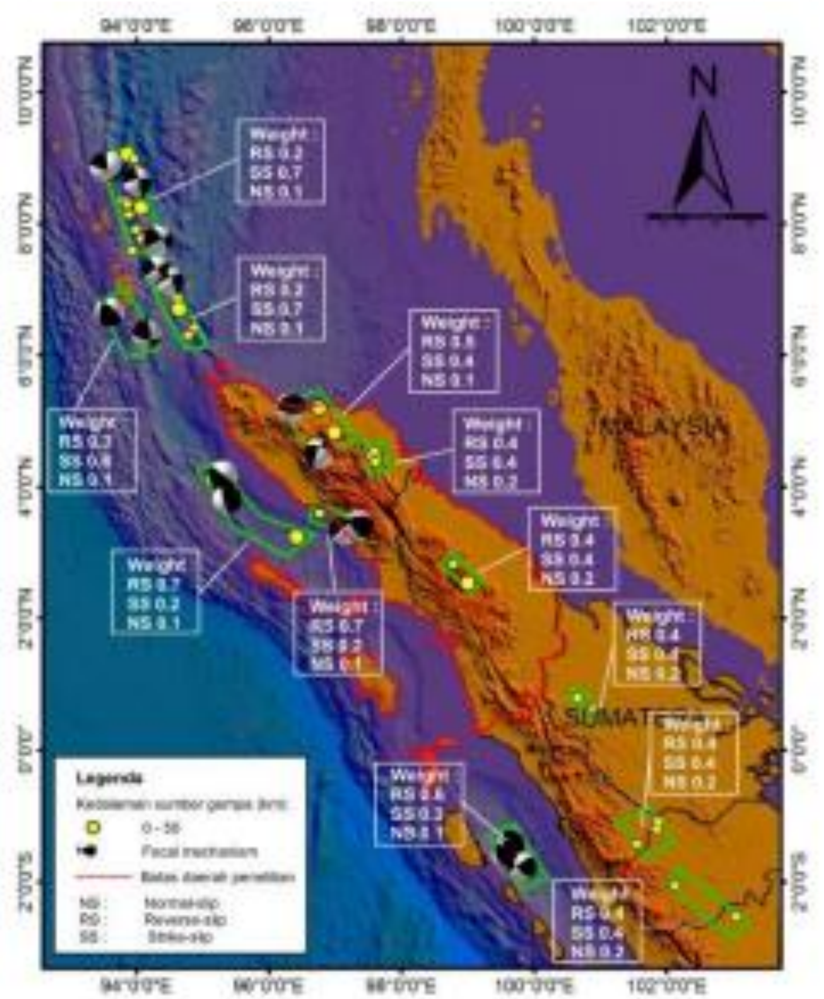

Figure 3.4 : Map of model shallow earthquke for Sumatra from Island (Source: A Yahya et al, 2016).

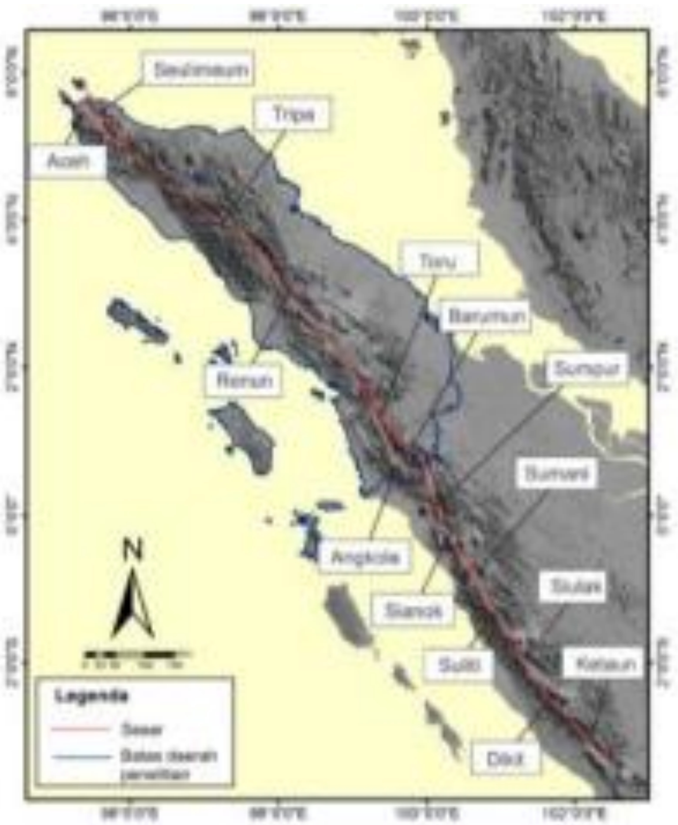

Figure 3.5 : Map of fault mechanism used for PSHA study (Source: A Yahya et al, 2016).

A Yahya et al (2016) stated that there are no specific attenuation function for Indonesia region, attenuation function derived for other regions and worldwide was used. Table 3.1 below explained the function attenuation used in the Banda Aceh hazard analysis.

Table 3.1 : Function attenuation for Banda Aceh hazard analysis (A Yahya et al, 2016).

Earthquake Source	**Attenuation Function**
Megathrust	Youngs et al (1997)
	Zhao et al (2006)
	Atkinson-Boore, Worldwide (2003)
Benioff	Atkinson-Boore, Worldwide (2003)
	Atkinson-Boore, Cascadia (2003)
	Youngs et al (1997)
Faults and shallow background	Campbell-Bozorgnia, NGA (2008)
	Boore-Atkinson, NGA (2008)
	Chiou-Youngs, NGA (2008)

A computer software called EZ-Frisk used to perform the seismic hazard on Banda Aceh. PGA and SA in the period spectra 0.2 and 1 second was obtained. PSHA was carried out on the layer of bedrock with Vs_{30} at 750 m/s. Grid for a 50 km of the fault zone was set to be 0.1^o x 0.1^o and for 0.5^o x 0.5^o for the zone outside from the fault zone. The seismic acceleration from each grid was mapped using ArcGIS 9.3 software. The result obtained from the study was a seismic hazard map for Banda Aceh with 2475 year return period. The hazad map was presented on Figure 3.6 to Figure 3.8.

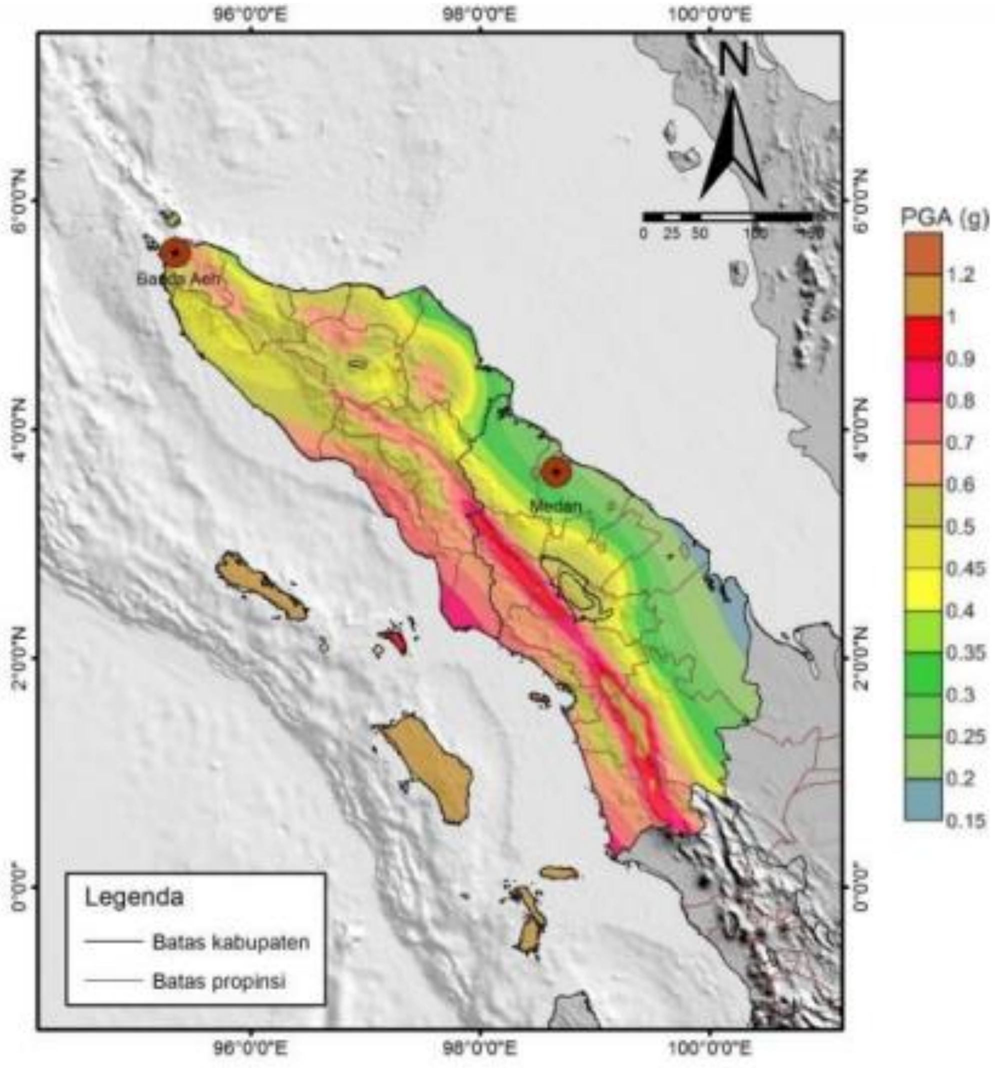

Figure 3.6 : PGA hazard conditions in the bedrock over a period of 2475 years for Banda Aceh and Northern Sumatra region. PGA value was ranged from 0.15g to 1.3g (Source: A Yahya et al, 2016).

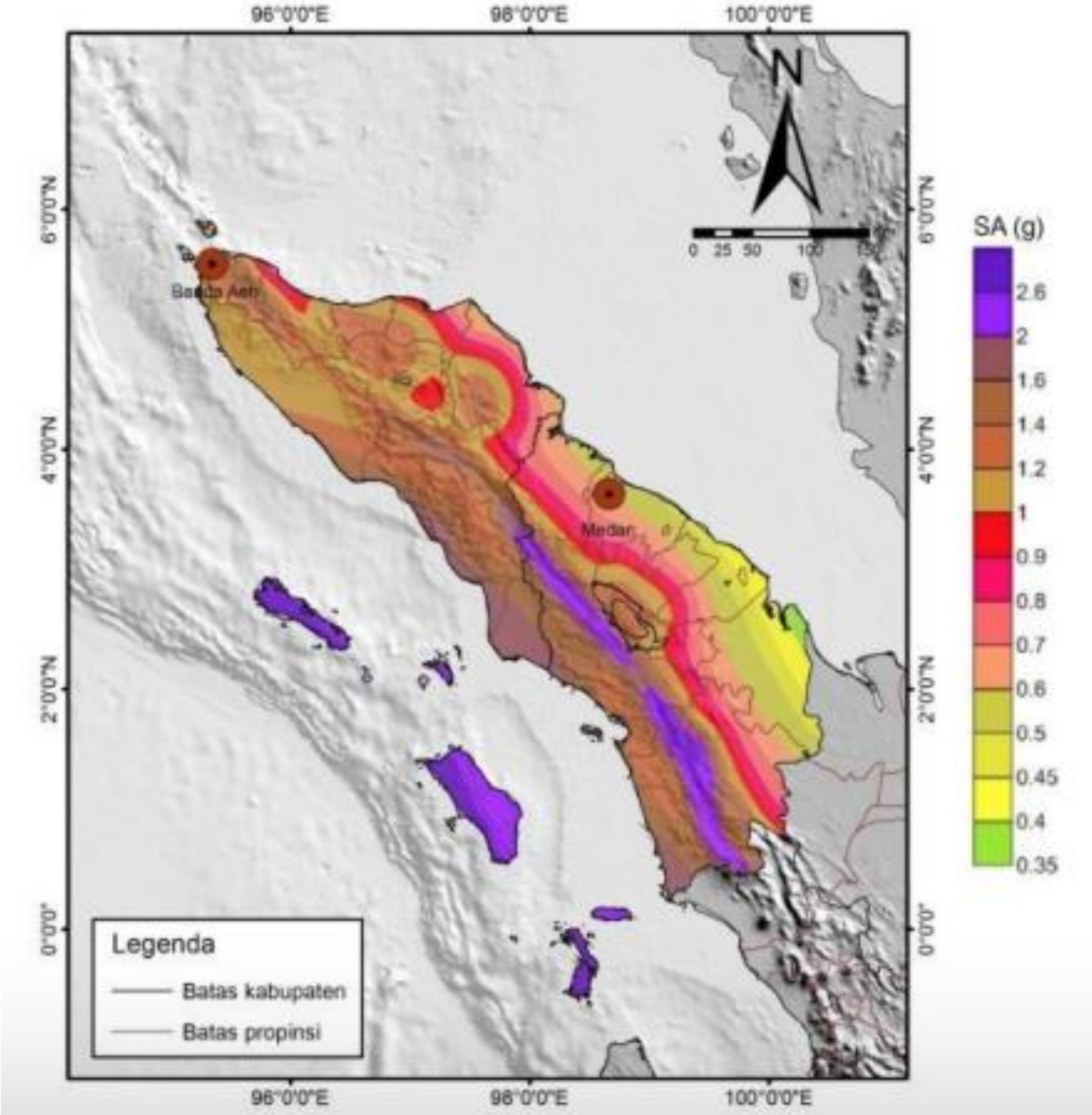

Figure 3.7 : Map of hazard conditions SA 0.2 seconds in the bedrock over a period of 2475 years for Banda Aceh and Northern Sumatra region. SA value was ranged from 0.35g to 2.8g (Source: A Yahya et al, 2016).

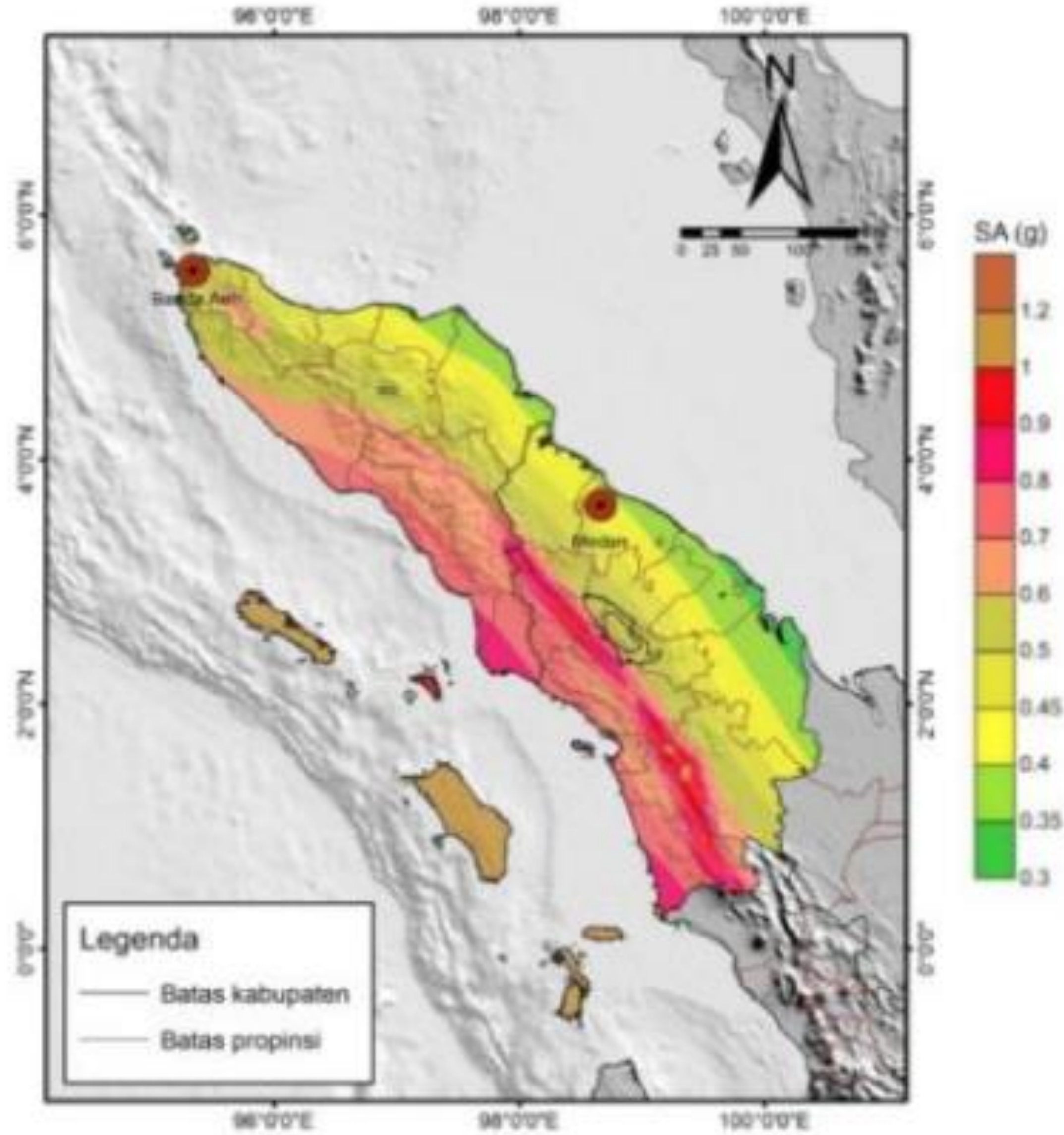

Figure 3.8 : Map of hazard conditions SA 1 seconds in the bedrock over a period of 2475 years for Banda Aceh and Northern Sumatra region. SA value was ranged from 0.30g to 1.30g (Source: A Yahya et al, 2016).

Hazard curve for Banda Aceh area was presented in Figure 3.9 to Figure 3.11 below. According to the hazard curves obtained for Banda Aceh, the most prevalent source or the earthquake fault segments are megathrust in Aceh and Andamant segment as both provide higher hazard than other seismic sources.

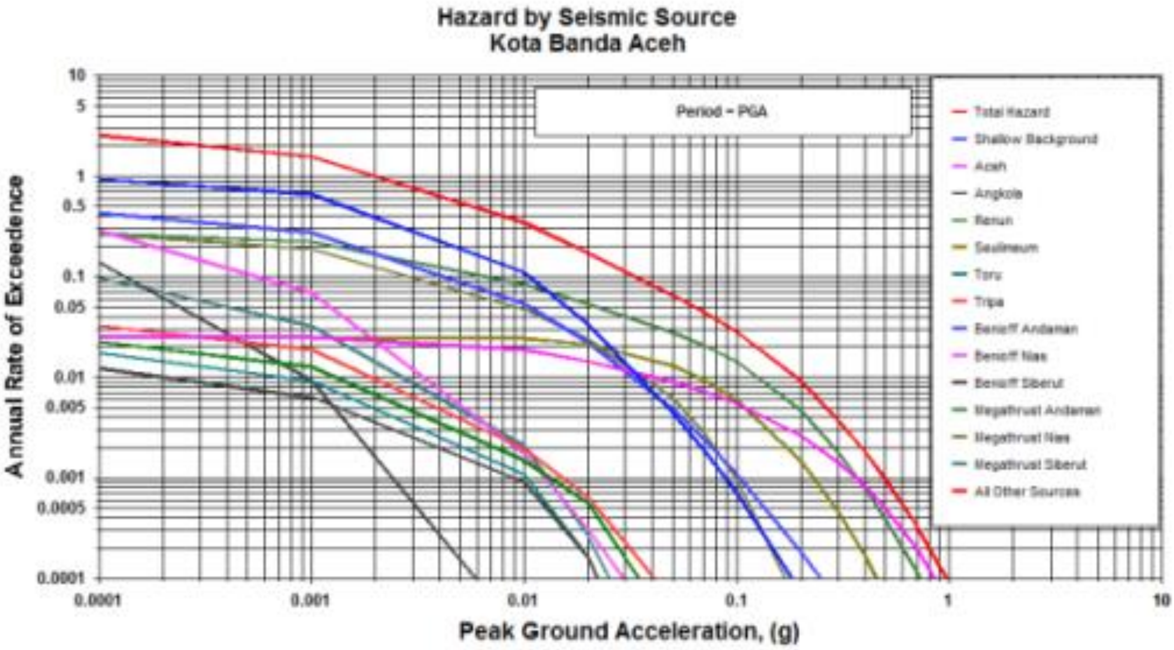

Figure 3. 9 : Curve hazard conditions in the bedrock PGA Banda Aceh (Source: A Yahya et al, 2016).

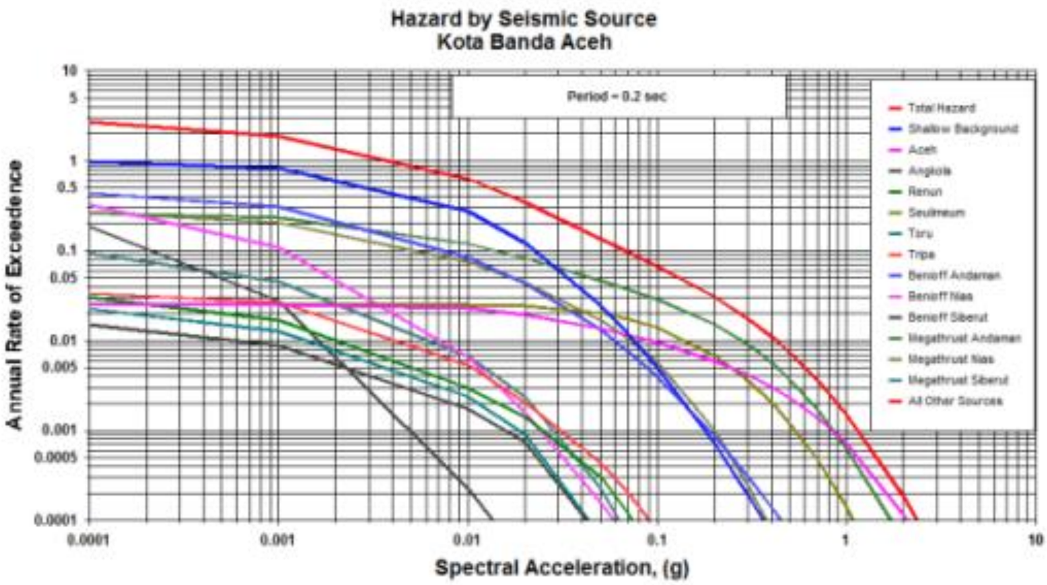

Figure 3. 10 : Curve SA 0.2 seconds hazard conditions in the bedrock Banda Aceh (Source: A Yahya et al, 2016).

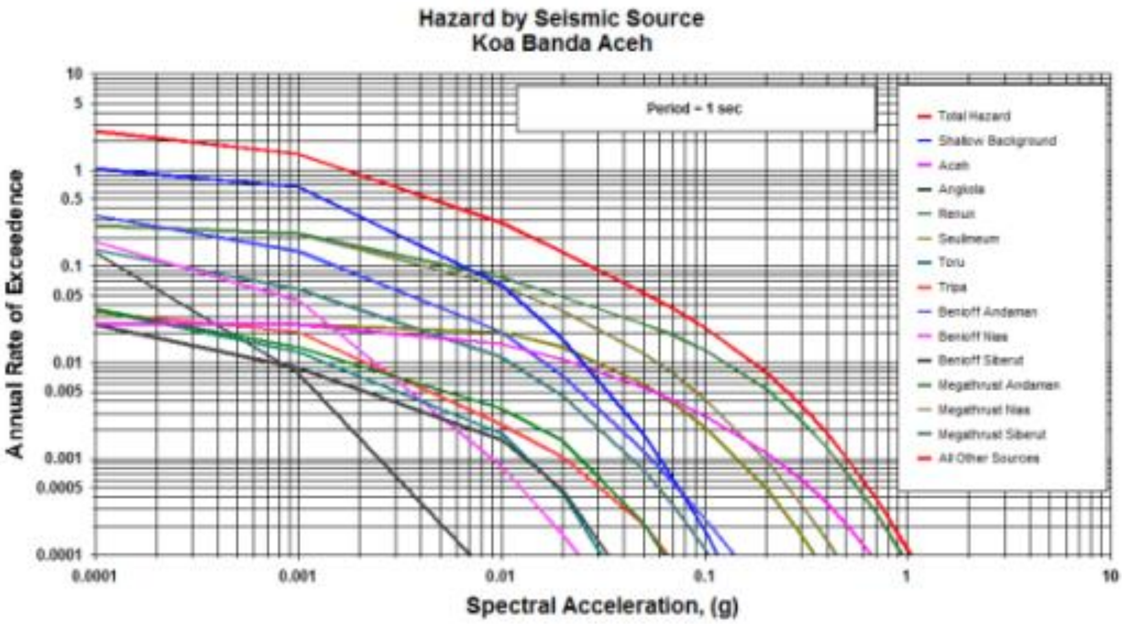

Figure 3. 11 : Curve SA 1 seconds hazard conditions in the bedrock Banda Aceh (Source: A Yahya et al, 2016).

4. DEVELOPMENT OF UNIFORM HAZARD GROUND MOTION RESPONSE SPECTRA

Site response analysis is one of the derivatives from earthquake hazard, that is ground motion hazard. Site response is a prediction of how a soil deposit would respond due to earthquake excitation, see Figure 4.1. Seismic waves are amplified or damped when they travel from the source of earthquake into rocks or soils (Kramer, 1996).

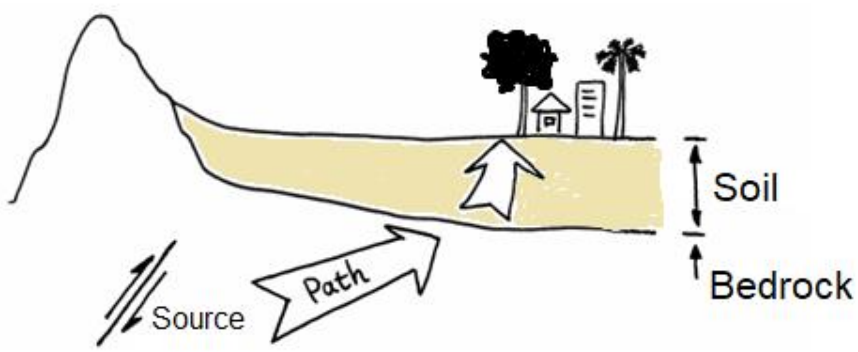

Figure 4.1 : Illustration of site response analysis (Kramer, 1996).

4.1 Earthquake Input Ground Motion

Input motion is the earthquake record obtained in strong ground motion stations. For ensuring the appropriate representation of ground motion intensity for Banda Aceh earthquake motions representing the seismicity of the region must be selected.

4.1.1 Sumatra-Andaman earthquake

Sumatra-Andaman is by far the most devastating seismic event that ever happened in Indonesia. According to the report written by Fehr et al., (2004) indicated that the earthquake caused 174,500 grievous losses of life, 51,500 people went missing and roughly 1.5 million people were displaced in Indonesia, Malaysia, Thailand, India, Myanmar, Sri Langka, Maldives and some little part of the coastal area of Africa.

4.1.2 Characteristics of the earthquake

Andaman Earthquake occurs on a boxing day, December 26, 2004 at 00:58:53 UTC or 07.53 a.m. by local time. The earthquake epicentered on 3.295°N 95.982°E (approximately 250 km south-southeast of Banda Aceh). The moment magnitude reported was varied between M9.0 to M9.3. Location for 2004 Sumatra-Andaman Earthquake is shown in figure 4.2.

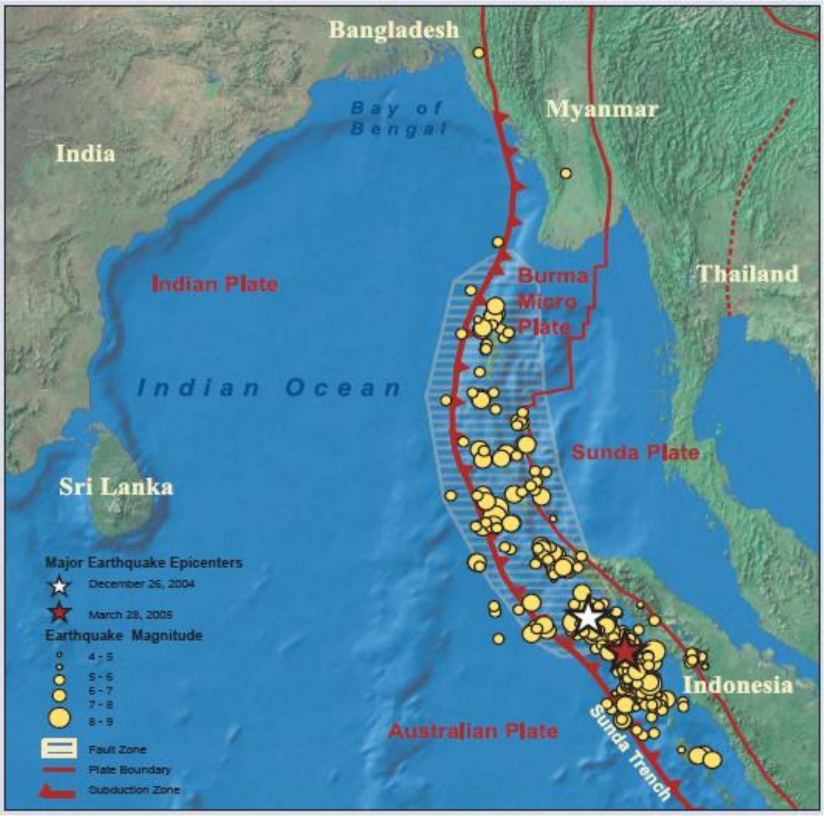

Figure 4.2 : Map of the epicenter, aftershocks, and area of the major fault rupture for the Sumatra-Andaman Earthquake (Fehr et al., 2004).

The map above indicate that earthquake occured on the east of Sunda trench, located in between of Autralian plate and Sunda plate. The earthquake took place on a subduction and fault zone at a depth of 30.0 km.

4.1.3 Fault surface rupture

According to Tanioka et al., (2006) the mechanism of Sumatra-Andaman earthquake on 26 December 2004 was thrust type faulting (strike = 329◦, dip = 8◦, rake = 110◦). The fault rupture spreaded toward the north-northwest direction at a velocity of about 2.5 km/s, expanded 1200 to 1300 km through the Andaman sea.

Tanioka et al. (2006) as quoted from Park et al (2005) stated that seismic moment of the earthquake was 6.5×10^{22} Nm (Mw 9.15) with rupture duration lasted up to 600 seconds.

4.1.4 Earthquake effects on Banda Aceh

Because the limited digitalized and recorded earthquake acceleration data, earthquake input motion used in this study was taken from simulated one produced by Sørensen et al in 2007 as shown in Figure 4.3.

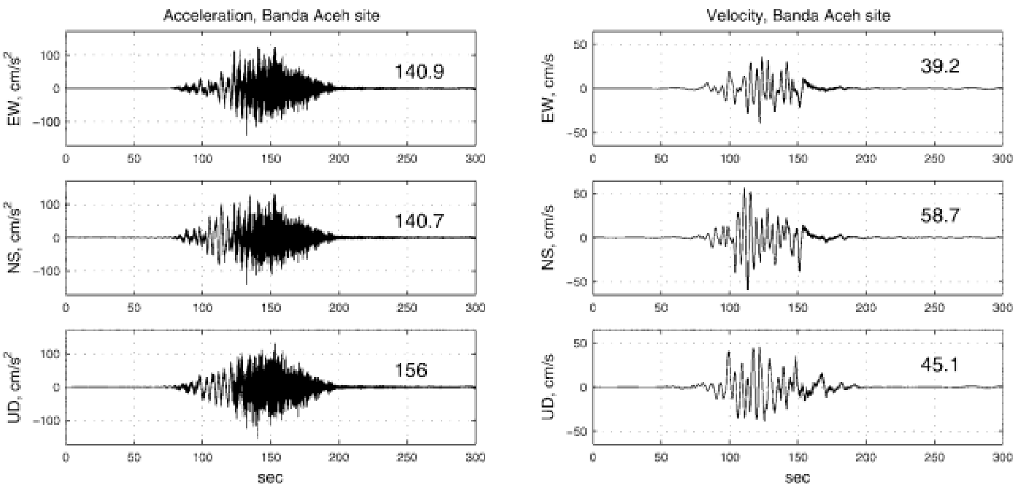

Figure 4.3 : A Simulated acceleration and velocity waveforms for Banda Aceh for 2004 Sumatra-Andaman earthquake proposed by Sørensen et al. (2007).

4.2 Site Characterization of Banda Aceh

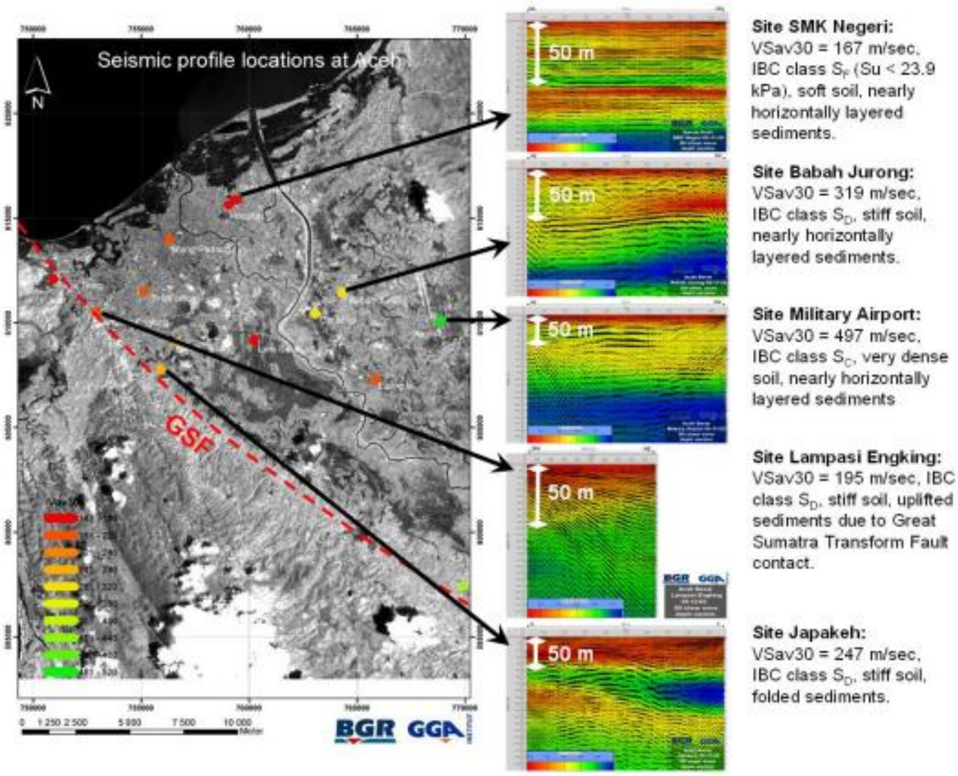

Figure 4.4 : Banda Aceh and nearby area shear wave velocity (Polom et al., 2008).

For this study, 3 sites from Banda Aceh were selected for analyses. Figure 4.4 give an overview on shear wave velocity condition in Banda Aceh. Due to the lack of shear wave velocity (V_S) profile measurements, for CPT data, Vs was calculated using a method proposed by Mayne and Rix (1995).

$$Vs = 1.75\ qc^{0.627} \tag{4.1}$$

Meanwhile SPT data, V_S profiles ware calculated using the correlation between SPT and V_S proposed by Marto et al. (2013) was used to determine the VS profiles. This correlation expressed as:

$$Vs = 77.13\ N^{0.377} \tag{4.2}$$

4.3 Soil Dynamic Properties

In an elastic homogenous soil mass, three types of seismic waves travel at different steps. These are P waves, S waves and Rayleigh waves. The velocity of rayleigh wave is less than shear wave (Kramer, 1996). The relationship between P wave and S wave is defined as

$$Vs \leq 707 \leq Vp \; 0 \leq 0. \tag{4.3}$$

Shear wave velocity data can be obtained from field tests or by using empirical correlations. Survey on site response analysis pointed out that most of the researchers used empirical correlations to obtain shear wave velocity (Kramer, 1996). Shear modulus can be obtained by using mass density of soil and shear wave velocity computed by making field measurements.

$$G = \rho \times Vs^2 \tag{4.4}$$

4.4 Methods of One-Dimensional Site Response Analysis

There are three constitutive models defined for site response analysis, linear elastic, equivalent linear and nonlinear. One-dimensional ground response assessments are based on the premise that all boundaries are horizontal and that SH-waves propagating vertically from the underlying bedrock are the primary cause of a soil deposit's response. In the case of one-dimensional, the soil and bedrock surface are supposed to extend indefinitely in ground response analysis in the horizontal plane. A brief description is presented for each method to calculate the response of SDOF systems and to solve the dynamic equilibrium equation defined as (Chopra, 1995; Newmark, 1959):

$$m\ddot{u} + c\dot{u} + ku = -m\ddot{u}_g \tag{4.5}$$

where m, c and k are the mass, the viscous damping and the system stiffness of the SDOF system respectively. $\ddot{u}$, $\dot{u}$ and u are the nodal relative accelerations, relative velocities and relative displacements respectively and $\ddot{u}_g$ is the exciting acceleration at the base of the SDOF.

4.4.1 Linear analysis

The simplest model is the linear elastic model, in which stress is proportional to strain. Linear model used both time-domain and frequency domain in its analysis.

For the ground response analysis, transfer function can be used to express various response parameters, such as displacement, velocity, acceleration, shear stress, and shear strain to an input motion parameter such as bedrock acceleration (Kramer, 1996). When an input motion (time history) is represented as a fourier series, after it multiplied by the transfer function then the output of this calculation is fourier series of the ground surface motion. The transfer function is a key factor to determine how each frequency in the bedrock input motion is amplified or deamplified by the soil deposit.

Transfer function equation for undamped soil can be expressed as follows. The influence of frequency on steady state response for undamped linear elastic layer shown in Figure 4.5 below.

$$F(\omega) = \frac{\text{Amplitude of the motion at surface (x=0)}}{\text{Amplitude of the motion at the base (x=H)}} = \frac{1}{\cos\left(\frac{\Omega H}{V_S}\right)} = \frac{1}{\cos\left(\frac{\pi 4fH}{2\, V_S}\right)} \tag{4.6}$$

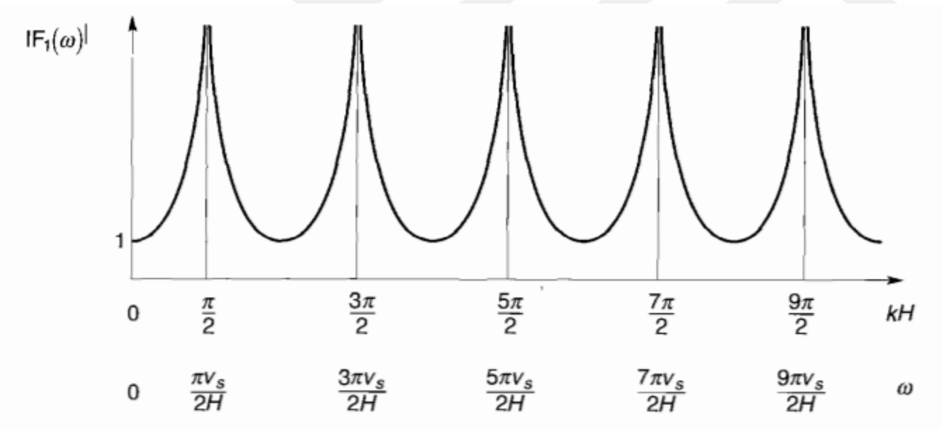

Figure 4.5 : The influence of frequency on steady state response for undamped linear elastic layer (Source: Kramer 1996).

Meanwhile, transfer function for dumped soil and the influence of frequency on steady state response for damped linear elastic layer shown in Figure 4.6 below.

$$F(\omega) = \frac{\text{Amplitude of the motion at surface (x=0)}}{\text{Amplitude of the motion at the base (x=H)}} = \sqrt{\frac{1}{sinh^2\left(\frac{\Omega H}{V_S} tan\frac{\delta}{2}\right) + \cos^2\left(\frac{\Omega H}{V_S}\right)}} \tag{4.8}$$

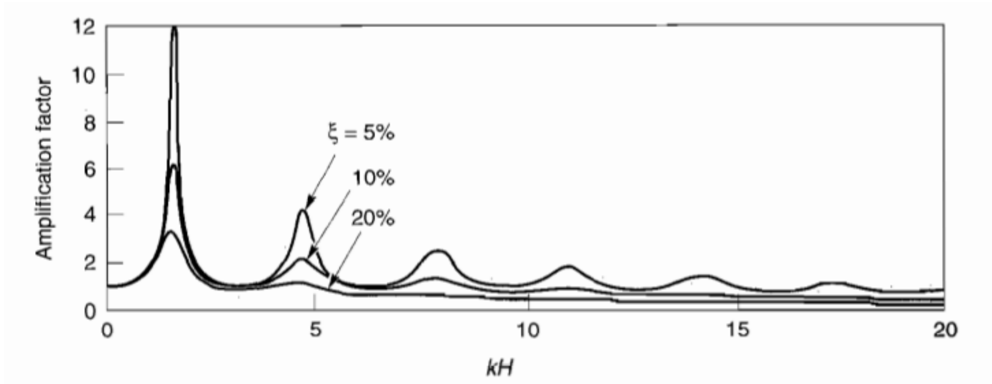

Figure 4.6 : The influence of frequency on steady state response for damped linear elastic layer (Source: Kramer 1996).

Fundamental frequency of soil profile:

$$\omega_0 = \frac{\pi V_s}{2H} = \frac{2\pi}{T_s} \tag{4.9}$$

Fundamental period of soil:

$$T_s = \frac{4H}{V_s} = \frac{4H^2}{\sum_{i=1}^{n}(h_i.V_{s,i})} \tag{4.10}$$

Linear approach is simple and fast to use, because the derived transfer function used in equation produced direct solution from input motion to output motion. However, because of the linear analysis' assumption of the dynamics properties like Vs, G and ξ do not change with strain. The stress-strain relationship in reality is technically nonlinear, the linear elastic model is not suitable for actual field practices.

4.4.2 Equivalent linear analysis

The equivalent linear method was first introduced by a computer software SHAKE, this model uses an iterative approach to choose the shear modulus and damping ratio soil parameters. Discrete points or the soil parameters that constitute the backbone curve of one of the nonlinear models can be used to define these attributes. The option of defining the soil curves using discrete points is only applicable for the equivalent linear analysis. For this option, the G/Gmax and damping ratio (%) are defined as functions of shear strain (%).

Figure 4.7 below shown both of harmonic and transient shear strain time histories with the same peak cyclic shear strain. Although their peak values are equal, the harmonic record depicts a more severe loading state than the transient record. As a result, it's typical to describe the transient record's strain level in terms of an effective shear strain, which has been empirically determined to range between 50 and 70% of the maximum shear strain. However, the computed response is unaffected by this proportion, and the effective shear strain is frequently assumed to be 65 percent of the peak strain. Because the computed strain level is dependent on the equivalent linear property values, an iterative method is required to guarantee that the properties utilized in the study are compatible with the calculated strain levels in all layers.

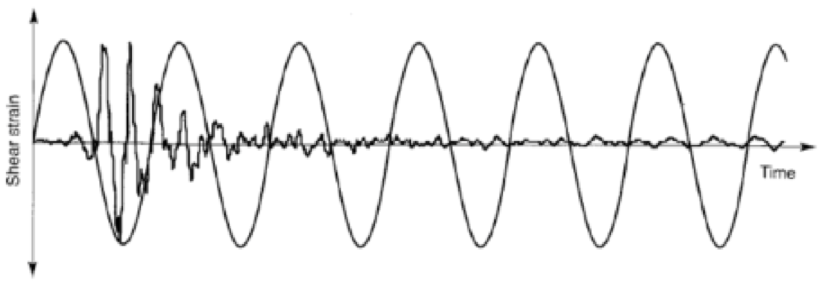

Figure 4.7 : Two shear strain time histories with identical peak shear strains. For the transient motion of an actual earthquake, the effective shear strain is usually taken as 65% of the peak strain (Source: Kramer, 1996).

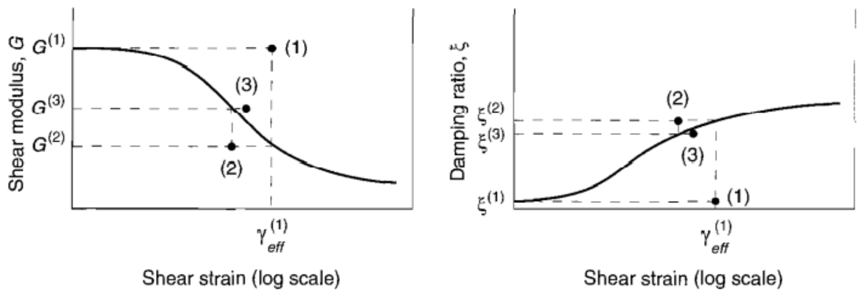

Figure 4.8 : Iteration toward strain-compatible shear modulus and damping ratio in equivalent linear analysis (Source: Kramer, 1996).

Figure 4.8 above shown an illustration on how equivalent linear procedures is done. In order to performed equivalent linear analysis, there are some steps that needed to be followed. First, just like any others iteration procedures, initial value of G and ξ should be guessed. After that, linear site response analysis for a layered system is performed to obtained shear strain time histories for every layer. Second steps are value of maximum strain, γ_{max} for each layer should be identified. For the third steps, the effective shear strain, γ_{eff} for each layer is computed using formula as follows:

$$\gamma_{eff} = R_{\gamma}(\gamma_{max}) \tag{4.11}$$

R_{γ} is the ratio of the effective shear strain to maximum shear strain. Its values depend on earthquake magnitude and can be estimated using equation proposed by Idriss and Sun (1992) as follows.

$$R_{\gamma} = \frac{M-1}{10} \tag{4.12}$$

For the fourth steps, the new estimated equivalent linear values, $G^{(i+1)}$ and $\xi^{(i+1)}$ are choosen for the next iteration. The second steps of iteration need to be repeated until at some point of tolerance is acceptable (Kramer, 1996).

4.4.3 Nonlinear analysis

Nonlinear is a time domain based calculation. Different aspects, such as updated stress-strain relationships and pore-pressure production, are included in the constitutive models. These features, which are not present in the comparable linear model, enable for more precise soil behavior estimations. One of the most important aspect of the nonlinear approach is it constitutive model (load-unload behaviour). Nonlinear models can translate the nonlinearity behavior of soil using various constitutive soil models (Hashash, 2020).

Most of nonlinear method use some modification of Masing criteria. Kramer (1996) explained the loading-unloading rules for the nonlinear method. The first rule is for initial loading, the stress-strain curve follows the backbone curve. The second rule stated that if the stress reversal occurs at a point defined by (γ_r, τ_r), the stress-strain curve follow a path given by:

$$\frac{\tau-\tau_r}{2} = F_{bb}\left(\frac{\gamma-\gamma_r}{2}\right) \quad (4.13)$$

The equation above imply that the unloading and reloading curve have the same shape as the backbone curve (with the origin shifted to the loading reversal point) but is enlarged by factor of 2. These first two rules which describe Masing behavior proposed by Masing (1926). But these two rules are insufficient to describe soil response under general cyclic loading. Other rules that added to nonlinear approach stated that if the unloading or reloading curve exceed the maximum past strain and intersects the backbone curve, it follows the backbone curve until the next stress reversal. If an unloading or reloading curve crosses an unloading or reloading curve from the previous cycle, the stress-strain curve follows that of the previous cycle.

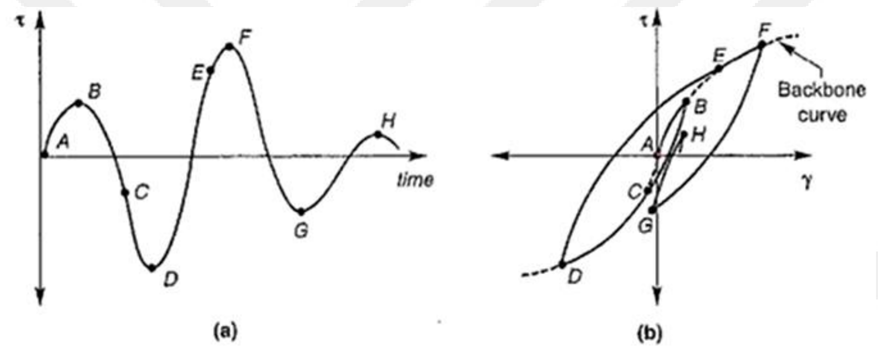

Figure 4.9 : Extended masing criteria for nonlinear method (a) variation with time; (b) resulting stress-strain behavior (backbone criteria indicated by dashed line (Source: Kramer, 1996).

The four rules stated above is called a Extended Masing models. Figure 4.9 shown an example of Extended Masing models.

The procedure of computing the linear site response analysis summarized from Kramer (1996) explained as follows. At the start of each time step, the particle velocity, $\dot{u}_{i,t}$ and total displacement ui,t are known at each layer boundary. Use the particle displacement profile to compute shear strain in each layer. Use the loading-unloading rules to compute the corresponding shear stress in each layer. Increment the time step in the ground motion at the base of model. Working from the bottom to the top, the motion at each layer boundary is calculated. Repeat steps 1 – 5 to evaluate the response for the entire time history.

In this research, DEEPSOIL v7.0 was used to perform equivalent linear and nonlinear 1-D site response analyses, General Quadratic/Hyperbolic Model (GQ/H) model was used. The variables that is required to develope the nonlinear curves for each layer are plasticity index (PI), the coefficient of lateral earth pressure (K_o), over consolidation ratio (OCR), number and frequency of cycles (N) and loading frequency (f). Because of the unavailability of site-specific index properties, PI for the sand and clay was assumed as 0% and 14% respectively, whereas OCR was taken as 1. N and f were set to 10 and 1, respectively.

4.5 Seismic Code for Soil and Earthquake Design

The lastest design codes that regulated the earthquake design and construction in Indonesia are SNI 1726:2019 about Earthquake Resilience Planning Procedures for Building and Non-Building Structures and SNI 2847:2019 about Structural Concrete Requirements for Buildings and Explanations. The lattest earthquake map zonation was updated on 2017. It divided Indonesia into 15 different zones due to the expected ground acceleration values (Figure 4.10).

Figure 4.10 : Indonesian Earthquake Zonation Map (2017).

5. CASE STUDY: EQUIVALENT LINEAR AND NONLINEAR SITE RESPONSE ANALYSIS OF BANDA ACEH

A total of and 3 soil boring samples with Standard Penetration Testing (SPT) profiles were collected from Banda Aceh city. Vs data are not available, so the correlation is made using equation (4.1) and (4.2) for SPT data as stated in Chapter 4.

The results of SPT site investigation are presented in Figure 4.1. They are noted as SPT – 1, SPT– 2 and SPT – 3. Both SPT – 1 and SPT – 2 are done offshore, under sea water level, meanwhile SPT – 3 are done onshore. In general, the soil type from this soil profile are clay and sandy soil.

Figure 5.1 : The location details of the boreholes.

Table 5.1 : Summary of location from soil profile selected for this study.

Case	District	Final Depth (m)	Latitude	Longitude	GWT (m)
SPT-1	Lampulo	20	5°35'10.97"N	95°19'11.01"E	0
SPT-2	Lampulo	20	5°35’06”N	95°19’14”E	0
SPT-3	Pasar Aceh	12	5°33’22”N	95°18’55”E	-0.30

5.1 In-situ Soil Testing

SPT was done with Raymond Split Spoon Sampler with hammer weighteed 63.5 kg, from a specific height 76 cm. Because of limited information N-SPT from this data, the soil profile is then corrected. The information about soil unit weight is given in Table 5.2 and the picture of soil profile was given in Figure 5.2.

Tabel 5.2 : SPT-1 unit weight information.

No.	Depth (m)	N-SPT	γ (kN/m2)
1	2	50	20
2	4	50	20
3	6	50	20
4	8	50	12
5	10	28	16
6	12	25	16
7	14	8	12
8	16	14	12
9	18	19	13
10	20	37	18
11	22	48	18
12	24	50	18

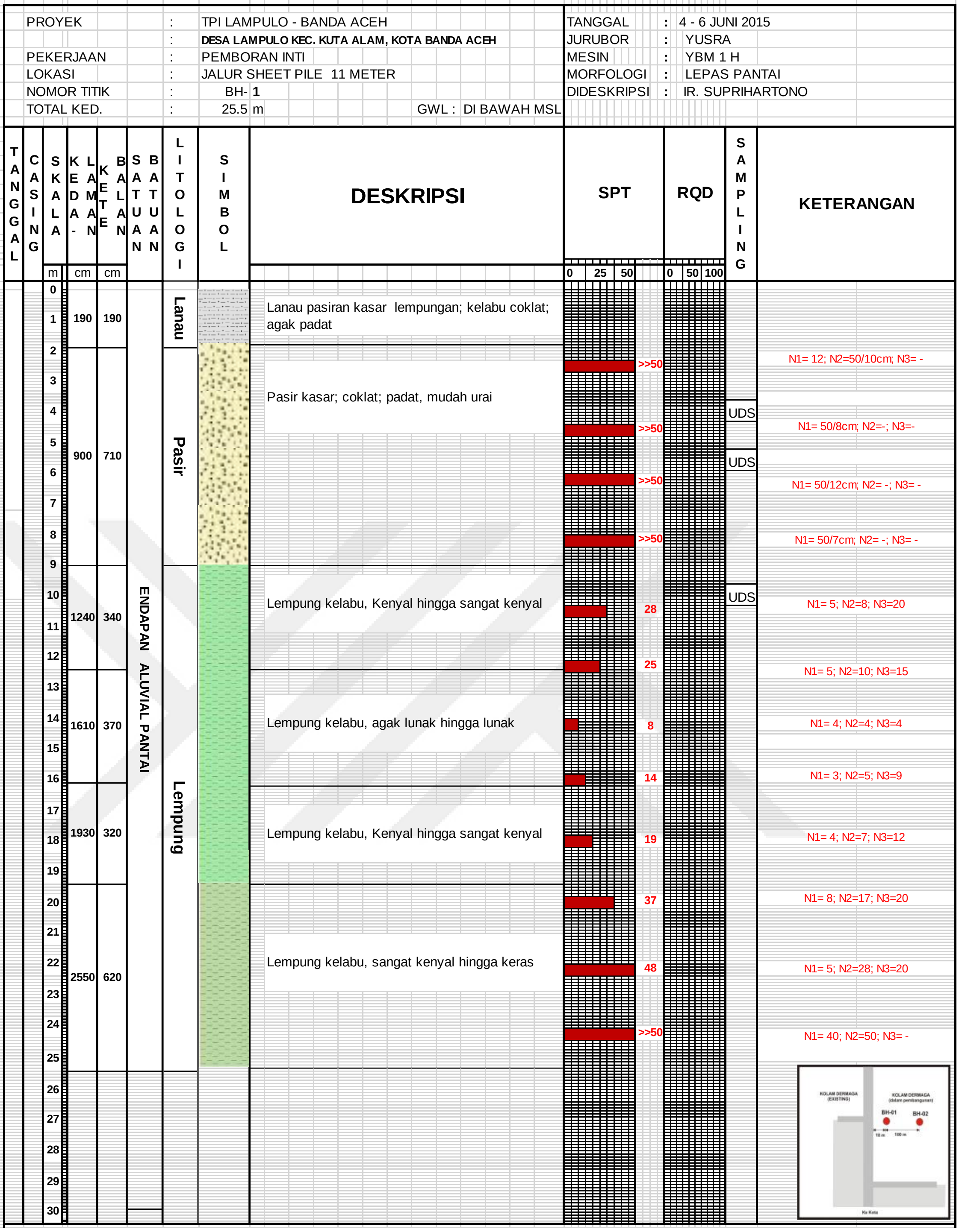

Figure 5.2 : SPT-1 Soil Profile.

The corrected N-SPT was done for this study was done using method suggested by Youd et al (2001) as shown below.

$$(N_1)_{60} = C_N.C_E.C_R.C_B.C_S.N_m \qquad (5.1)$$

Whereas, C_N is a overburden correction factor, C_E is hammer energy ratio correction factor, C_R is rod length correction factor, C_B is borehole diameter correcction factor, C_S is correction factor for using split spoon with room for liners, N_m is the measured SPT blow count. The correction factor is given at Table 5.3. Meanwhile, the corrected N-SPT for SPT-1 was shown in Table 5.4 below.

Table 5.3 : Correction Factor for N-SPT (Youd et al, 2001).

Factor	Equipment Variable	Term	Correction
Overburden Pressure		C_N	for Pa=100 kPa
Energy ratio	Donnut Hammer	C_E	0.5 to 1.0
	Safety Hammer		0.7 to 1.2
	Automatic-Trip Donut Hammer		0.8 to 1.3
Borehole diameter	65 mm to 115 mm	C_B	1.0
	150 mm		1.05
	200 mm		1.15
Rod length	3 m to 4 m	C_R	0.75
	4 m to 6 m		0.85
	6 m to 30 m		0.95
	>30 m		1.0
Sampling method	Standard sampler	C_S	1.0
	Sampler without liners		1.1 to 1.3

Table 5.4 : Corrected N-SPT Values for SPT-1.

Depth (m)	**N-SPT**	**Soil Type**	**Unit Weight (kN/m^3)**	**σ (kPa)**	**σ' (kPa)**	**C_E**	**C_B**	**C_R**	**C_S**	**C_N**	**$(N_1)_{60}$**
2	50	Silt	20	40	20.4	0.75	1	0.8	1	1.70	50.00
4	50	Coarse Sand	18	76	36.8	0.75	1	0.85	1	1.62	50.00
6	50	Coarse Sand	18	112	53.2	0.75	1	0.95	1	1.34	47.91
8	50	Coarse Sand	12	136	57.6	0.75	1	0.95	1	1.29	46.05
10	28	Clay	12	160	62	0.75	1	1	1	1.25	26.16
12	25	Clay	16	192	74.4	0.75	1	1	1	1.14	21.32
14	8	Clay	16	224	86.8	0.75	1	1	1	1.05	6.32
16	14	Clay	12	248	91.2	0.75	1	1	1	1.03	10.79
18	19	Clay	12	272	95.6	0.75	1	1	1	1.00	14.30
20	37	Clay	16	304	108	0.75	1	1	1	0.94	26.20
22	48	Clay	16	336	120.4	0.75	1	1	1	0.89	32.19
24	50	Clay	18	372	136.8	0.75	1	1	1	0.84	31.45

The corrected $(N_1)_{60}$ and shear wave velocity for SPT– 1 are plotted in graph below as shown in Figure 5.3 and Figure 5.4.

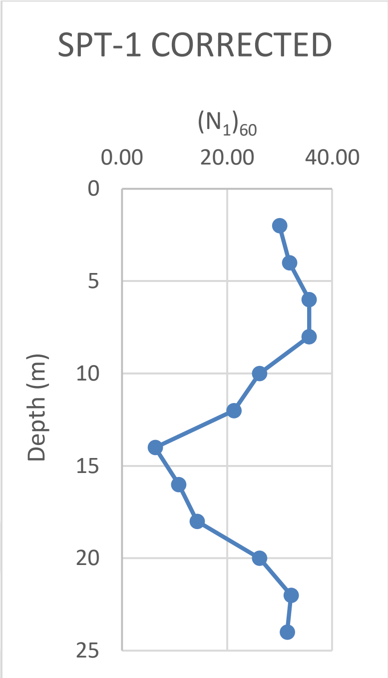

Figure 5.3 : The corrected N Value Graph for SPT-1.

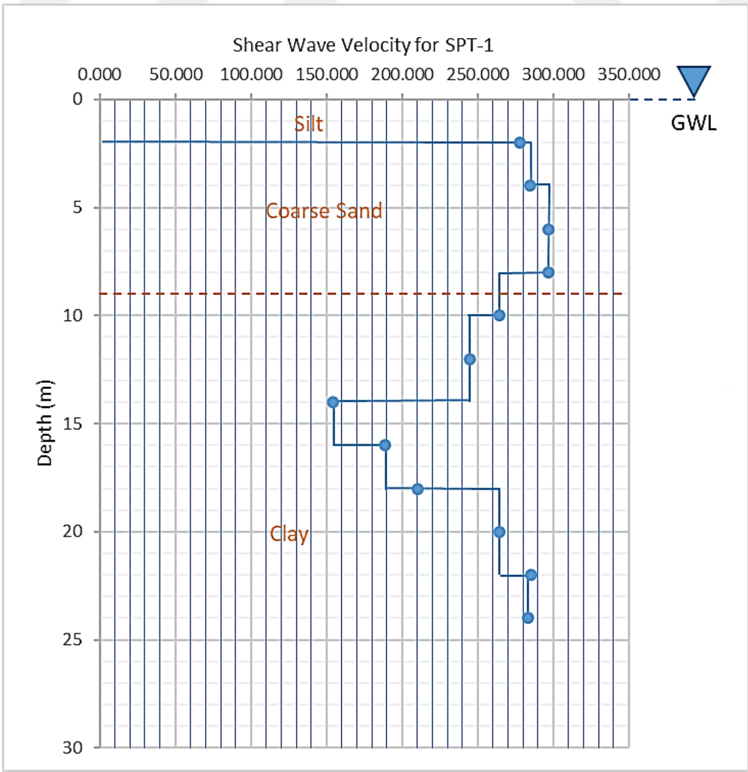

Figure 5.4 : Shear wave velocity for SPT-1.

5.2 Equivalent Linear Analysis Using Deepsoil

The ELA steps done using Deepsoil software will be explained in this section.

Step 1

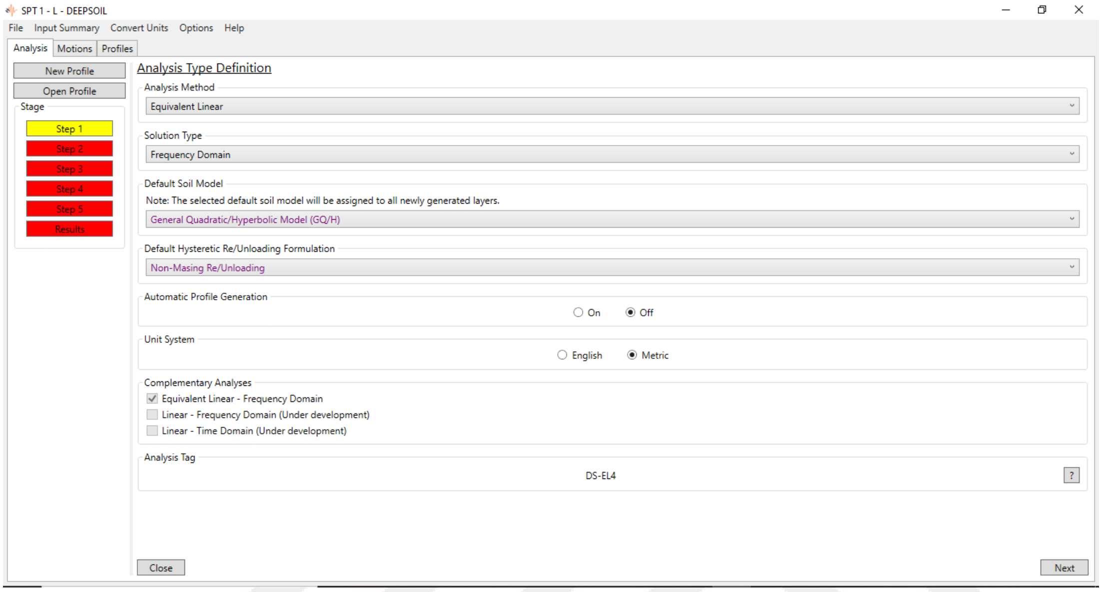

Figure 5.5 : Analysis type definition.

The first step is can be seen in Figure 5.5 above. We determine the definition and type of analysis. Equivalent linear is selected. Solution type selected is frequency domain. General Quadratic/Hyperbolic Model (GQ/H) model was used. Non masing hysteretic loading was selected. Metric unit system is chosen. Another complimentary method was not selected.

Step 2

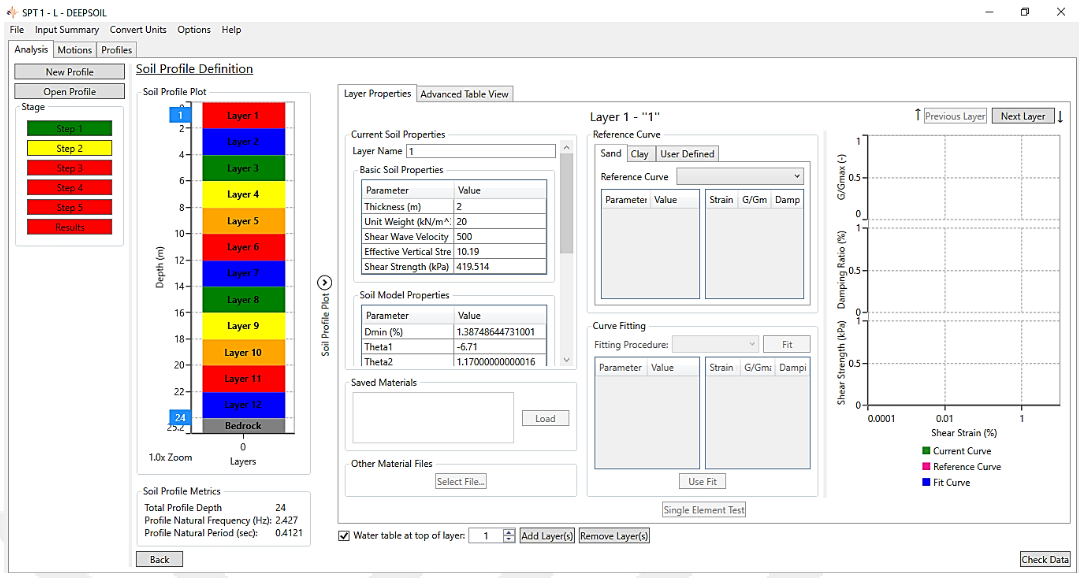

Figure 5.6 : Input soil profile to Deepsoil.

In the next step, soil layer for SPT-1 is inputted. Soil properties was determined. Soil profile can be saved to be used in later time, see Figure 5.6.

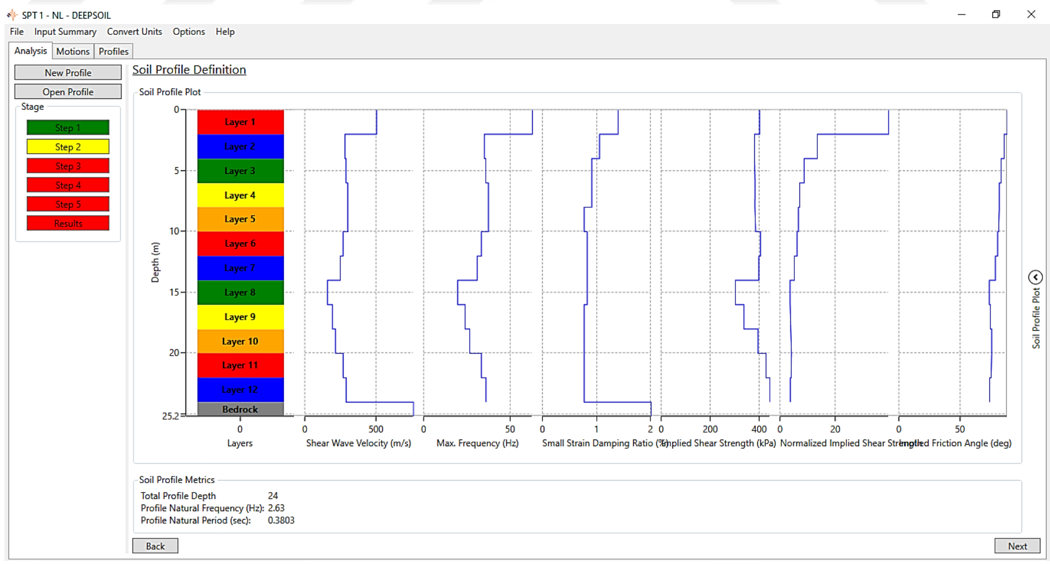

Figure 5.7 : Deepsoil software generating the soil profile definition.

Figure 5.7 shown the soil profile generated from the information inputted. Shear wave velocity, max. frequency, small strain damping ratio, normalized implied shear strength and friction angle was plotted.

Step 3

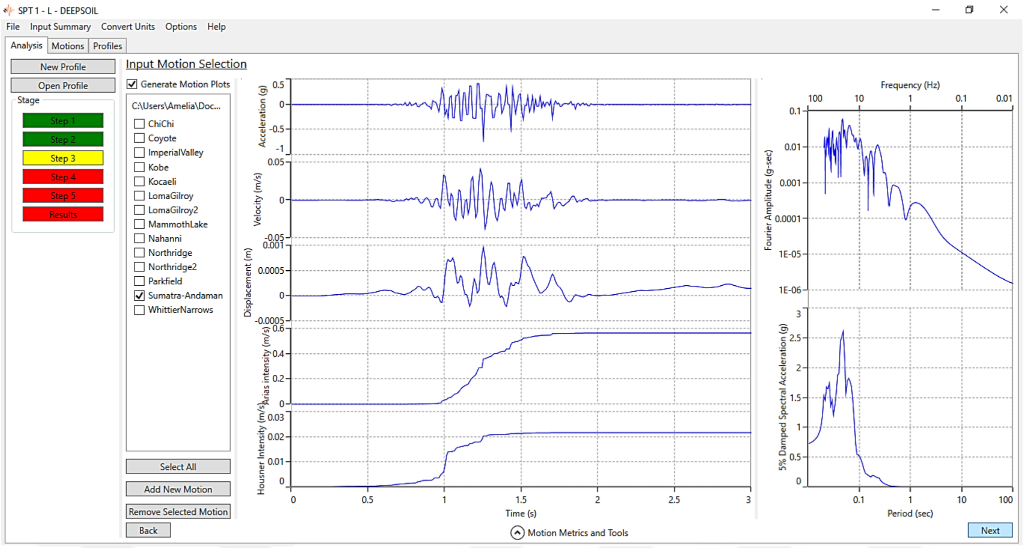

Figure 5.8 : SPT-1 EL earthquake input motion selection.

The next step can be seen in Figure 5.8. Input motion used in this study was 2004 Sumatra-Andaman that was artificially simulated by Soransen (2007).

Step 4

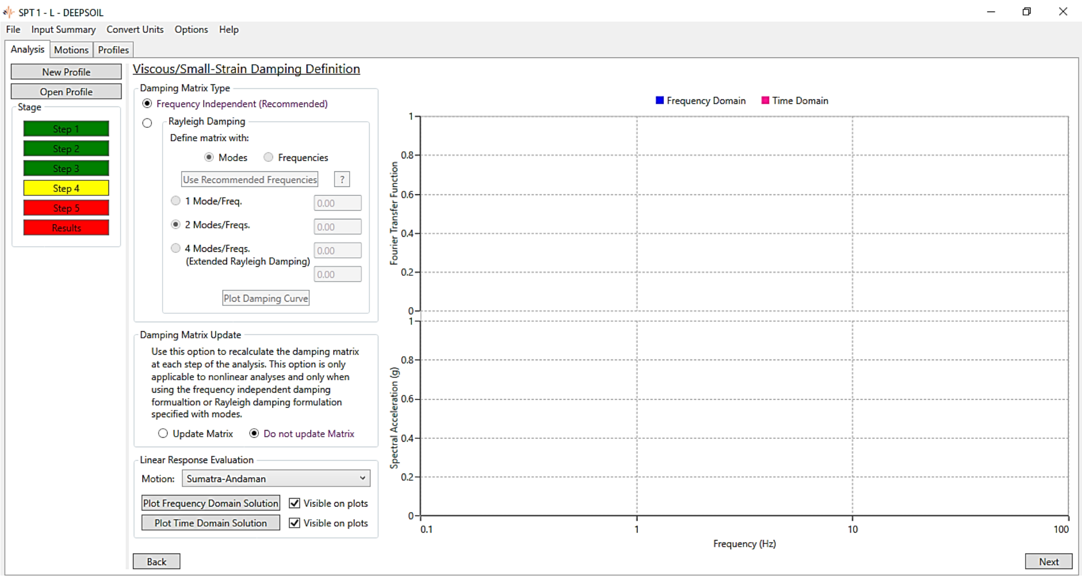

Figure 5.9 : SPT-1 EL viscous/small strain damping definition.

The next step shown in Figure 5.9 was the selection of viscous/small-strain damping definition. Rayleigh model was selected.

Step 5

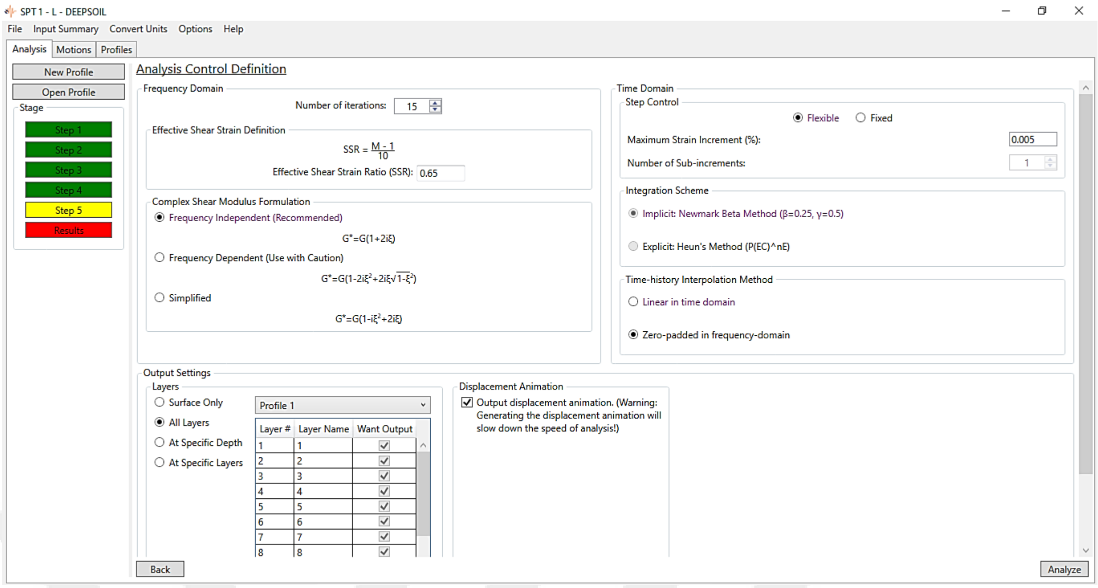

Figure 5.10 : Analysis control definition.

In the last step of ELA, analysis control definition was done. Complex shear modulus formulation selected for this study is Frequency Indepent as it was recommended by Deepsoil (Figure 5.10).

Result

Result from this EL analysis can be seen in Figure 5.11 to Figure 5.17 as follows.

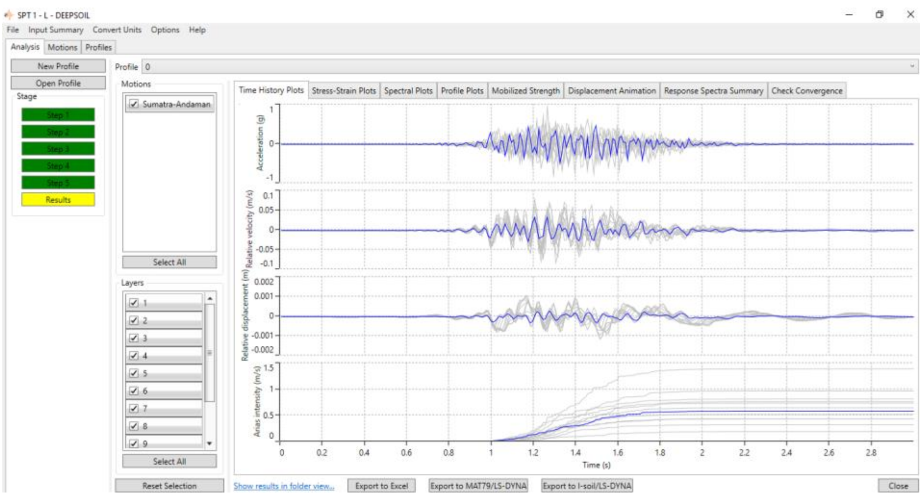

Figure 5.11 : SPT-1 EL time history plot.

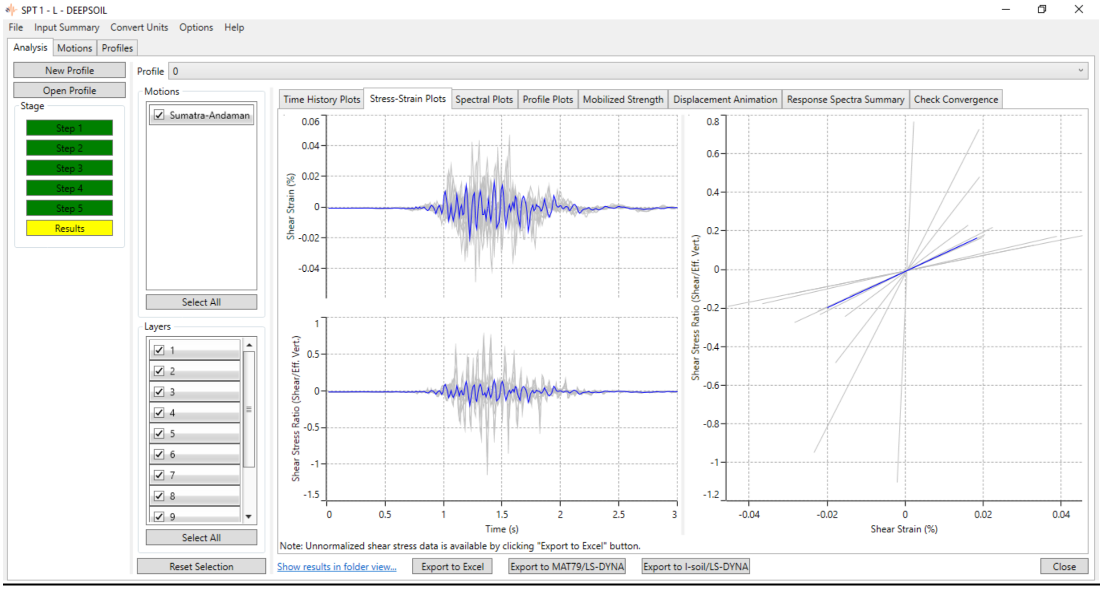

Figure 5.12 : SPT-1 EL stress-strain plot.

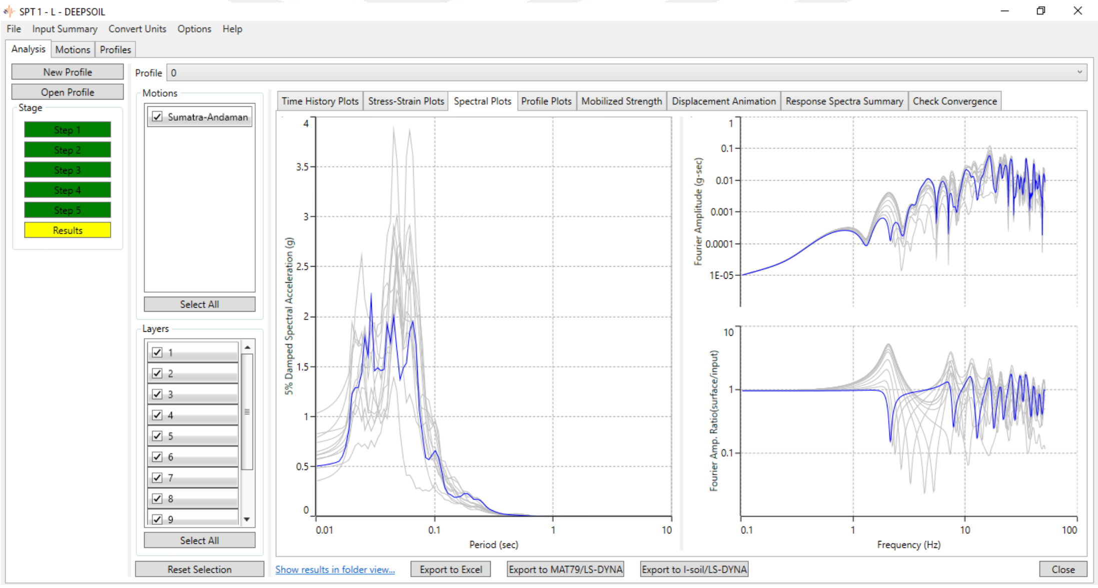

Figure 5.13 : SPT-1 EL spectral plot.

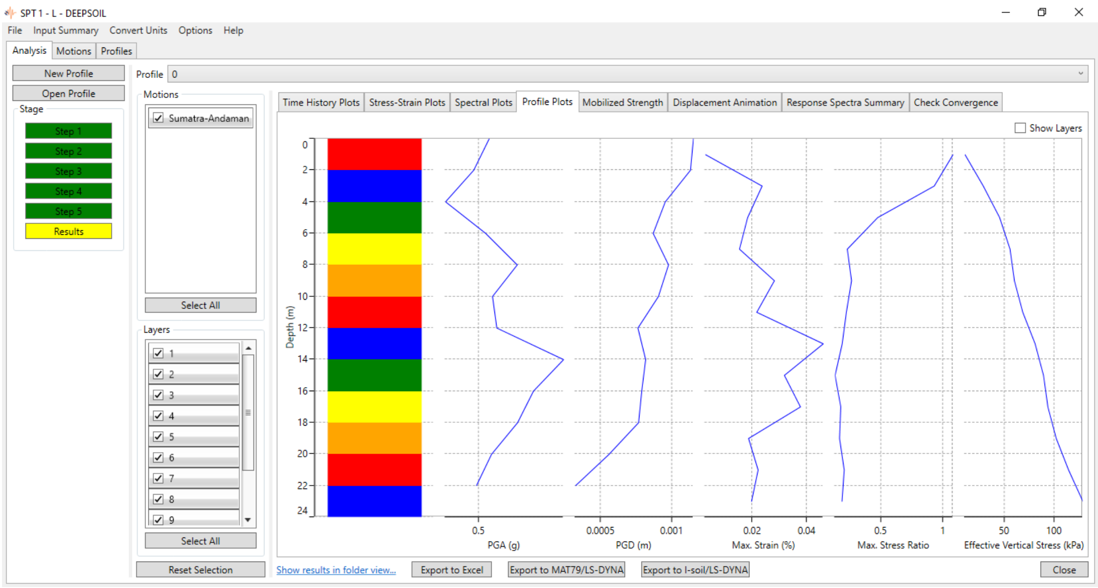

Figure 5.14 : SPT-1 EL profile plot.

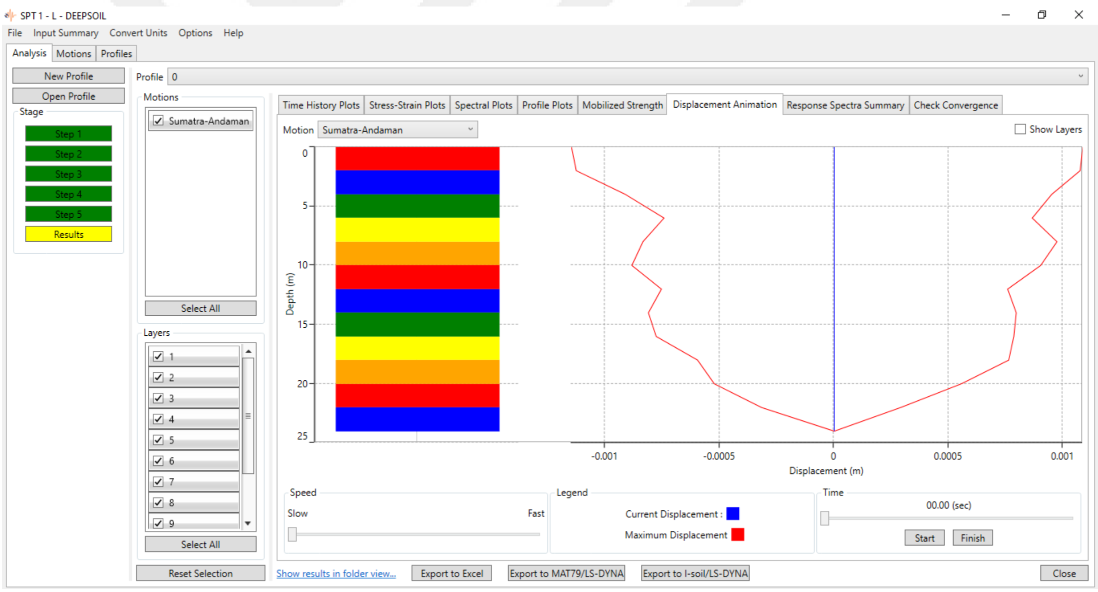

Figure 5.15 : SPT-1 EL displacement plot.

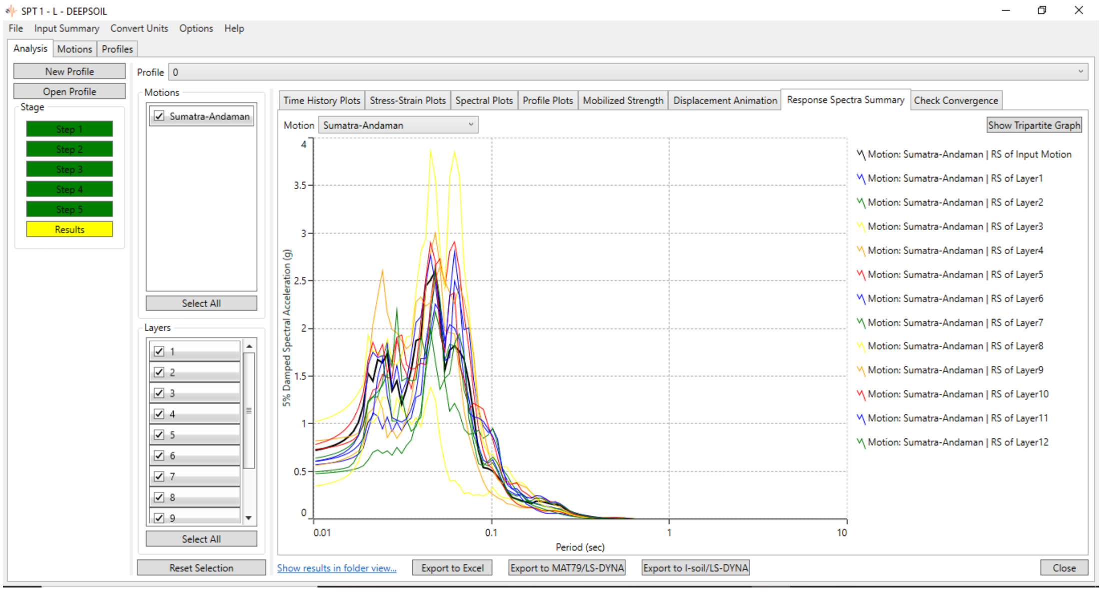

Figure 5.16 : SPT-1 EL response spectra plot.

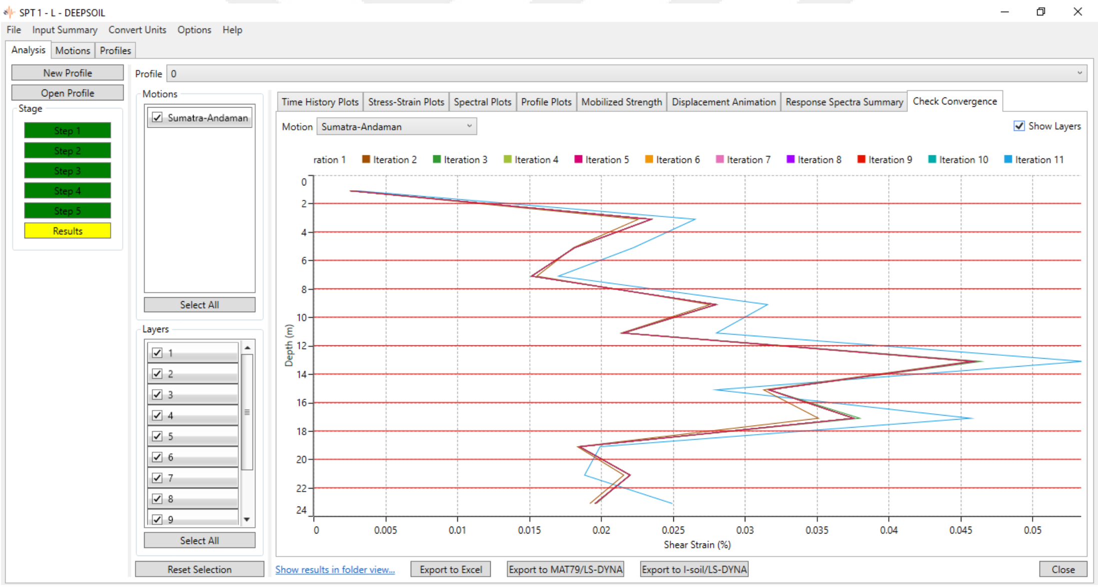

Figure 5.17 : SPT-1 EL check convergence.

5.3 Nonlinear Analysis Using Deepsoil

Step 1

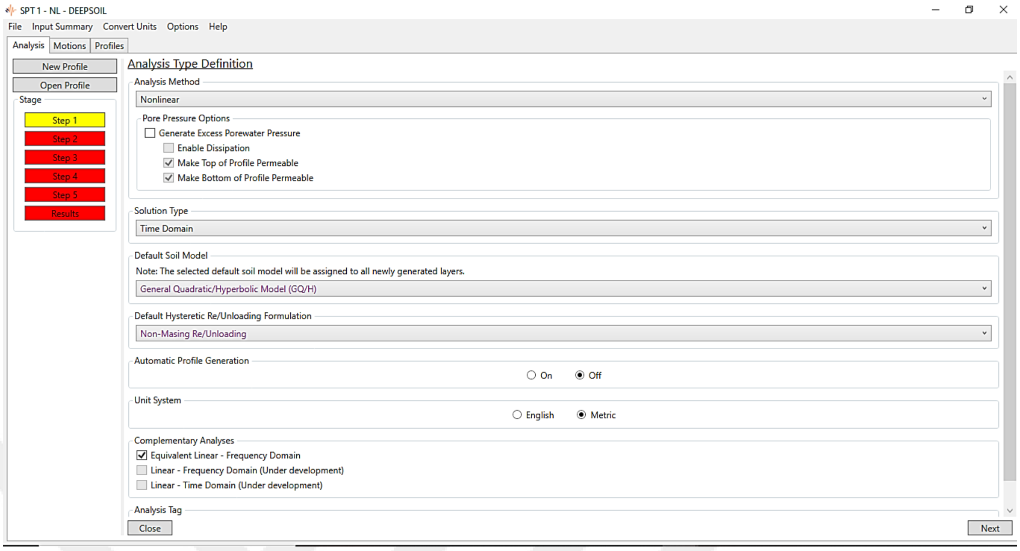

Figure 5.18 : Analysis type definition for NL SPT-1.

The first step is can be seen in Figure 5.18 above. We determine the definition and type of analysis. Nonlinear is selected. Solution type selected is time domain. General Quadratic/Hyperbolic Model (GQ/H) model was used. Masing hysteretic loading was selected. Metric unit system is chosen. Equivalent linear method was selected as nother complimentary method.

Step 2

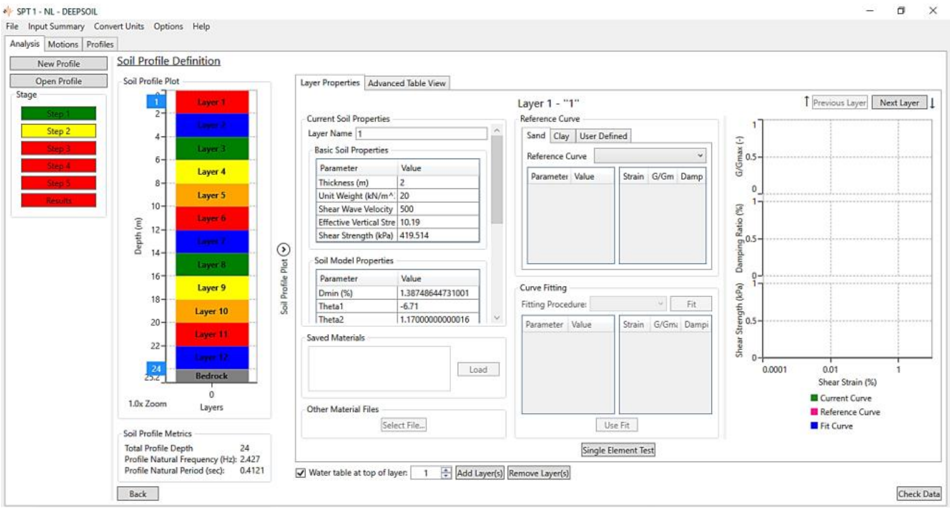

Figure 5.19 : NL SPT-1 input soil profile to Deepsoil.

In the next step for NLA (Figure 5.19) is same with ELA method, soil layer for SPT-1 is inputted. Soil properties was determined.

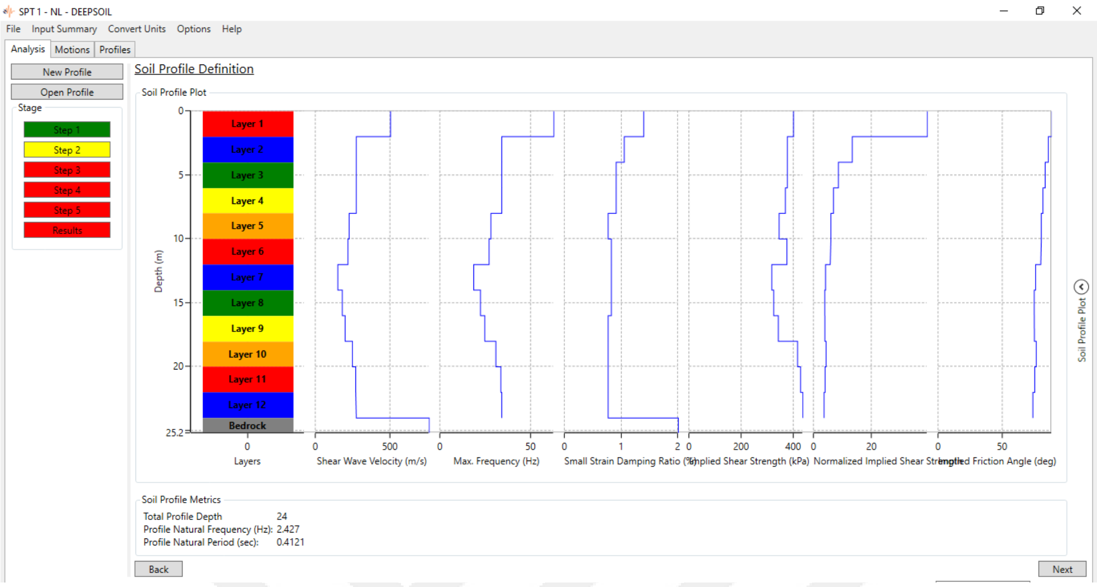

Figure 5.20 : NL SPT-1 Deepsoil software generating the soil profile definition.

The soil profile generated from the information inputted was shown in Figure 5.20. Shear wave velocity, max. frequency, small strain damping ratio, normalized implied shear strength and friction angle was plotted.

Step 3

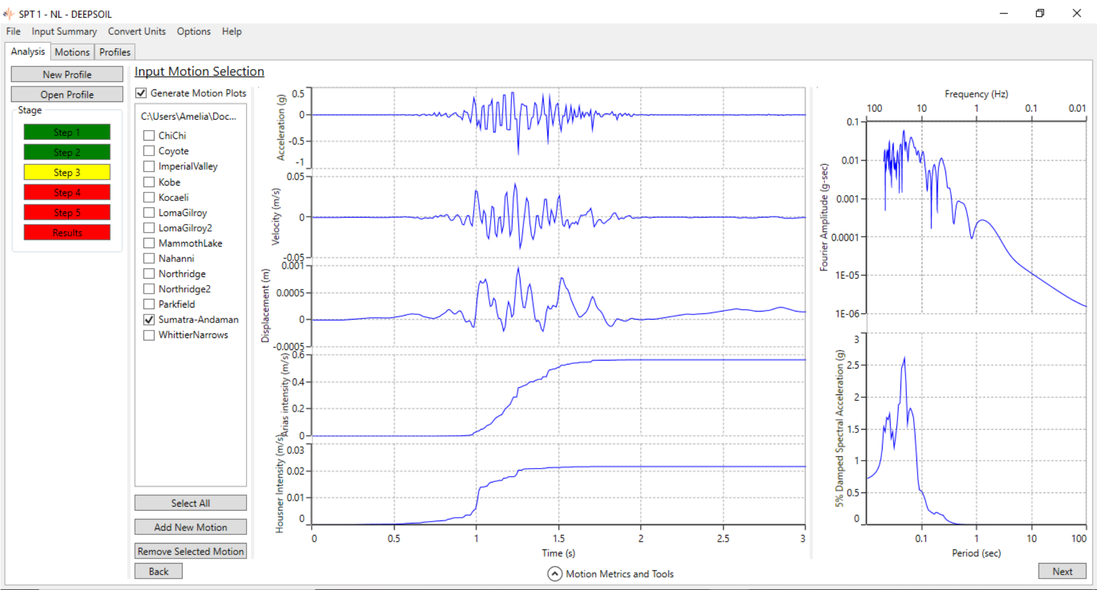

Figure 5.21 : NL SPT-1 input motion selection.

The next step can be seen in Figure 5.21. Input motion used in this study was 2004 Sumatra-Andaman that was artificially simulated by Soransen (2007). Both ELA and NLA method used the same earthquake input motion.

Step 4

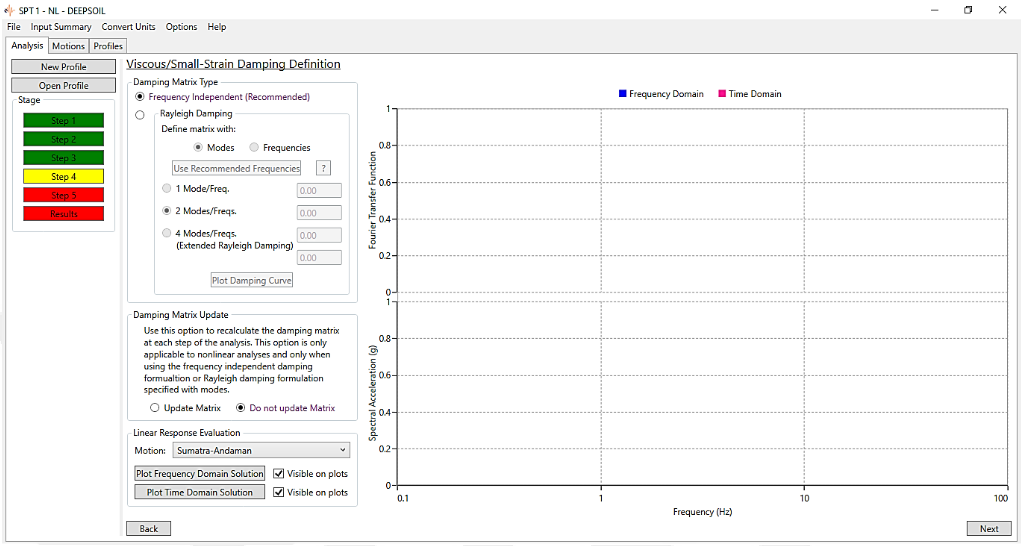

Figure 5.22 : NL SPT-1 viscous/small strain damping definition.

The next step shown in Figure 5.22 was the selection of viscous/small-strain damping definition. Rayleigh model was selected for this study.

Step 5

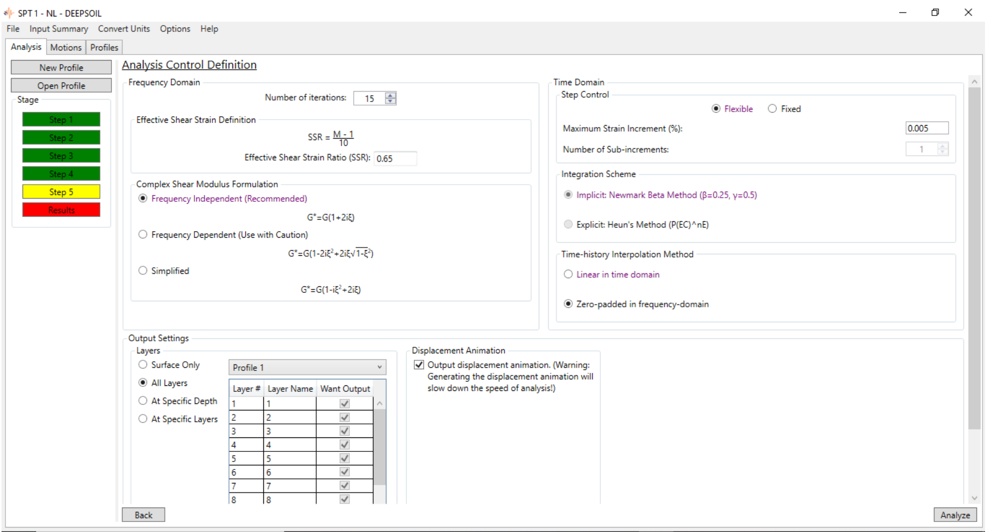

Figure 5.23 : NL SPT-1 analysis control definition.

In the last step of NLA, analysis control definition was done (See Figure 5.23). Complex shear modulus formulation selected for this study is Frequency Indepent as it was recommended by Deepsoil.

Result

The result for NLA method is shown in Figure 5.24 to Figure 5.31

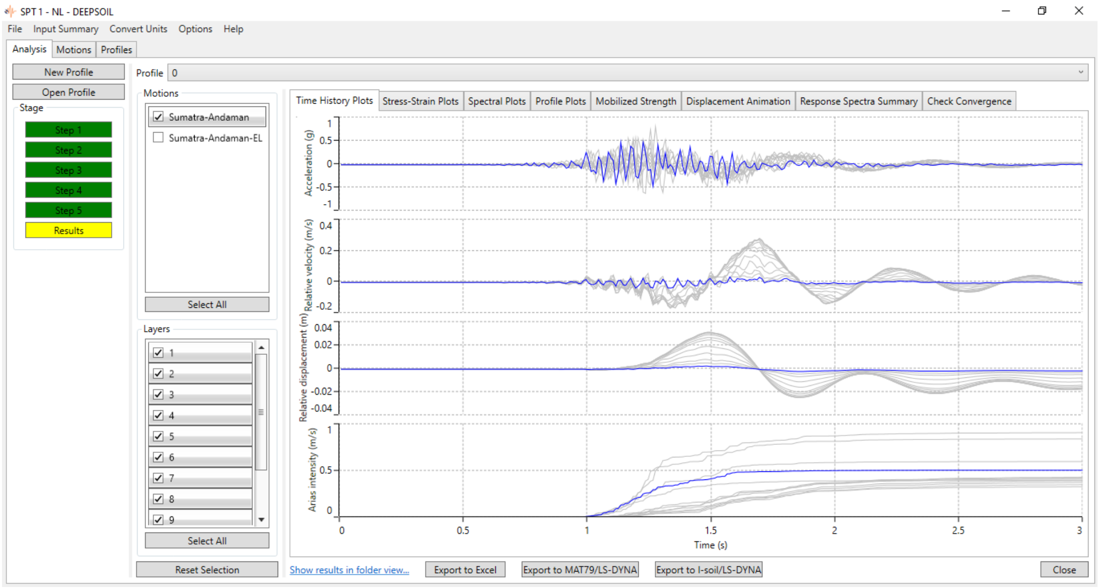

Figure 5.24 : NL SPT-1 time history plot.

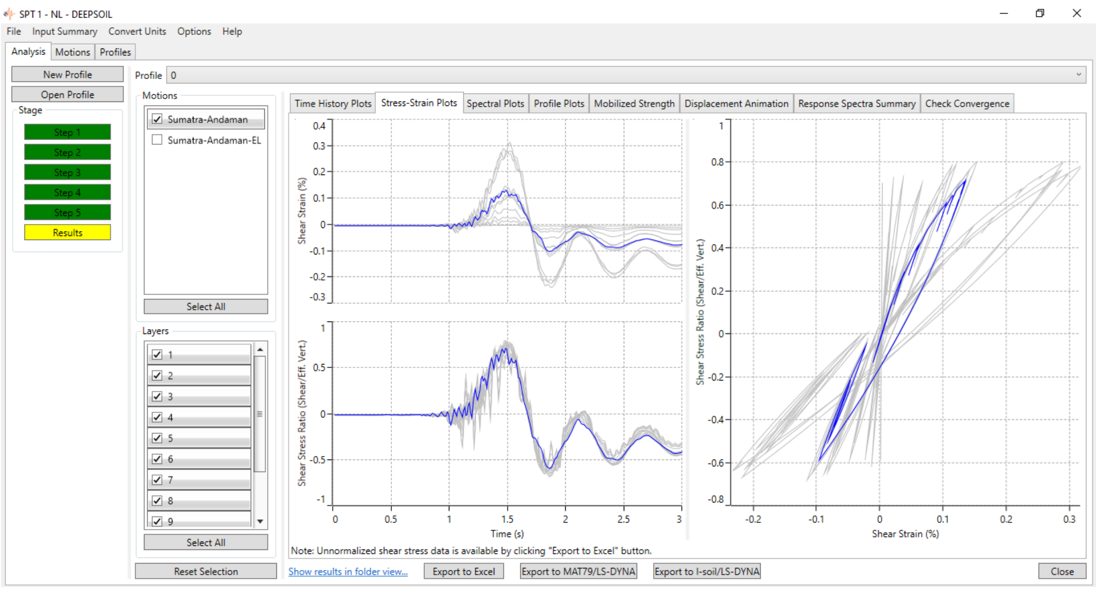

Figure 5.25 : NL SPT-1 stress-strain plot.

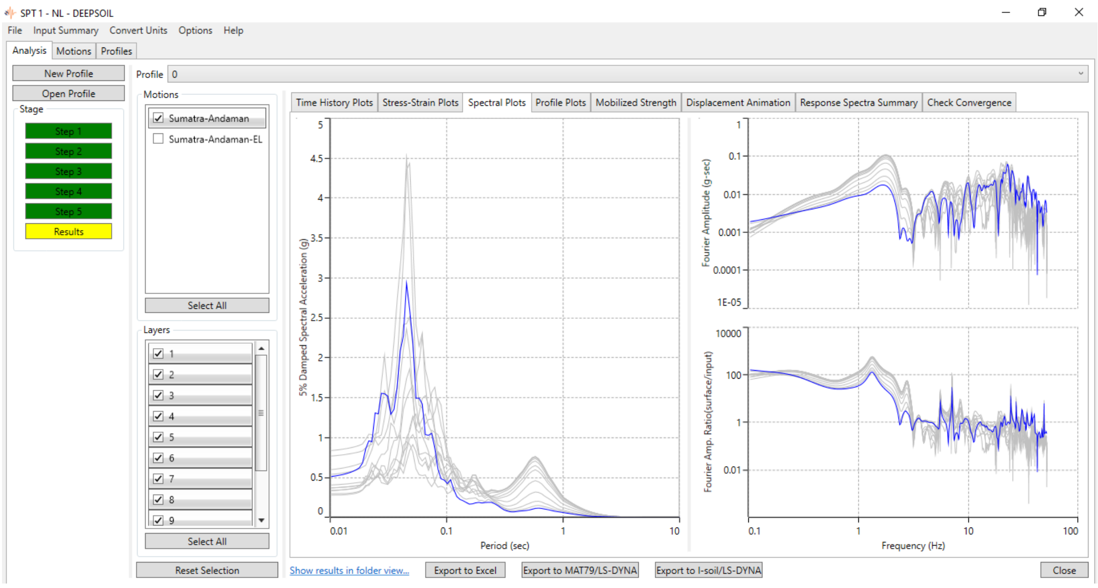

Figure 5.26 : NL SPT-1 spectral plot.

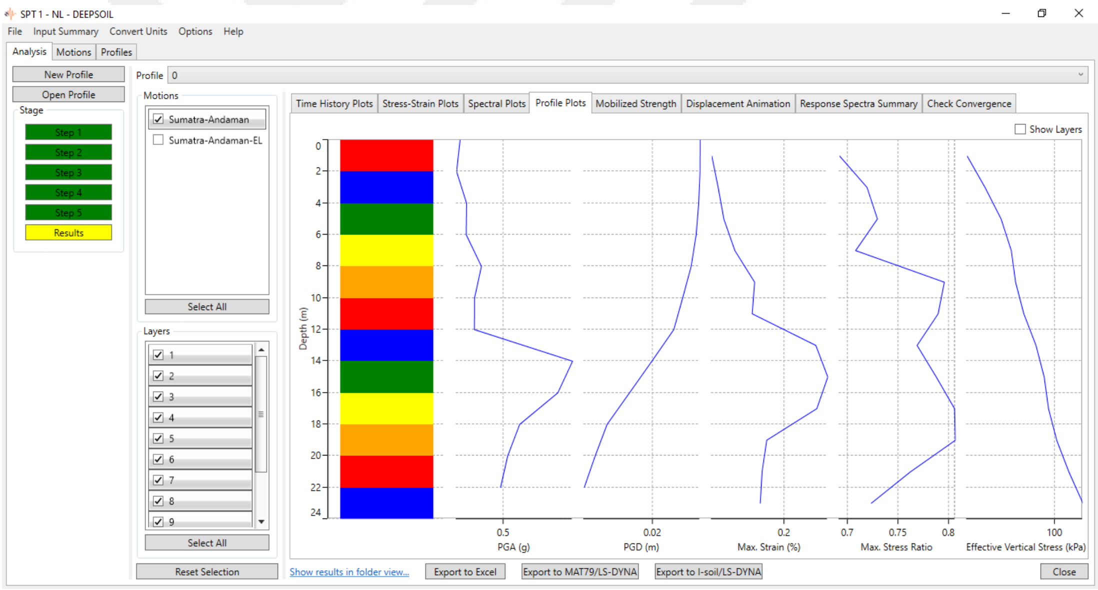

Figure 5.27 : NL SPT-1 profile plot.

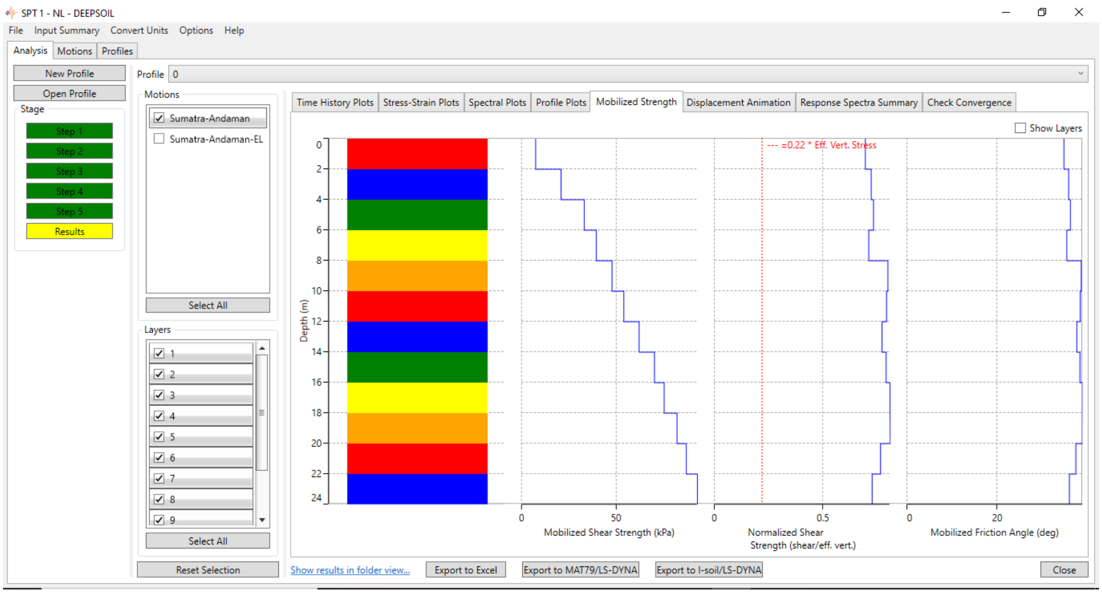

Figure 5.28 : SPT-1 NL mobiled strength plot.

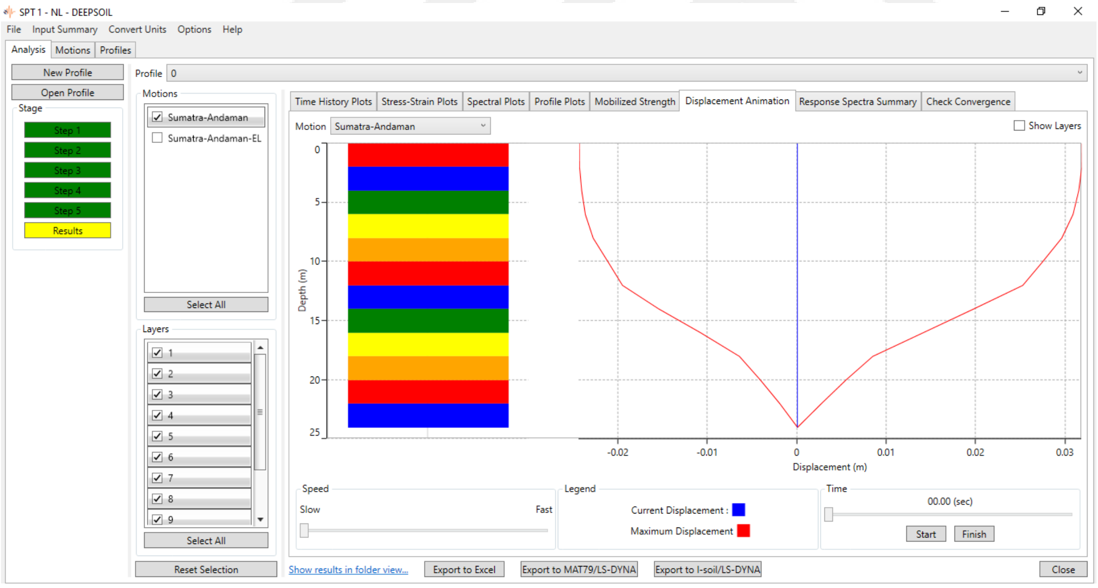

Figure 5.29 : NL SPT-1 displacement plot.

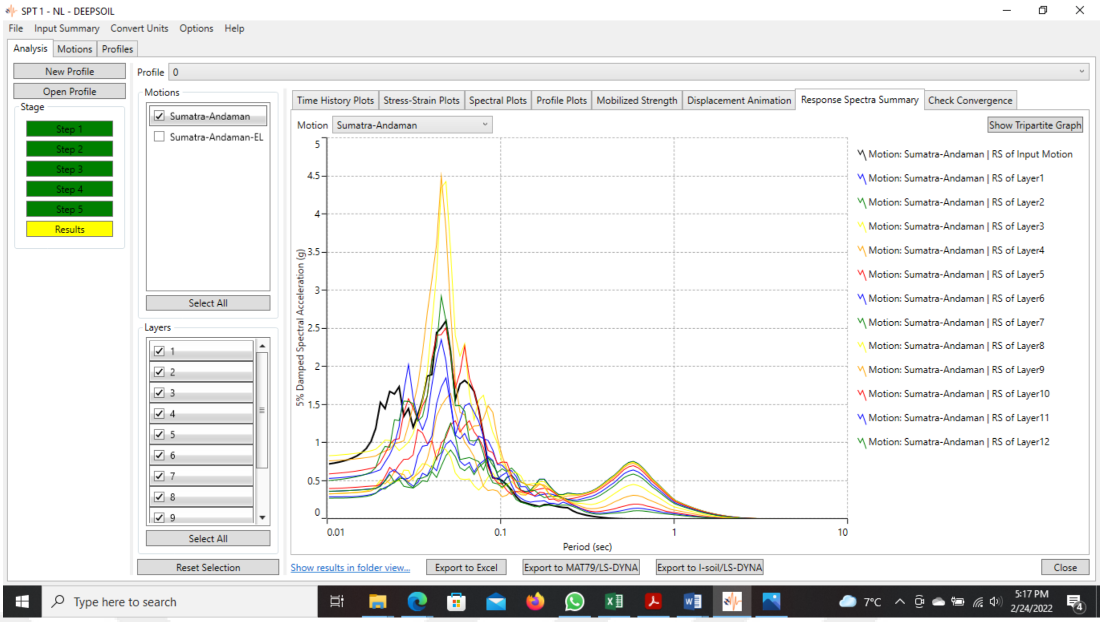

Figure 5.30 : NL SPT-1 response spectra plot.

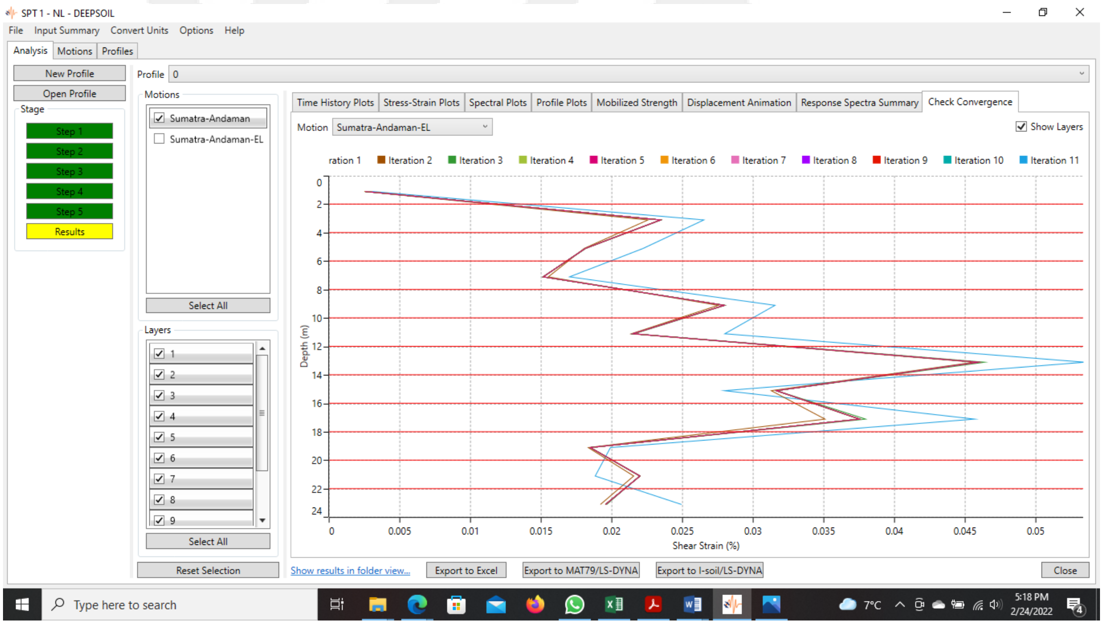

Figure 5.31 : NL SPT-1 check convergence.

5.4 Comparison Between ELA and NLA

The site response analysis calculation was shown in Appendix A. Table 5.5 and Table 5.6 below summarize the comparison site response analysis between equivalent linear and nonlinear methods. Both ELA and NLA methods demonstrate that the soil profiles from Banda Aceh have a tendency to amplify the earthquake motion, with the only exception was only the upper layer of SPT-1 with NLA method that shown a different result.

Table 5.5 : Comparison between ELA and NLA in terms of response spectra.

Borehole	ELA			NLA		
	Response Spectra on Bedrocks	Response Spectra on Ground Surface	Difference	Response Spectra on Bedrocks	Response Spectra on Ground Surface	Difference
SPT-1	2.62 g	3.41 g	30.15% ↑	2.62 g	2.18 g	16.79 % ↓
SPT-2	2.62 g	3.77 g	43.89 % ↑	2.62 g	3.22 g	22.9 % ↑
SPT-3	2.64 g	2.78 g	5.30 % ↑	2.62 g	2.80 g	6.87 % ↑

Table 5.6 : Comparison between ELA and NLA in terms of PGA.

Borehole	ELA			NLA		
	PGA on Bedrocks	PGA on Ground Surface	Difference	PGA Bedrocks	PGA on Ground Surface	Difference
SPT-1	0.50 g	0.76 g	52 % ↑	0.49 g	0.45g	8.0 % ↓
SPT-2	0.58 g	0.80 g	37.9 % ↑	0.49 g	0.55 g	12.24 ↑
SPT-3	0.46 g	1.13 g	145.53% ↑	0.50 g	0.76 g	52 % ↑

5.5 Liquefaction Analysis

In site response analysis studies, another issue that is as important as the effects of soils on the propagation of earthquake waves is the evaluation of the liquefaction potential of the soil under dynamic loadings. It is stated that the soil deposits with clay content may be evaluated as non-liquefiable (Youd et. al., 2001). For this study, liquefaction analysis was conducted solely to saturated sand layers.

The stress-based approach of liquefaction potential analysis was pioneered by Seed and Idriss (1967). For this study, the simplified method that compares CRR (Cyclic

Resistance Ratio) that is the resistance of a soil layer agaist liquefaction to CSR (Cyclic Stress Ratio) was used to determine the factor of safety (FS) of the given soil. The formulas and table used was based on method proposed by Idriss and Boulanger (2014).

Earthquake-induced cyclic stress ratio (CSR)

The earthquake induced CSR is expressed as equivalent uniform value equal to 65% of the maximum cyclic shear stress ratio (Idriss and Boulanger, 2014).

$$CSR_{M,\sigma'_v} = 0.65 \frac{\sigma_v}{\sigma'_v} \frac{\alpha_{max}}{g} r_d \tag{5.2}$$

Where σ_v = vertical total stress at depth z, α_{max}/g = maximum horizontal acceleration at the ground surface, and r_d = shear stress reduction factor actor that accounts for the dynamic response of the soil profile.

Cyclic resistance ratio (CRR)

The cyclic resistance ratio (CRR) is usually correlated to an in-situ parameter such as SPT blow count, CPT penetration resistance or shear wave velocity, Vs and effective overburden stress.

$$CRR_{M,\sigma'_v} = CRR_{M=7.5,\,\sigma'_v=1atm}.MSF.K_\sigma \tag{5.3}$$

Shear stress reduction parameter, r_d

According to Idriss and Boulanger (2014) in terms of evaluating the liquefaction potential procedures, the parameter r_d could be read from graphic in Figure 5.32 or numerically calculated using formula below.

$$r_d = exp[\alpha(z) + \beta(z).M] \tag{5.4}$$

$$\alpha(z) = -1.012 - 1.126\, sin\left(\frac{z}{11.73} + 5.133\right) \tag{5.5}$$

$$\beta(z) = 0.106 + 0.118 \sin\left(\frac{z}{11.28} + 5.142\right) \tag{5.6}$$

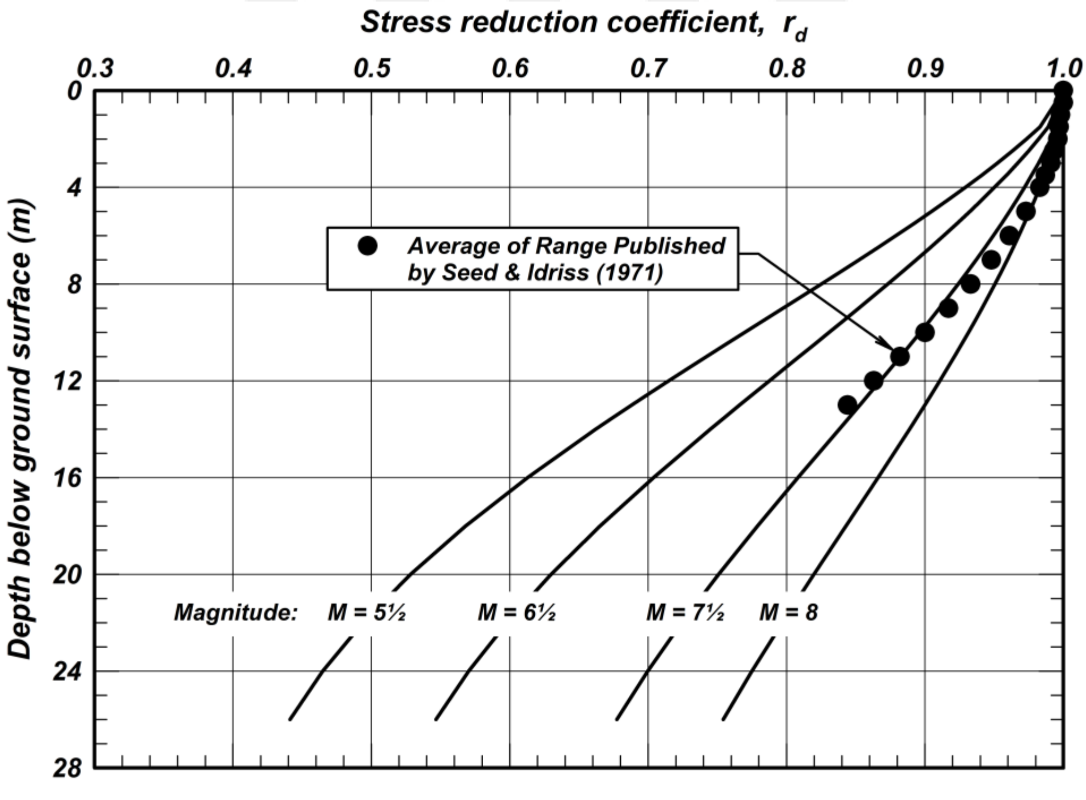

Figure 5.32 : Shear stress reduction factor, r_d, ground surface depth, and earthquake magnitude relationship (Source: Idriss and Boulanger, 2014).

Overburden correction factor

The K_σ for SPTrelationship was initially developed by Boulanger in 2003. Idriss and Boulanger (2008) suggested that the relatioship between K_σ and $(N_1)_{60cs}$ values as follows:

$$K_\sigma = 1 - C_\sigma \ln\left(\frac{\sigma'_v}{P_a}\right) \leq 1.1 \tag{5.7}$$

$$C_\sigma = \frac{1}{18.9 - 2.55\sqrt{(N_1)_{60cs}}} \leq 0.3 \tag{5.8}$$

The relatioship above is plotted in Figure 5.33 below. The limit value of 1.1 from K_σ relationship reached its maximum value at vertical effective stress less than 40 kPa. This limit was imposed because the function were not validated for very low effective stress. Idriss and Boulanger (2014) stated that omitting the limit of 1.1 for the maximum value of K_σ on the liquefaction analysis deemed as essentially unimportant.

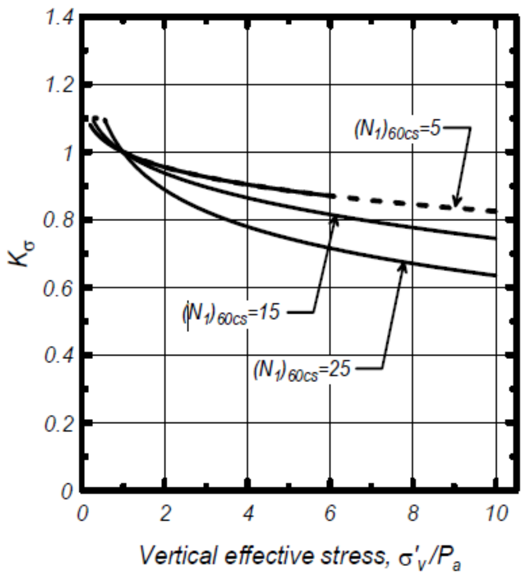

Figure 5.33 : Overburden correction factor (K_σ) and vertical effective stress relationship (Source: Idriss and Boulanger, 2014).

Idriss and Boulanger (2014) also suggested another overburden pressure correction factor denoted as C_N which can be expressed in terms of q_{c1Ncs} or $(N_1)_{60cs}$ as follows:

$$C_N = \left(\frac{P_a}{\sigma'_v}\right)^m \leq 1.7 \qquad (5.9)$$

$$m = 1.338 - 0.249(q_{c1Ncs})^{0.264} \qquad (5.10)$$

$$m = 0.784 - 0.0768\sqrt{(N_1)_{60cs}} \qquad (5.11)$$

<u>Magnitude Scalling Factor, MSF</u>

Comparison of some magnitude scaling factor (MSF) relationship was shown in Figure 3.4. The magnitude Scalling Factor (MSF) relatioship for sands was recommended by Idriss (1999) as follow:

$$MSF = 6.9.exp\left(\frac{-M}{4}\right) - 0.058 \leq 1.8 \qquad (5.12)$$

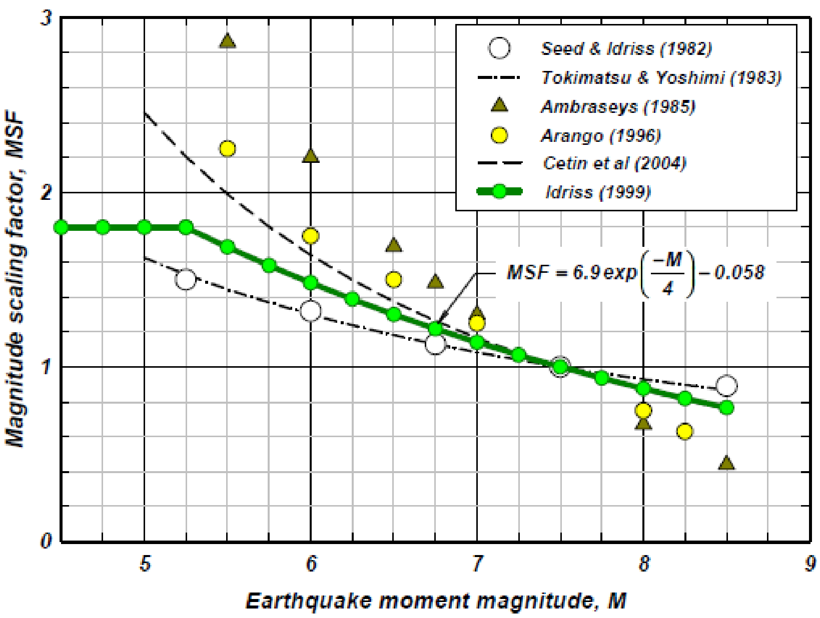

Figure 5.34 : Comparison of some magnitude scaling factor (MSF) relationship (Source: Idriss and Boulanger, 2014).

Equivalent clean sand adjustment for fine content

The equivalent clean sand adjustment is developed empirically from the liquefaction case history data, and it incorporates the impacts of fines content on both the CRR and the SPT blow count. The liquefaction triggering correlation shifts to the left as the fines content (FC) increases, according to the liquefaction case histories. The equivalent clean sand adjustment suggested by Idriss and Boulanger (20014) is shown below, FC value is in percent.

$$\Delta(N_1)_{60} = exp\left(1.63 + \frac{9.7}{FC+0.01} - \left(\frac{15.7}{FC+0.01}\right)^2\right) \tag{5.13}$$

For CPT based calculation, the equivalent clean sand adjustment can be calculated by formulas recommended by Idriss and Boulanger (2014) as follows:

$$\Delta q_{c1N} = \left(11.9 + \frac{q_{c1N}}{14.6}\right) exp\left(1.63 - \frac{9.7}{FC+2} - \left(\frac{15.7}{FC+2}\right)^2\right) \tag{5.14}$$

Liquefaction triggering correlation

The correlation between the SPT based cyclic resistance ratio (CRR) adjusted to M=7.5 and σ'_v=1 atm and the equivalent clean sand $(N_1)_{60cs}$ value for cohesionless soils, developed by Idriss and Boulanger (2008), is expressed as,

$$CRR_{M=7.5,\, \sigma'_v=1atm} = exp\left(\frac{(N_1)_{60cs}}{14.1} + \left(\frac{(N_1)_{60cs}}{126}\right)^2 - \left(\frac{(N_1)_{60cs}}{23.6}\right)^3 + \left(\frac{(N_1)_{60cs}}{25.4}\right)^4 - 2.8\right) \tag{5.15}$$

The summary of the liquefaction analysis for SPT – 1 are given in Table 5.6 below. SPT-1 is an offshore borehole with GWT under sea water level. Considering all of the liquefaction susceptibility criteria for the investigated soil profiles, it is concluded that the examined soil profile has a liquefaction potential. Calculation of site response analyses other soil profilea are attached in Appendix-1.

Table 5.7 : Liquefaction evaluation of the SPT-1 soil profiles.

Depth (m)	**N-SPT**	**Soil Type**	**Unit Weight (kN/m^3)**	**σ (kPa)**	**σ' (kPa)**	**C_E**	**C_B**	**C_R**	**C_S**	**C_N**	**$(N_1)_{60}$**
(1)	(2)	(3)	(4)	(5)	(6)	(7)	(8)	(9)	(10)	(11)	(12)
2	50	Coarse Sand	20	40	20.4	0.75	1	0.8	1	1.00	30.00
4	50	Coarse Sand	18	76	36.8	0.75	1	0.85	1	1.00	31.88
6	50	Coarse Sand	18	112	53.2	0.75	1	0.95	1	1.00	35.63
8	50	Coarse Sand	12	136	57.6	0.75	1	0.95	1	1.00	35.63
10	28	Clay	12	160	62	0.75	1	1	1	1.25	26.16
12	25	Clay	16	192	74.4	0.75	1	1	1	1.14	21.32
14	8	Clay	16	224	86.8	0.75	1	1	1	1.05	6.32
16	14	Clay	12	248	91.2	0.75	1	1	1	1.03	10.79
18	19	Clay	12	272	95.6	0.75	1	1	1	1.00	14.30
20	37	Clay	16	304	108	0.75	1	1	1	0.94	26.20
22	48	Clay	16	336	120.4	0.75	1	1	1	0.89	32.19
24	50	Clay	18	372	136.8	0.75	1	1	1	0.84	31.45

Table 5.7 (continued) : Liquefaction evaluation of the SPT-1 soil profiles.

Depth (m)	**Finese Content**	**Δ $N_{1(60)}$**	**$N_{1(60)cs}$**	**r_d**	**CSR**	**MSF**	**$K_σ$**	**CRR for $M_{7.5}$**	**CRR for $M_{9.0}$**	**SF**
(1)	(13)	(14)	(15)	(16)	(17)	(18)	(19)	(20)	(21)	(22)
2	5.9	0.004	30.004	0.875	0.669	0.650	1.000	0.485	0.315	0.471
4	5.9	0.004	31.879	0.550	0.443	0.650	1.000	0.632	0.411	0.927
6	5.9	0.004	35.629	0.303	0.249	0.650	1.000	1.268	0.824	3.312
8	5.9	0.004	35.629	0.168	0.155	0.650	1.000	1.268	0.824	5.323
10	5.9	0.004	26.167	0.099	0.100	0.650	1.000	0.321	0.208	Clay
12	5.6	0.002	21.327	0.064	0.064	0.650	1.000	0.223	0.145	Clay
14	5.6	0.002	6.320	0.045	0.045	0.650	1.000	0.094	0.061	Clay
16	5.6	0.002	10.788	0.035	0.037	0.650	1.000	0.124	0.080	Clay
18	5.6	0.002	14.299	0.030	0.033	0.650	1.000	0.150	0.098	Clay
20	5.6	0.002	26.197	0.027	0.030	0.650	1.000	0.321	0.209	Clay
22	5.6	0.002	32.187	0.026	0.028	0.650	1.000	0.663	0.431	Clay
24	5.6	0.002	31.455	0.026	0.027	0.650	1.000	0.593	0.385	Clay

6. CONCLUSIONS AND RECOMMENDATIONS

The city of Banda Aceh is possibly exposed to a high seismic hazard in terms of earthquake risk. Estimating the city's seismic site amplification is critical for any mitigation actions involving a future unanticipated seismic event and seismic site amplification. Analytical models have demonstrated that they can simulate reasonably well the seismic ground motions amplification.

This study focuses on Banda Aceh-Indonesia which is founded on thick alluvium. Historical time history and developed subsurface models across the city were used to estimate the seismic site amplification of Banda Aceh’s soft soil. The site response analysis results reveal the ground motions amplification of Banda Aceh’s soils of up is relatively high. Thus, applying the seismic site amplification for structural design at Banda Aceh can be further works.

Response spectra and PGA in ELA shown that the amplification of the soil acceleration was observed by SPT-1, SPT-2, and SPT-3. Meanwhile, the response spectra and PGA in NLA shown that upper layers of the SPT-2 and SPT-3 soil soil profile that amplify the earthquake motion. The possibility of SPT-1 upper layer did not show the soil amplification in NLA method could be because of the liquefactions that occurs with the 2004 Sumatra-Andaman earthquake motion.

From the liquefaction analysis, the soil profile SPT-1 and SPT-2 are succeptible for liquefaction and SPT-3 sand layer was not liquefy. However, further study need to be done.

REFERENCES

Ammon, C. J., Ji, C., Thio, H. K., Robinson, D., Ni, S., Hjorleifsdottir, V., … Wald, D. (2005). Rupture process of the 2004 Sumatra-Andaman earthquake. *Science*, *308*(5725), 1133–1139. https://doi.org/10.1126/science.1112260

Ansal, Atilla (2004). Non-Linear Soil Models for Site Response; European Experience, International Workshop on the Uncertainties in Nonlinear Soil Properties and their Impact on Modeling Dynamic Soil Response, California, USA

Bappenas (2005) Indonesia: lhe preliminary damage and loss assessmellllhe 26 December 2004 natural disaster, a technical report

Chlieh, M., Avouac, J.-P., Hjorleifsdottir, V., Song, T.-R., Ji, C., Sieh, K., Sladen, A., Hebert, H., Prawirodirdjo, L., Bock, Y. and Galetzka, J. (2007). Coseismic slip and afterslip of the Great (Mw 9.15) Sumatra—Andaman Earthquake of 2004, Bulletin of the Seismological Society of America, v. 97, no. 1A, p. S152-S173, DOI: 10.1785/0120050631

Cluff, Lloyd S. (2007). Effects of the 2004 Sumatra-Andaman Earthquake and Indian Ocean Tsunami in Aceh Province, The Bridge, Vol. 37, No. 1, p.12-16.

Culshaw, M. G., Duncan S. V., Sutarto N. R. (1979). Bulletin of the International Association of. *Bulletin of the International Association of Engineering Geology*, *19*, 40–47.

Fehr, I., Grossi, P., Hernandez, S., Krebs, T., Mckay, S., Muir-wood, R., Pomonis, A., Re, D., Souch, C., Windeler, D., & Xie, Y. (2004). *Managing Tsunami Risk in the Aftermath of the 2004 Indian Ocean Earthquake & Tsunami Editorial and Production Team.*

Ghobarah, A., Saatcioglu, M., & Nistor, I. (2006). The impact of the 26 December 2004 earthquake and tsunami on structures and infrastructure. *Engineering Structures*, *28*(2), p. 312–326. https://doi.org/10.1016/j.engstruct.2005.09.028

Gillespie et al. (2009). Assessment of Natural Hazard Damage and Reconstruction: A Case Study from Band Aceh, Indonesia, California Center for Population Research On-Line Working Paper Series, University of California, USA.

Gutenberg, B. (1957), Effects of ground on earthquake motion, Bulletin of the Seismological Society of America, 47(3), 221–250.

Hashash, Y.M.A., Musgrove, M.I., Harmon, J.A., Ilhan, O., Xing, G., Numanoglu, O., Groholski, D.R., Phillips, C.A., and Park, D. (2020)

"DEEPSOIL 7.0, User Manual". Urbana, IL, Board of Trustees of University of Illinois at Urbana-Champaign.

Hutchings, S. J., & Mooney, W. D. (2021). The seismicity of Indonesia and tectonic implications. Geochemistry, Geophysics, Geosystems, 22, e2021GC009812. https://doi.org/10.1029/2021GC009812.

Idriss, I. M. (1990). Response of soft soil sites during earthquakes. In: Proceedings Memorial Symposium to Honor Professor Harry Bolton Seed, Berkeley, California.

Idriss, I. M., Boulanger, R. W. (2014). CPT and SPT Based Liquefaction Triggering Procedures, Department Of Civil and Environmental Engineering College of Engineering University of California at Davis, USA.

Idriss, I. M., Seed, H. B. (1967). Response of Horizontal Soil Layers During Earthquakes. Soil Mechanics and Bituminous Materials Research Laboratory, University of California, Berkeley, Berkeley, CA.

Idriss, I. M., Seed, H.B. (1968). An analysis of ground motions during the 1957 San Francisco Earthquake. Bull. Seismol. Soc. Am. 58 (6), 2013–2032.

Idriss, I.M., Sun, J.I. (1992). User's Manual for SHAKE91: A Computer Program for Conducting Equivalent Linear Seismic Response Analyses of Horizontally Layered Soil Deposits.

International Federation of Red Cross and Red Cressent Societies (2005) Nias earthquake, infornlation bulletin no. 03n005

Jaffe, B.E., Borrero, J.C., Prasetya, G.S., Peters, R., McAdoo, B., Gelfenbaum, G., Morton, R., Ruggiero, P., Higman, B., Dengler, L., Hidayat, R., Kingsley, E., Kongko, W., Lukiyanto, Moore, A., Titov, V., and Yulianto, E. (2006), Northwest Sumatra and Offshore Islands Field Survey after the December 2004 Indian Ocean Tsunami, Earthquake Spectra, v. 22, n. S3, p. S105-S135.

Jalil, A., Fathani, T. F., Satyarno, I., & Wilopo, W. (2020). A study on the liquefaction potential in banda aceh city after the 2004 sumatera earthquake. *International Journal of GEOMATE*, *18*(65), 147–155. https://doi.org/10.21660/2020.65.94557

Kramer, S.L. (1996). Prentice Hall, Upper Saddle River, New Jersey. Geotechnical Earthquake Engineering.

Marto, A.; Tan, C.S.; Leong, T.K. (2013). Universal correlation of shear wave velocity and standard penetration resistance. Electron. J. Geotech. Eng. 18, 2727–2738.

Mayne, P. W., and Rix, G. J., (1995). Correlations between cone tip resistance and shear wave velocity in natural clay: Soils and Foundations, v. 35, no. 2, p. 107 - 110.

Moore, A., Nishimura, Y., Gelfenbaum, G., and Kamataki, T. (2006), Sedimentary deposits of the 26 December 2004 tsunami on the northwest coast of Aceh, Indonesia, Earth, Planets, and Space, v. 58, p. 253-258.

Natawidjaja, D. H. (2007). *Gempabumi dan tsunami di Sumatra dan upaya untuk mengembangkan lingkungan hidup yang aman dari bencana alam. Geospasial, Kementerian Lingkugan Hidup*, Jakarta.

Pan, T., Karim, K. R., You, X., Lim, C. L., & Leong, C. L. (2005). *the Great Sumatra-Andaman Islands Earthquake (M W = 9 . 0) of 26 December 2004 : Far-Field Response in Singapore*. *December 2004*, 2–5.

Schnabel, P.B., Lysmer, J., Seed, H.B. (2012). Computer Program SHAKE: A Computer Program for Earthquake Response Analysis of Horizontally Layered Sites. University of California, Berkeley, California.

Sugiyanto, D., Zulfakriza, Ismail, N., Adriansyah, F., Meilano, I., Hasanuddin, Z.A. (2011). *Analisa deformasi permukaan patahan aktif segmen Seulimum dan Segmen Aceh. Banda Aceh. Prosiding Hasil Penelitian Kebencanaan* TDMRC Unsyiah, Banda Aceh, 13-19 April 2011. pp. 72-77.

Sørensen, M. B., Atakan, K., & Pulido, N. (2007). Simulated strong ground motions for the great M 9.3 Sumatra-Andaman earthquake of 26 December 2004. *Bulletin of the Seismological Society of America*, *97*(1 A SUPPL.), 139–151. https://doi.org/10.1785/0120050608.

Tanioka, Y., Yudhicara, Kususose, T., Kathiroli, S., Nishimura, Y., Iwasaki, S. I., & Satake, K. (2006). Rupture process of the 2004 great Sumatra-Andaman earthquake estimated from tsunami waveforms. *Earth, Planets and Space*, *58*(2), 203–209. https://doi.org/10.1186/BF03353379.

Yahya, A., Palupi, M. I. R., & Suharsono. (2016). Seismic Hazard characterization study using an earthquake source with Probabilistic Seismic Hazard Analysis (PSHA) method in the Northern of Sumatra. *Journal of Physics: Conference Series*, *776*(1). https://doi.org/10.1088/1742-6596/776/1/012111

Yahya, A. S. (2014) Development of Seismic Microzonation Maps Using GIS, A Case Study of Banda Aceh, Indonesia. LAP Lambert Academic Pubblishing, Germany.

Youd, T.L., Idriss, I.M., Andrus, R.D., Arango, I., Castro, G., Christian, J.T., Dobry, R., Finn, L.W.D.,. Harder, L.F Jr, Hynes, M.E., Ishihara, K.J.P., Koester, S.S.C. Liao, W.F. Marcuson III, G.R. Martin, J.K. Mitchell, Y. Moriwaki, M.S. Power, P.K. Robertson, H.B. Seed,

K.H. Stokoe. (2001). Liquefaction Resistance of Soils: Summary Report from the 1996 NCEER and 1998 NCEER/NSF Workshops on Evaluation of Liquefaction Resistance of Soils, JGGE, 127(10).

Yunita, H., Setiawan, B., Saidi, T., & Abdullah, N. (2018). Site response analysis for estimating seismic site amplification in the case of Banda Aceh - Indonesia. *MATEC Web of Conferences*, *197*(April). https://doi.org/10.1051/matecconf/201819710002.

Offshore diesel generating power station swept inland < https://static.trip101.com/paragraph_media/pictures/002/269/764/large/1024px-PLTD_Apung.jpg?1603966730> erişim tarihi 11.1.2022

Think Hazard - Kota Bandaaceh - Landslide <https://thinkhazard.org/en/report/73705-indonesia-nangroe-aceh-darussalam-kota-bandaaceh/LS> erişim tarihi 10.01.2022

The Aftermath of 2004 Tsunami <https://www.sms-tsunami-warning.com/pages/tsunami-sumatra-2004#.Yd8jvdFBzIU> erişim tarihi 12.01.2022

Tsunamis and Earthquakes - 2005 Sumatra Survey, Subsidence - USGS PCMSC <https://cmgds.marine.usgs.gov/data/sumatra05/subsidence.html> erişim tarihi 10.10.2021

UNESCO < http://ioc3.unesco.org> erişim tarihi 07.01.2021

APPENDICES

APPENDIX A: SITE RESPONSE ANALYSES

APPENDIX A : SITE RESPONSE ANALYSES

Site Response For SPT-1

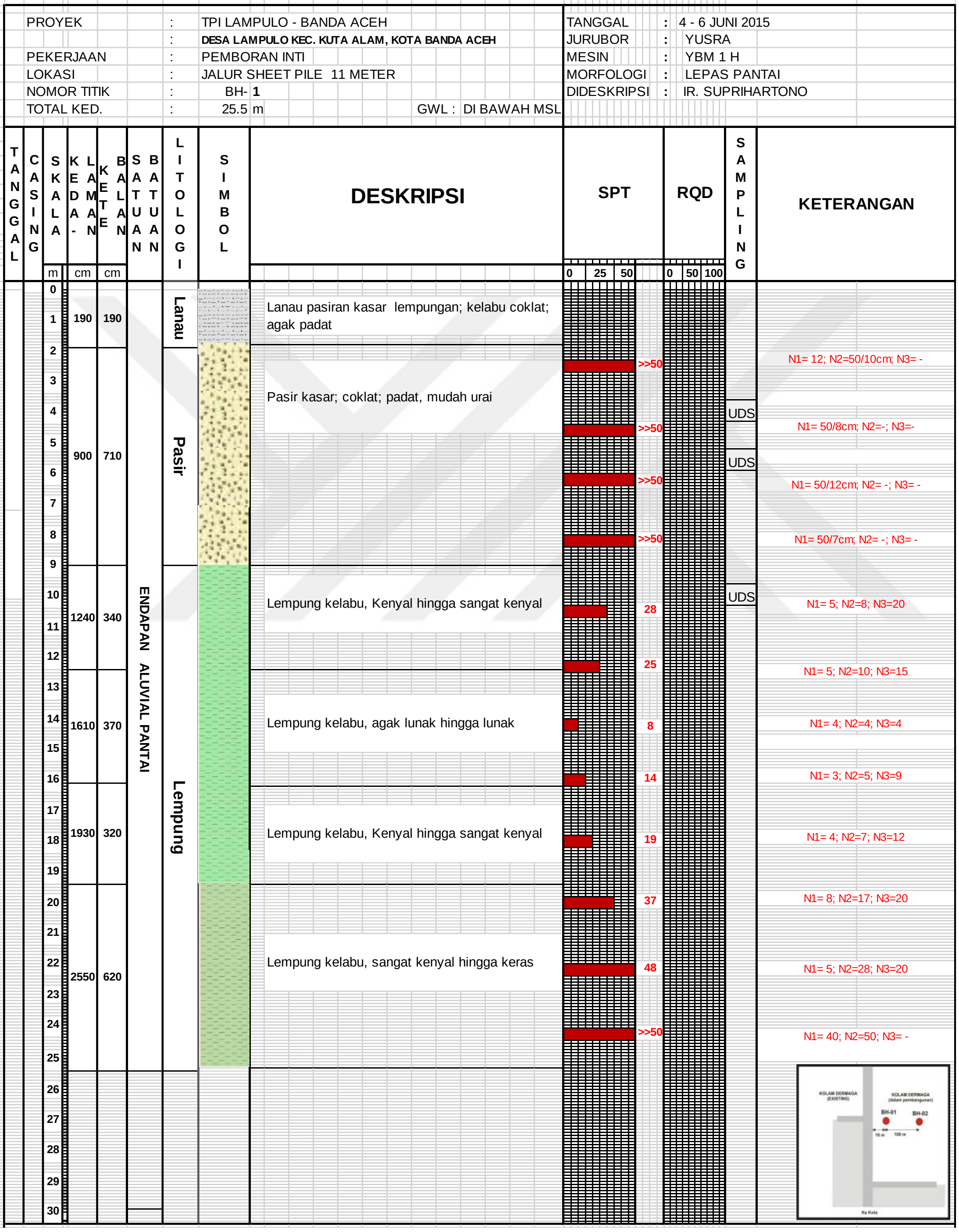

Figure A.1 : Soil Profile for SPT-1.

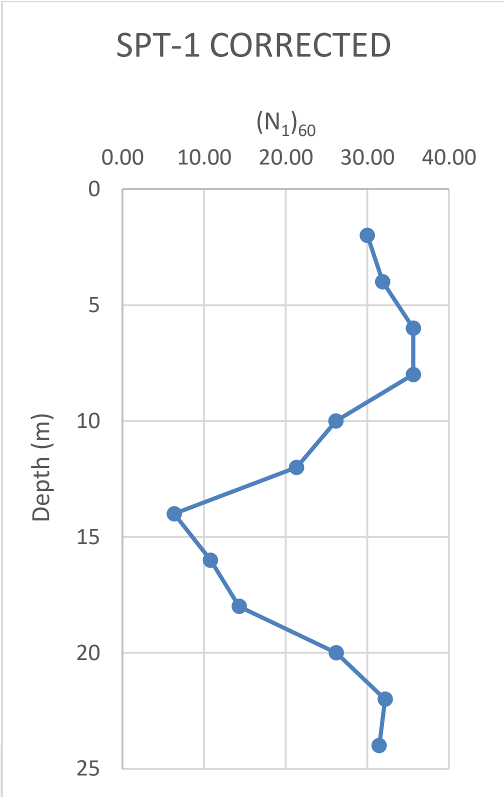

Figure A.2 : Corrected $(N_1)_{60}$ for SPT-1.

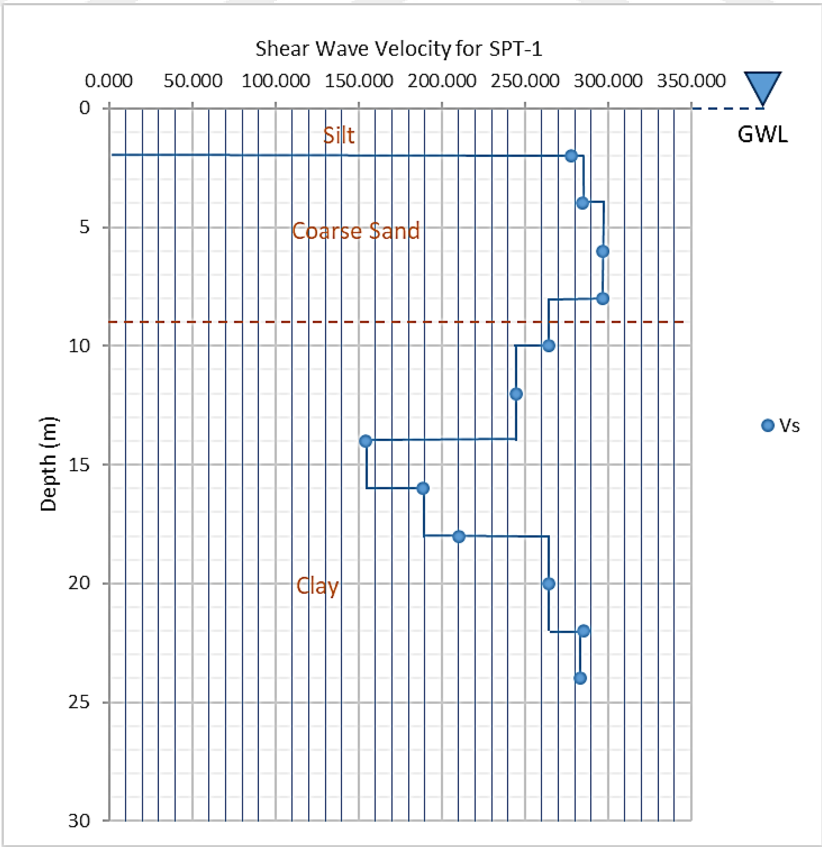

Figure A.3 : Shear Wave Velocity for SPT-1.

Equivalent Linear Site Response Analysis

<u>Response Spectra</u>

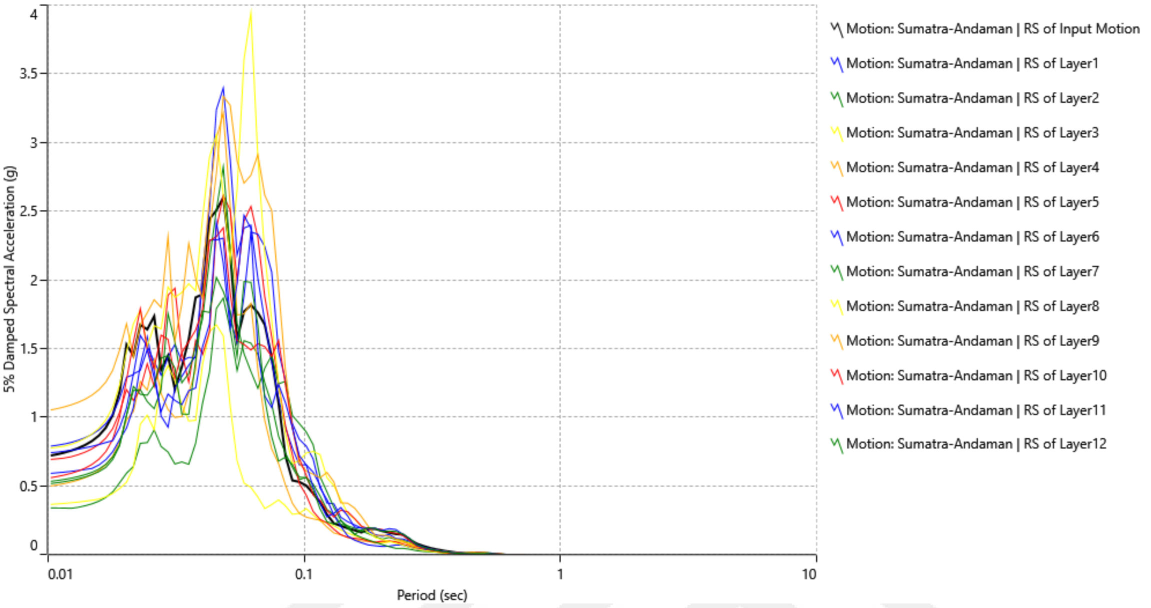

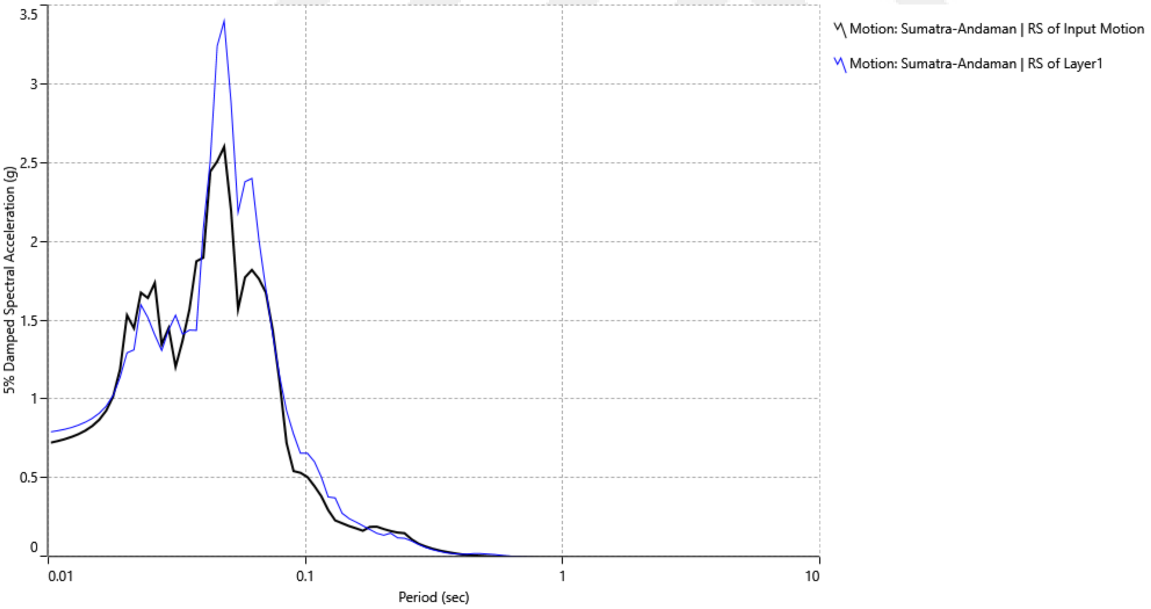

Figure A.4 : ELA Response Spectra for SPT-1.

Input motion = 2.62 g

Ground surface acceleration = 3.41 g

Earthquake motion was amplified by 30.15%

Peak Ground Acceleration

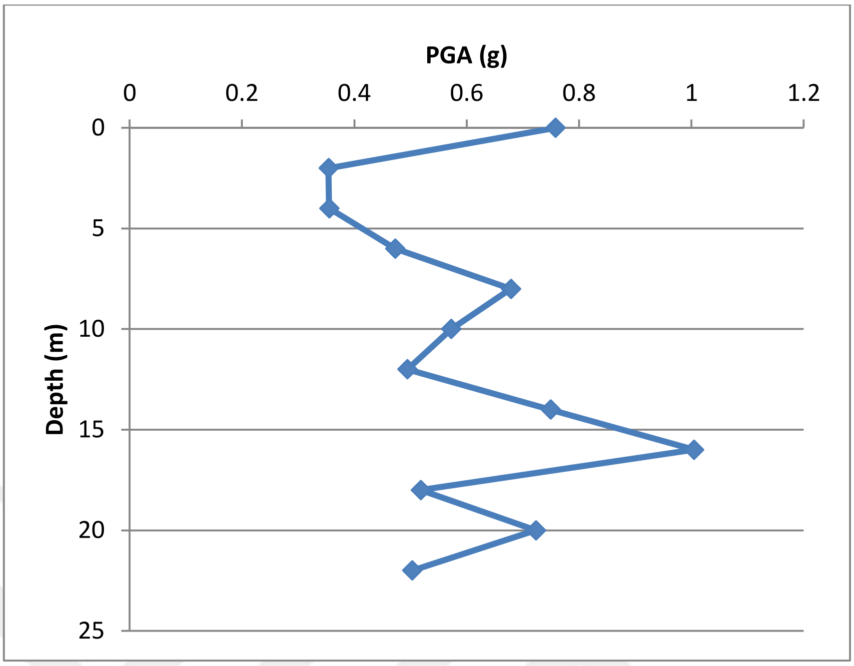

Figure A.5 : ELA Peak Ground Acceleration for SPT-1.

PGA at bedrocks = 0.50 g

PGA at ground surface = 0.76 g

PGA was amplıfied by 52%

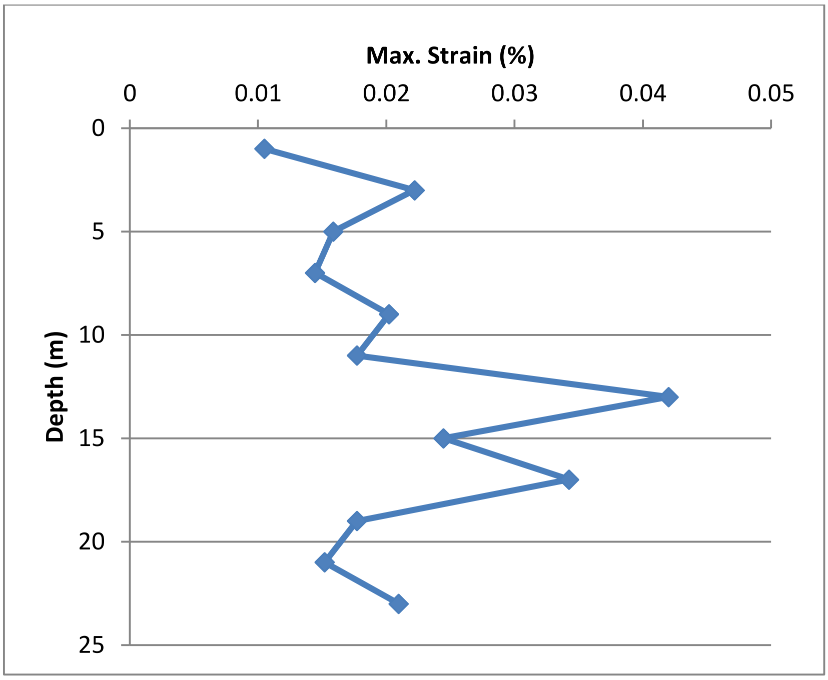

Figure A.6 : ELA Maximum Strain for SPT-1.

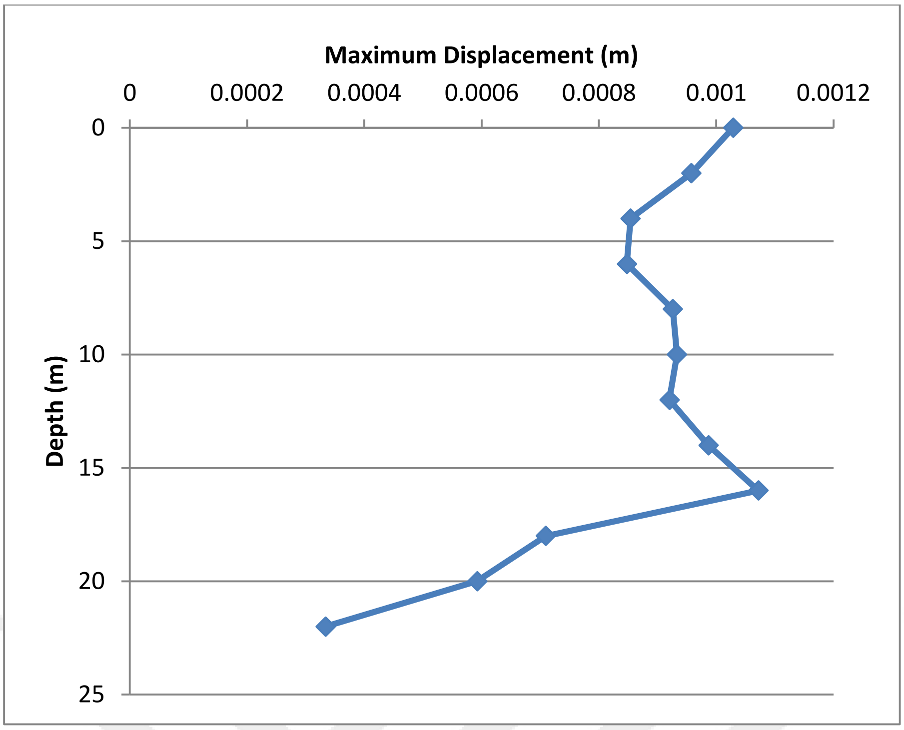

Figure A.7 : ELA Maximum Displacement for SPT-1.

Nonlinear Site Response Analysis

<u>Response Spectra</u>

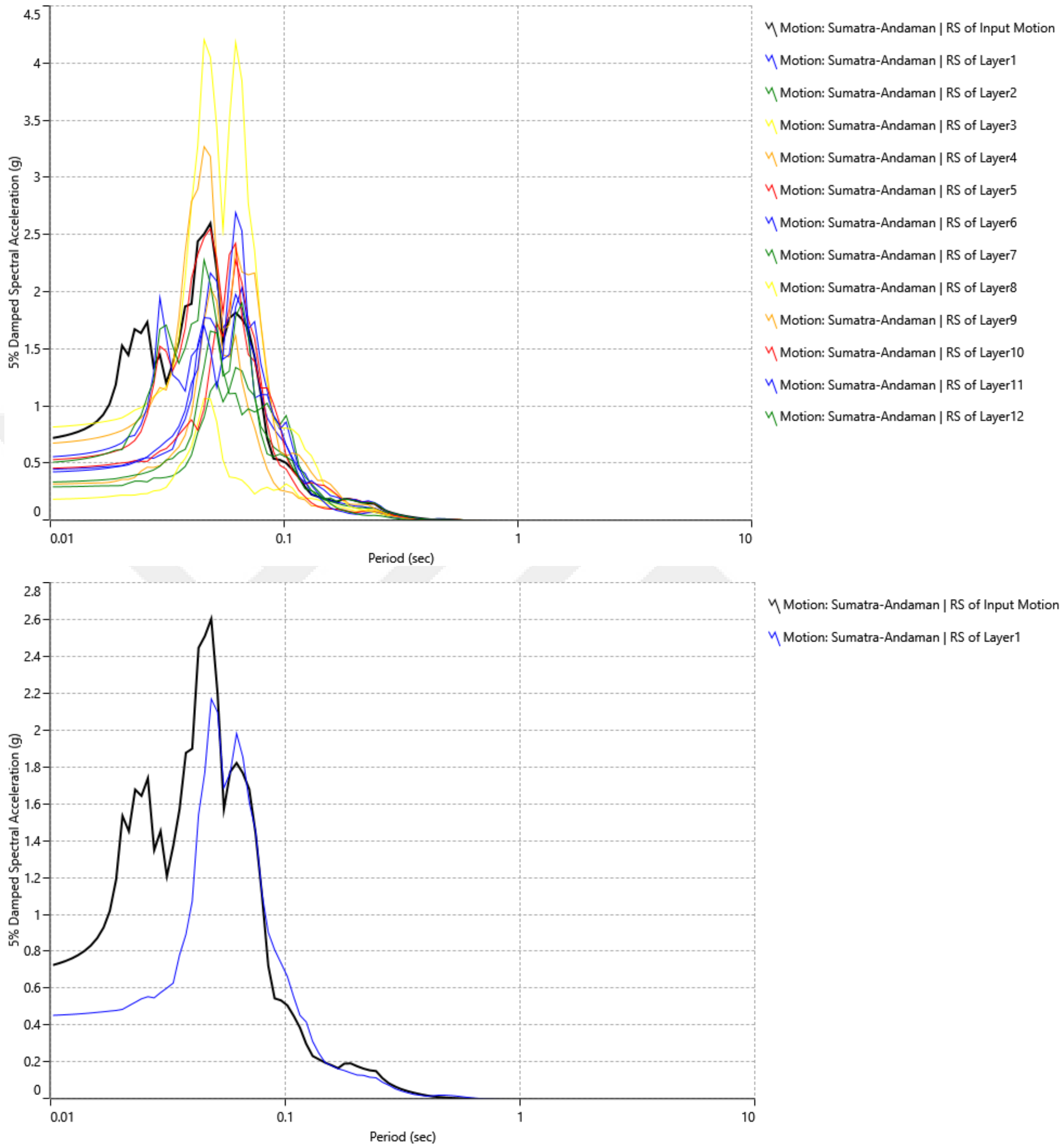

Figure A.8 : NLA Response Spectra for SPT-1.

Input motion = 2.62 g

Ground surface motion = 2.18 g

Earthquake motion was deamplified by 16.79%

Peak Ground Acceleration

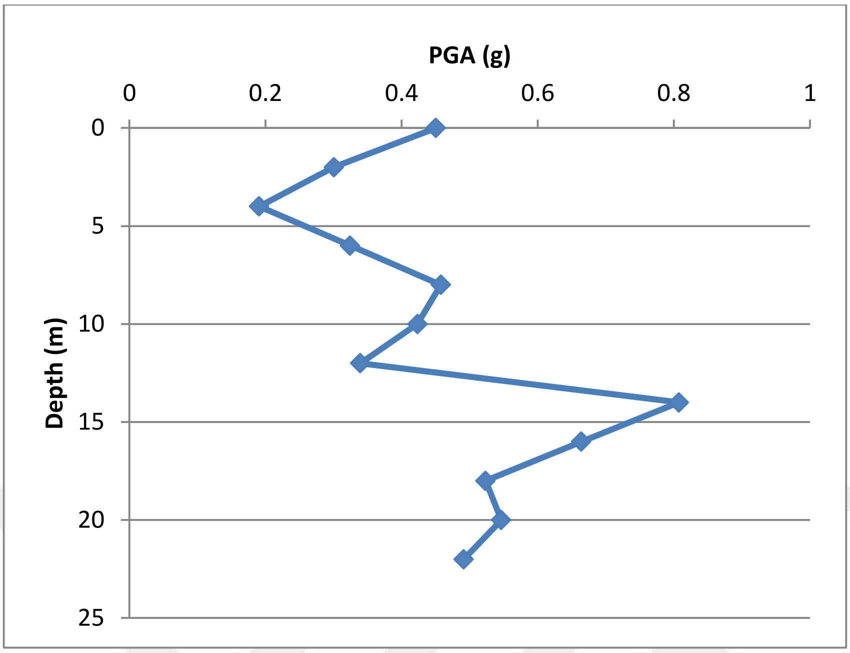

Figure A.9 : NLA Peak Ground Acceleration for SPT-1.

PGA at bedrocks = 0.49 g

PGA at surface = 0.45 g

PGA was decrease by 8%

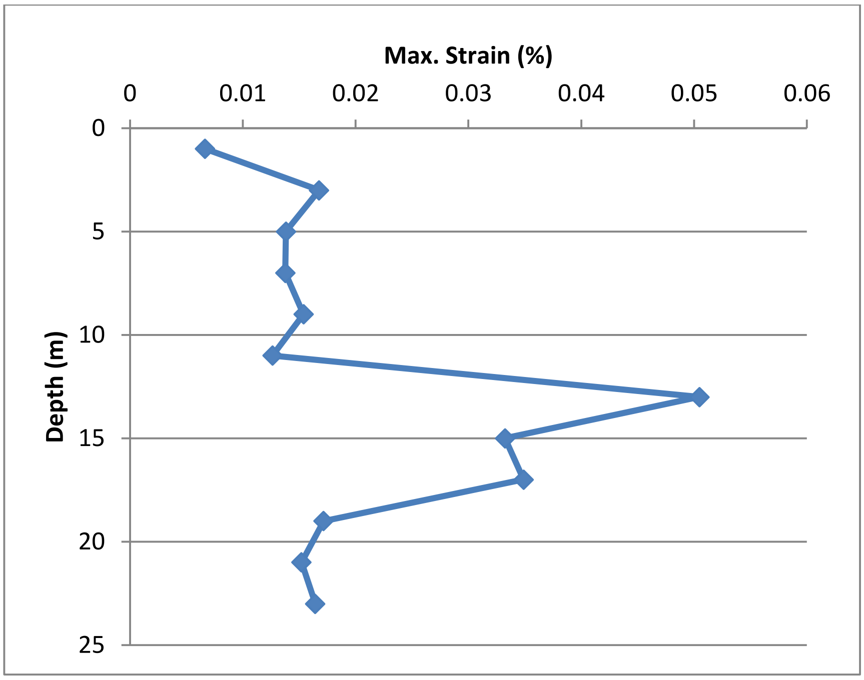

Figure A.10 : NLA Maximum Strain for SPT-1.

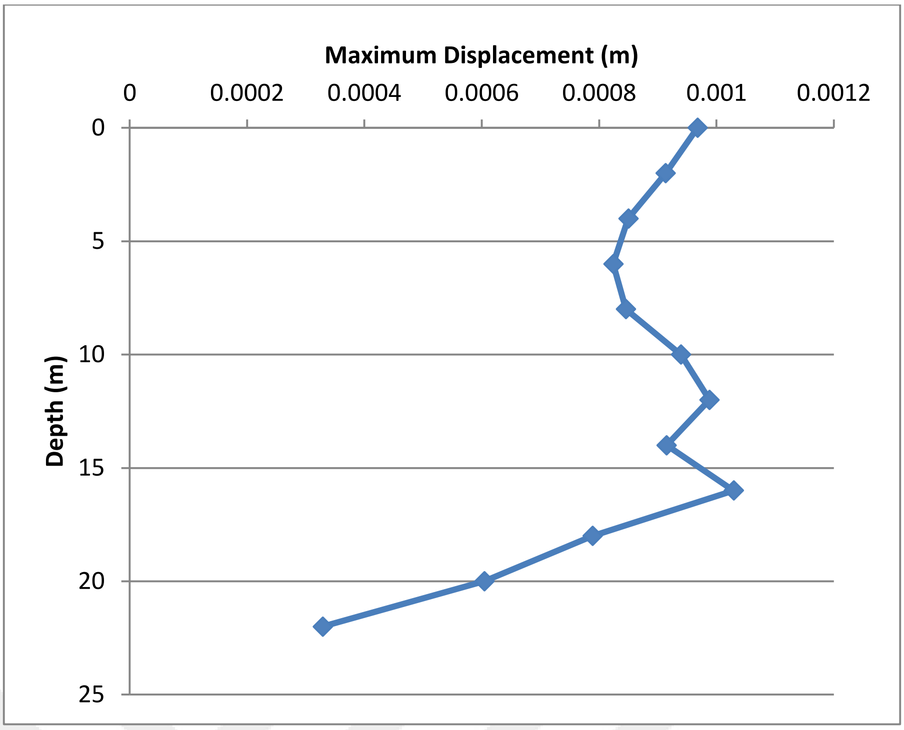

Figure A.11 : NLA Maximum Displacement for SPT-1.

Liquefaction Analysis

Table A.1 : Liquefaction evaluation of the SPT-1 soil profiles.

Depth (m)	**N-SPT**	**Soil Type**	**Unit Weight (kN/m^3)**	**σ (kPa)**	**σ' (kPa)**	**C_E**	**C_B**	**C_R**	**C_S**	**C_N**	**$(N_1)_{60}$**
(1)	(2)	(3)	(4)	(5)	(6)	(7)	(8)	(9)	(10)	(11)	(12)
2	50	Coarse Sand	20	40	20.4	0.75	1	0.8	1	1.00	30.00
4	50	Coarse Sand	18	76	36.8	0.75	1	0.85	1	1.00	31.88
6	50	Coarse Sand	18	112	53.2	0.75	1	0.95	1	1.00	35.63
8	50	Coarse Sand	12	136	57.6	0.75	1	0.95	1	1.00	35.63
10	28	Clay	12	160	62	0.75	1	1	1	1.25	26.16
12	25	Clay	16	192	74.4	0.75	1	1	1	1.14	21.32
14	8	Clay	16	224	86.8	0.75	1	1	1	1.05	6.32
16	14	Clay	12	248	91.2	0.75	1	1	1	1.03	10.79
18	19	Clay	12	272	95.6	0.75	1	1	1	1.00	14.30
20	37	Clay	16	304	108	0.75	1	1	1	0.94	26.20
22	48	Clay	16	336	120.4	0.75	1	1	1	0.89	32.19
24	50	Clay	18	372	136.8	0.75	1	1	1	0.84	31.45

Table A.1 (continued) : Liquefaction evaluation of the SPT-1 soil profiles.

Depth (m)	**Finese Content**	**$\Delta N_{1(60)}$**	**$N_{1(60)cs}$**	**r_d**	**CSR**	**MSF**	**K_σ**	**CRR for $M_{7.5}$**	**CRR for $M_{9.0}$**	**SF**
(1)	(13)	(14)	(15)	(16)	(17)	(18)	(19)	(20)	(21)	(22)
2	5.9	0.004	30.004	0.875	0.669	0.650	1.000	0.485	0.315	0.471
4	5.9	0.004	31.879	0.550	0.443	0.650	1.000	0.632	0.411	0.927
6	5.9	0.004	35.629	0.303	0.249	0.650	1.000	1.268	0.824	3.312
8	5.9	0.004	35.629	0.168	0.155	0.650	1.000	1.268	0.824	5.323
10	5.9	0.004	26.167	0.099	0.100	0.650	1.000	0.321	0.208	Clay
12	5.6	0.002	21.327	0.064	0.064	0.650	1.000	0.223	0.145	Clay
14	5.6	0.002	6.320	0.045	0.045	0.650	1.000	0.094	0.061	Clay
16	5.6	0.002	10.788	0.035	0.037	0.650	1.000	0.124	0.080	Clay
18	5.6	0.002	14.299	0.030	0.033	0.650	1.000	0.150	0.098	Clay
20	5.6	0.002	26.197	0.027	0.030	0.650	1.000	0.321	0.209	Clay
22	5.6	0.002	32.187	0.026	0.028	0.650	1.000	0.663	0.431	Clay
24	5.6	0.002	31.455	0.026	0.027	0.650	1.000	0.593	0.385	Clay

Liquefaction happened at the depth of 6 – 8 m.

Site Response For SPT-2

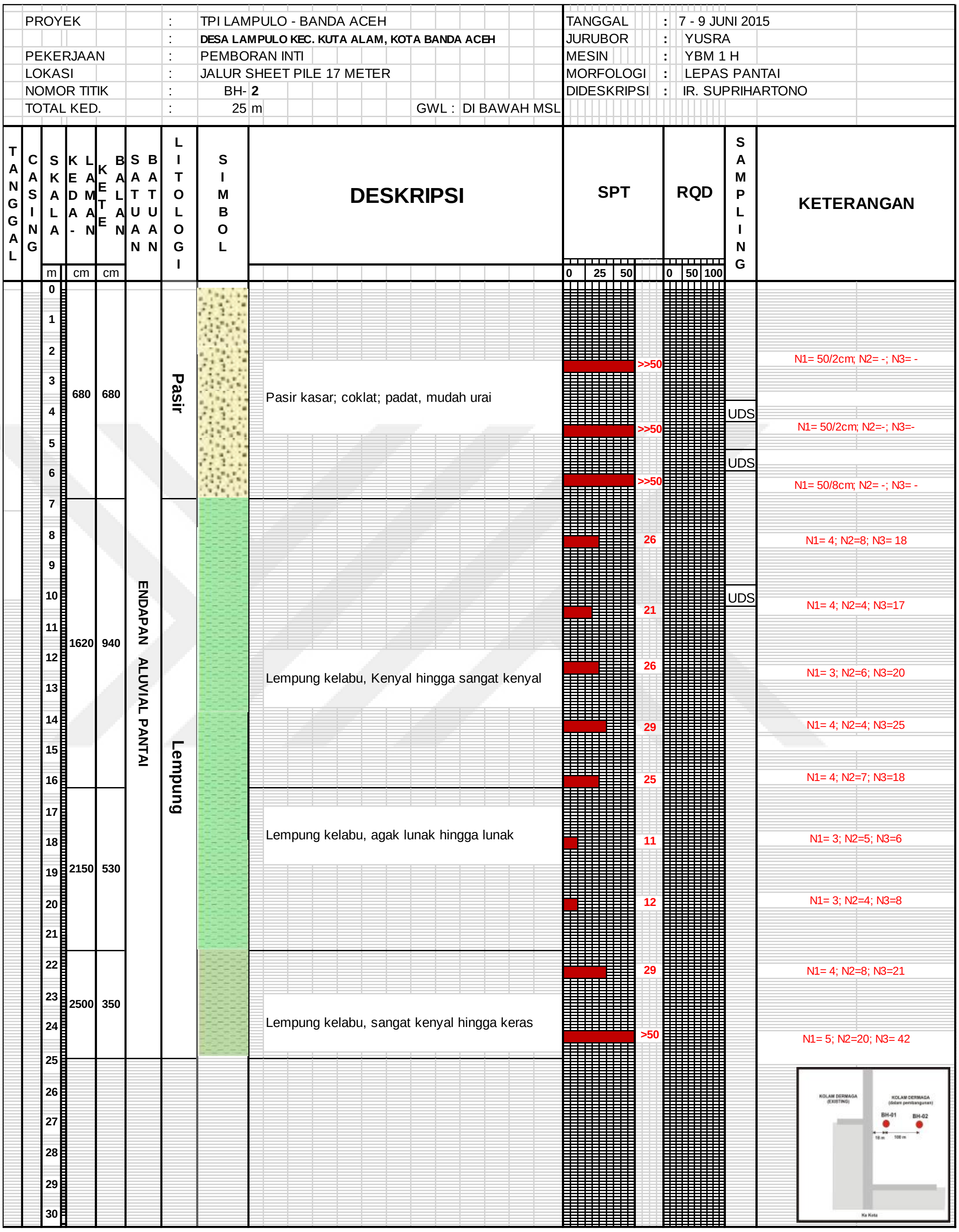

Figure A.12 : Soil profile for SPT-2.

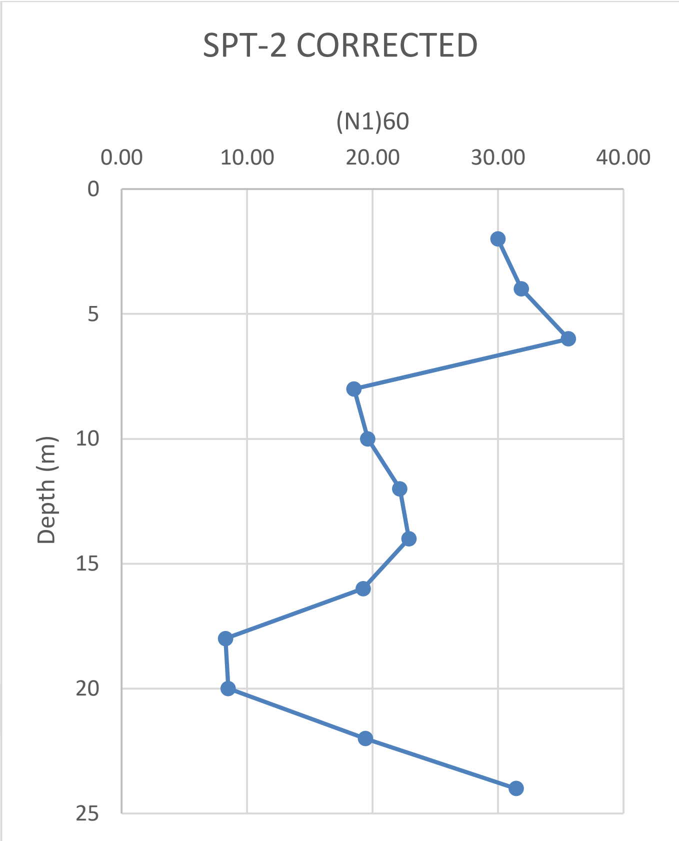

Figure A.13 : Corrected $(N_1)_{60}$ for SPT-2.

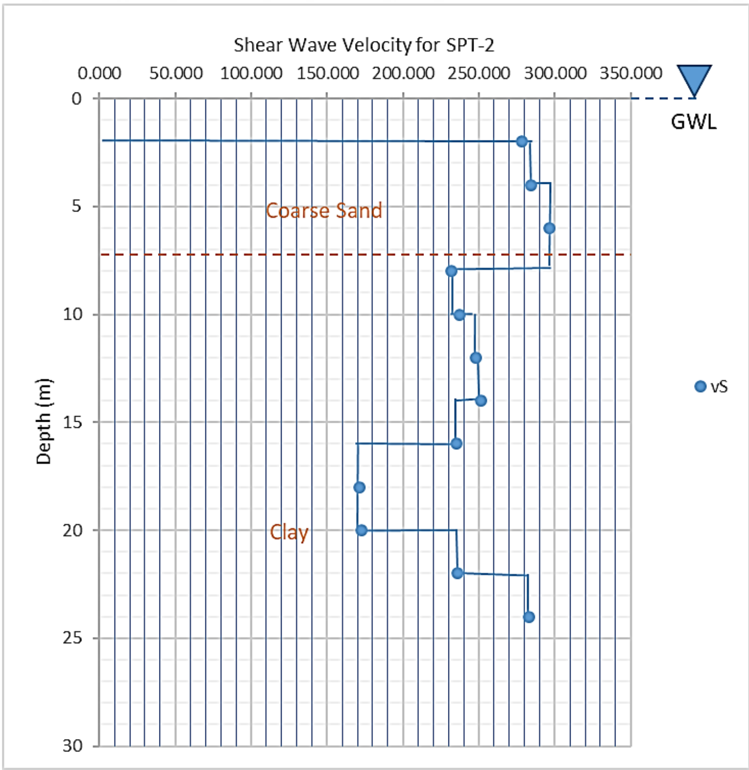

Figure A.14 : Shear wave velocity for SPT-2.

Equivalent Linear Site Response Analysis

<u>Response Spectra</u>

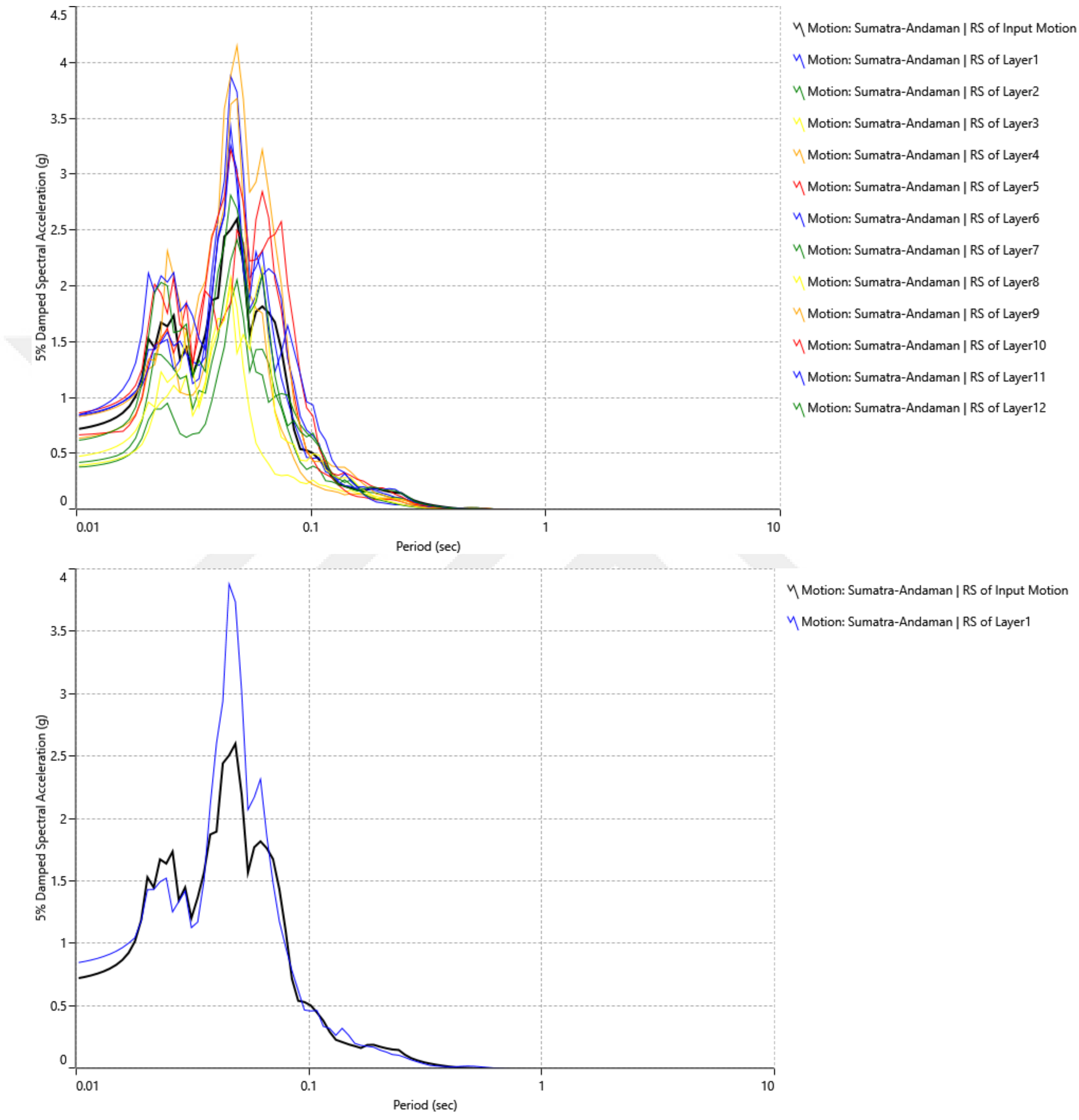

Figure A.15 : ELA Response Spectra for SPT-2.

Input motion = 2.62 g

Surface motion = 3.77 g

Earthquake motion was amplified by 43.89%

Peak Ground Acceleration

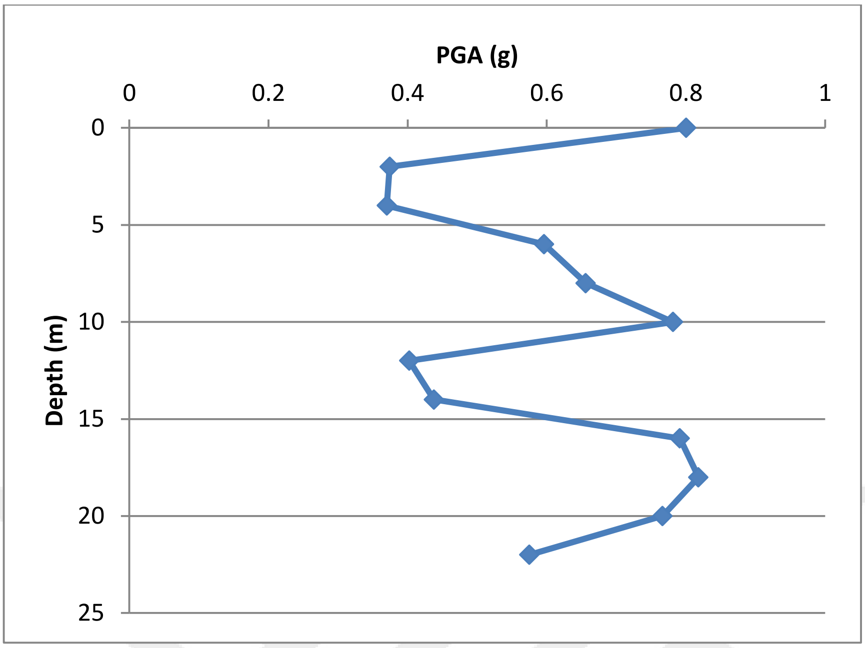

Figure A.16 : ELA Peak Ground Acceleration for SPT-2.

PGA at bedrocks = 0.58 g

PGA at surface = 0.80 g

PGA was increased by 37.9%

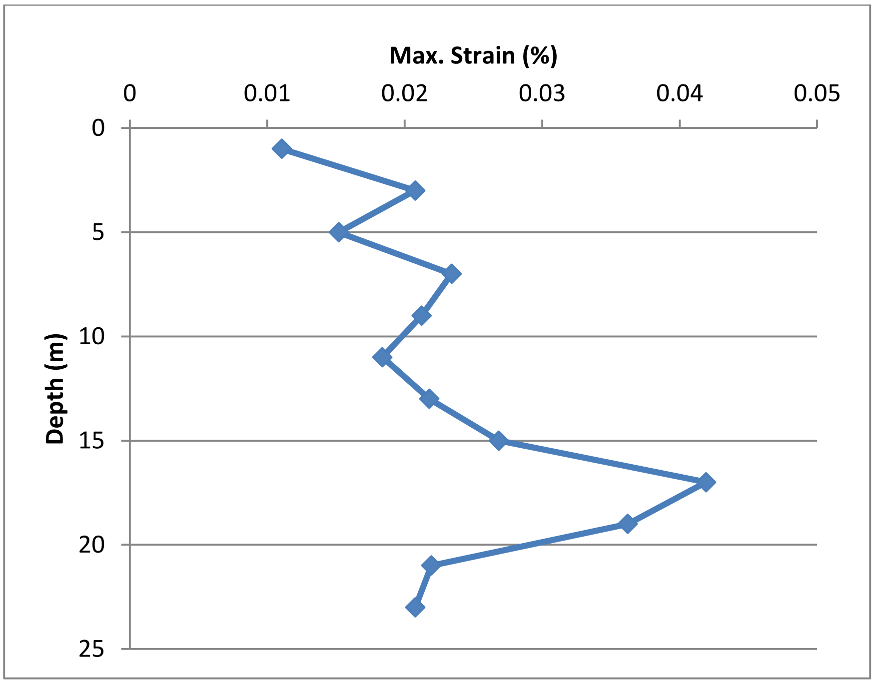

Figure A.17 : ELA Maximum Strain for SPT-2.

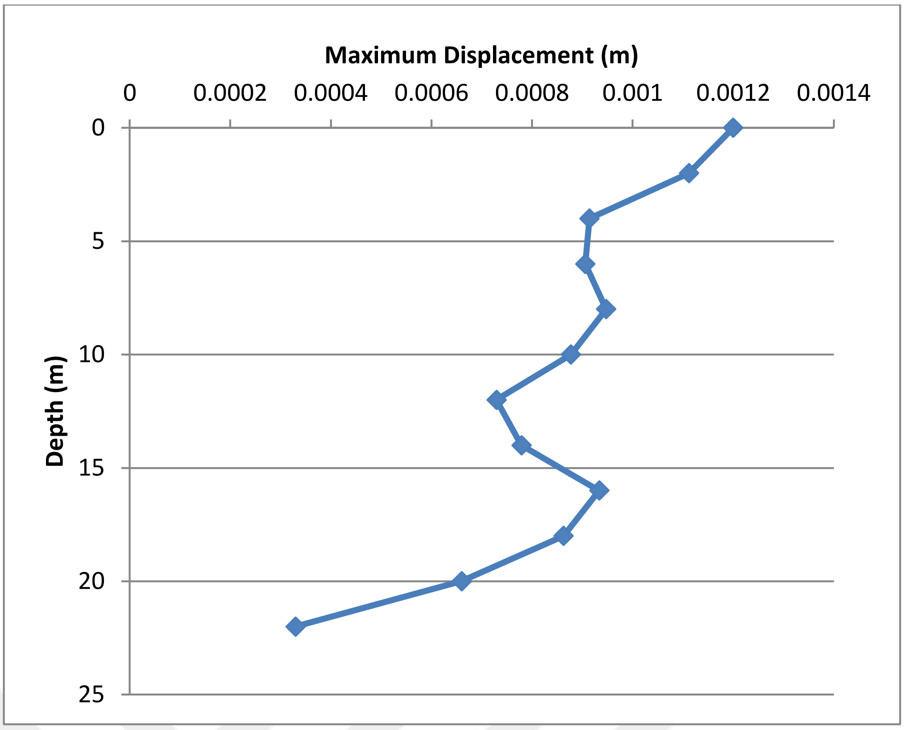

Figure A.18 : ELA Maximum Displacement for SPT-2.

Nonlinear Site Response Analysis

<u>Response Spectra</u>

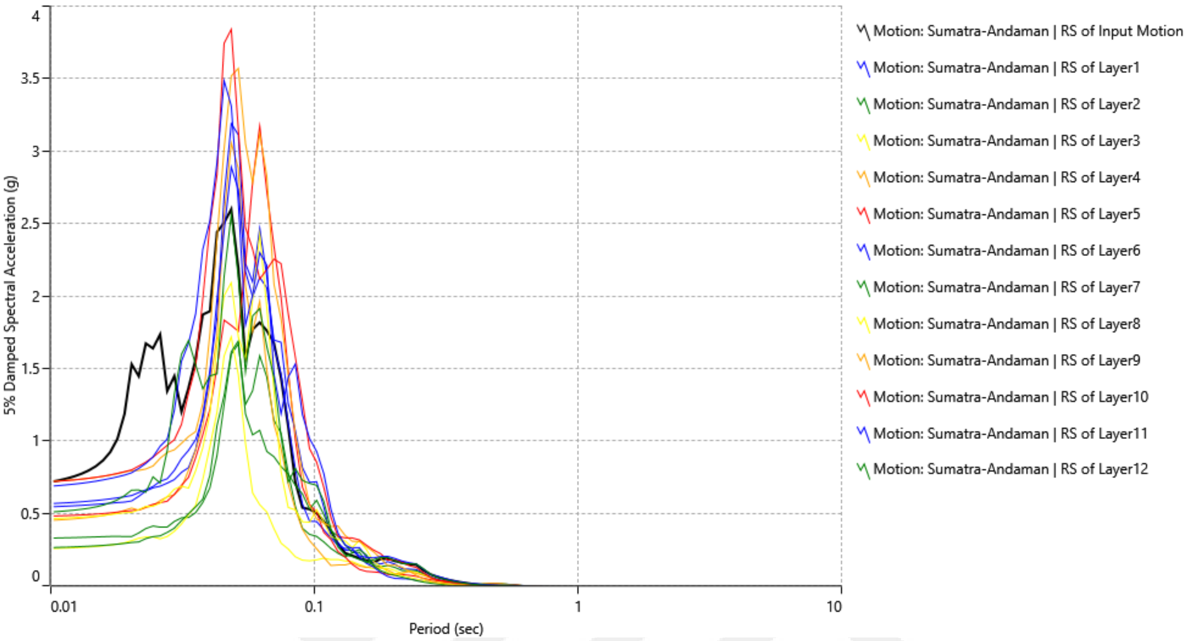

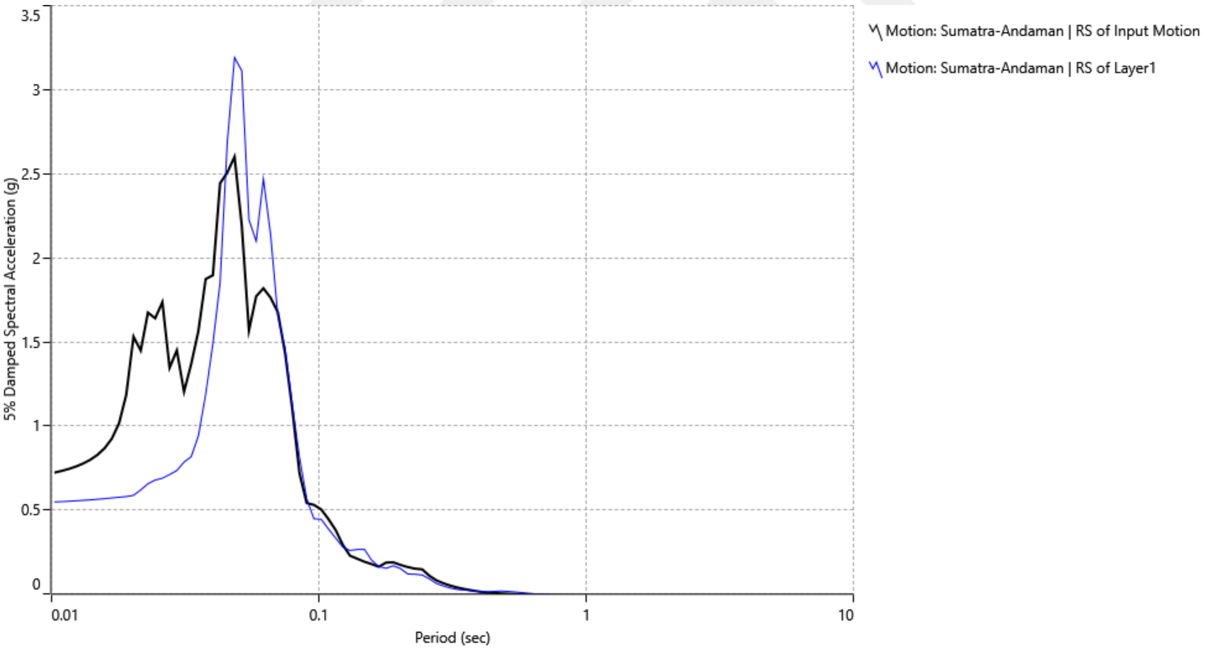

Figure A.19 : NLA response spectra for SPT-2.

Input motion = 2.62 g

Ground surface = 3.22 g

Earthquake motion was amplified by 22.9%

Peak Ground Acceleration

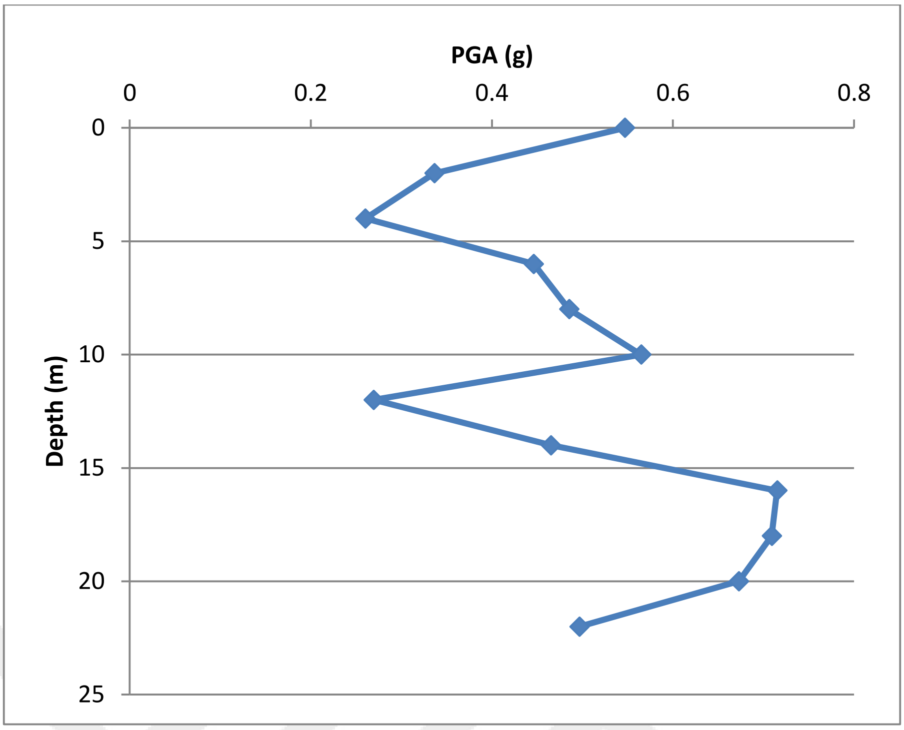

Figure A.20 : NLA Peak Ground Acceleration for SPT-2.

PGA at bedrocks = 0.49 g

PGA at surface = 0.55 g

PGA was increased by 12.24%

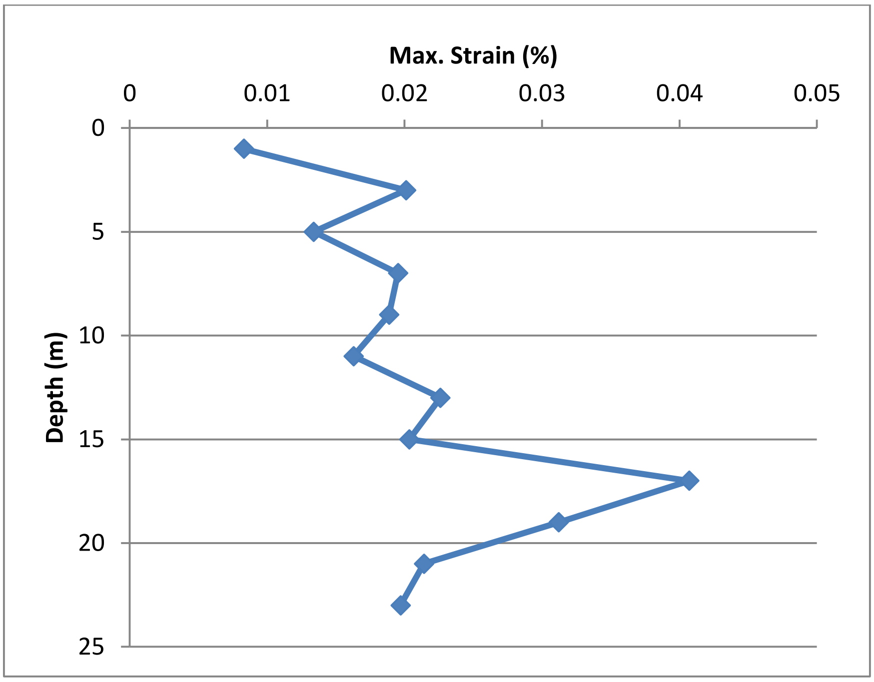

Figure A.21 : NLA Maximum Strain for SPT-2.

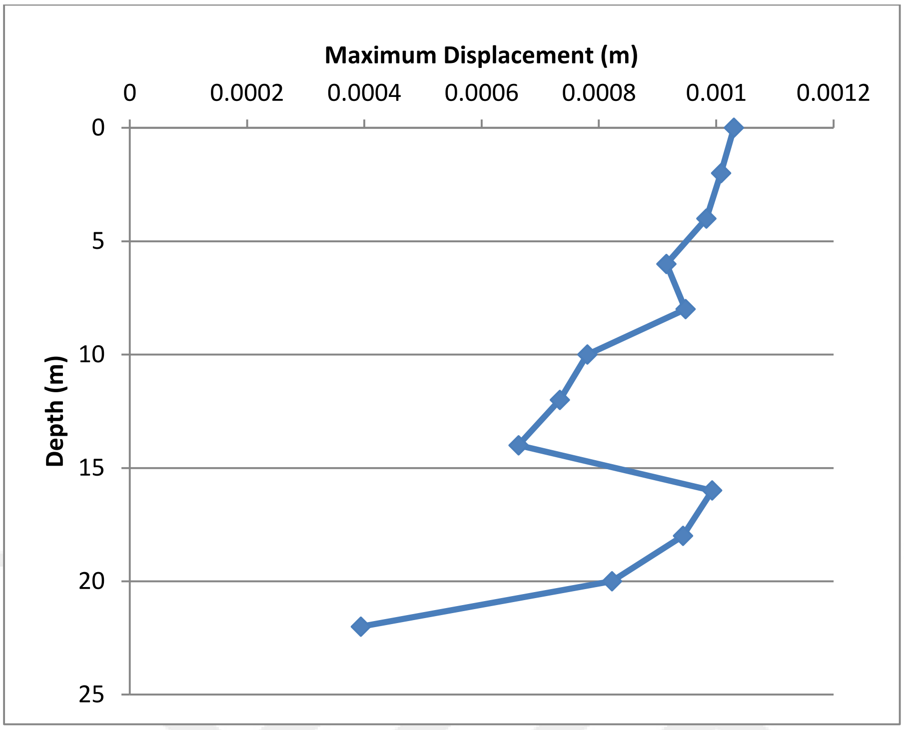

Figure A.22 : NLA Maximum Displacement for SPT-2.

Liquefaction Analysis

Table A.2 : Liquefaction evaluation of the SPT-2 soil profiles.

Depth (m)	**N-SPT**	**Soil Type**	**Unit Weight (kN/m^3)**	**σ (kPa)**	**σ' (kPa)**	**C_E**	**C_B**	**C_R**	**C_S**	**C_N**	**$(N_1)_{60}$**
(1)	(2)	(3)	(4)	(5)	(6)	(7)	(8)	(9)	(10)	(11)	(12)
2	50	Coarse Sand	20	40	20.4	0.75	1	0.8	1	1.00	30.00
4	50	Coarse Sand	18	76	36.8	0.75	1	0.85	1	1.00	31.88
6	50	Coarse Sand	18	112	53.2	0.75	1	0.95	1	1.00	35.63
8	26	Clay	12	136	57.6	0.75	1	0.95	1	1.00	18.53
10	21	Clay	12	160	62	0.75	1	1	1	1.25	19.62
12	26	Clay	16	192	74.4	0.75	1	1	1	1.14	22.18
14	29	Clay	16	224	86.8	0.75	1	1	1	1.05	22.90
16	25	Clay	12	248	91.2	0.75	1	1	1	1.03	19.26
18	11	Clay	12	272	95.6	0.75	1	1	1	1.00	8.28
20	12	Clay	16	304	108	0.75	1	1	1	0.94	8.50
22	29	Clay	16	336	120.4	0.75	1	1	1	0.89	19.45
24	50	Clay	18	372	136.8	0.75	1	1	1	0.84	31.45

Table A.2 (continued) : Liquefaction evaluation of the SPT-2 soil profiles.

Depth (m)	**Finese Content**	**$\Delta N_{1(60)}$**	**$N_{1(60)cs}$**	**r_d**	**CSR**	**MSF**	**K_σ**	**CRR for $M_{7.5}$**	**CRR for $M_{9.0}$**	**SF**
(1)	(13)	(14)	(15)	(16)	(17)	(18)	(19)	(20)	(21)	(22)
2	5.9	0.004	30.004	0.875	0.669	0.650	1.000	0.485	0.315	0.471
4	5.9	0.004	31.879	0.550	0.443	0.650	1.000	0.632	0.411	0.927
6	5.9	0.004	35.629	0.303	0.249	0.650	1.000	1.268	0.824	3.312
8	5.9	0.004	18.529	0.168	0.155	0.650	1.000	0.189	0.123	Clay
10	5.9	0.004	19.627	0.099	0.100	0.650	1.000	0.201	0.131	Clay
12	5.6	0.002	22.180	0.064	0.064	0.650	1.000	0.236	0.153	Clay
14	5.6	0.002	22.904	0.045	0.045	0.650	1.000	0.248	0.161	Clay
16	5.6	0.002	19.263	0.035	0.037	0.650	1.000	0.197	0.128	Clay
18	5.6	0.002	8.279	0.030	0.033	0.650	1.000	0.106	0.069	Clay
20	5.6	0.002	8.498	0.027	0.030	0.650	1.000	0.108	0.070	Clay
22	5.6	0.002	19.447	0.026	0.028	0.650	1.000	0.199	0.130	Clay
24	5.6	0.002	31.455	0.026	0.027	0.650	1.000	0.593	0.385	Clay

Liquefaction happened at the depth of 6 m.

Site Response For SPT-3

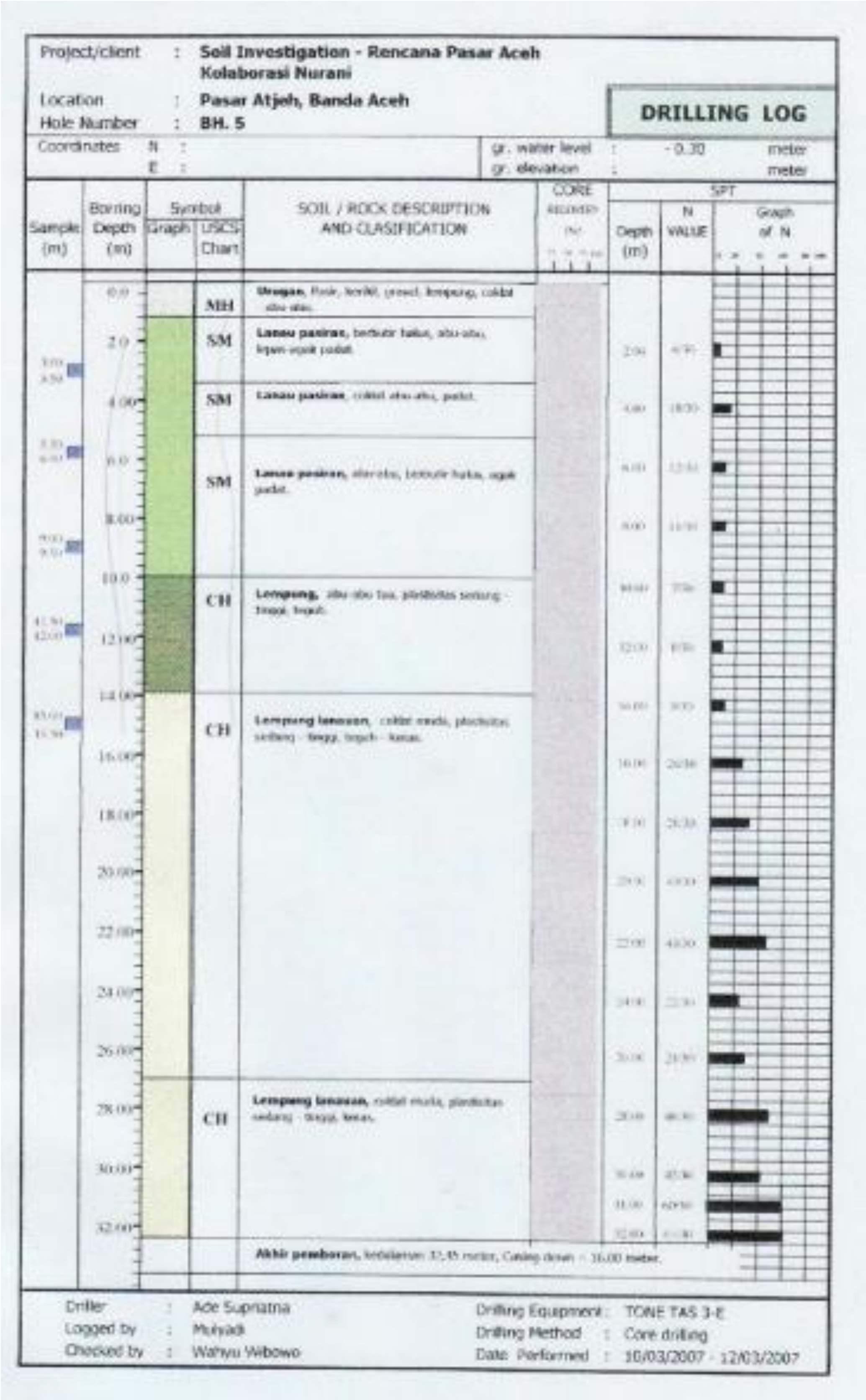

Figure A.23 : Soil profile for SPT-3.

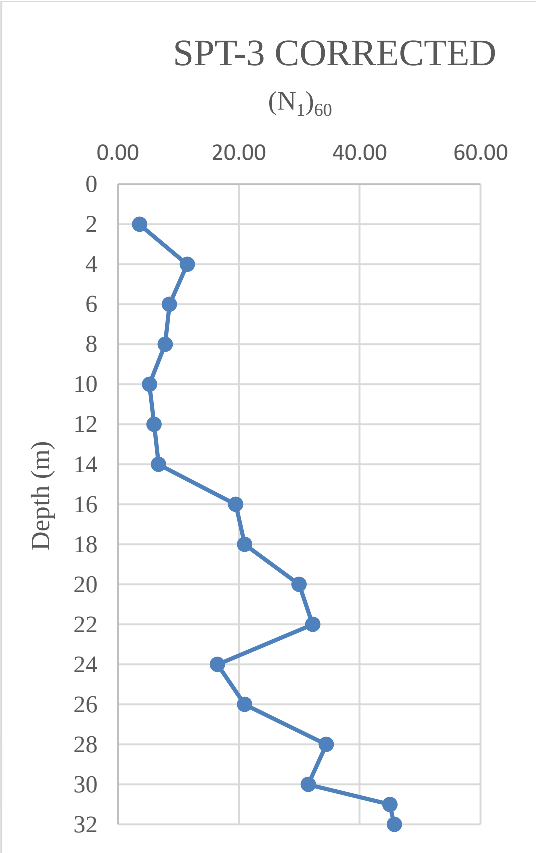

Figure A.24 : Corrected $(N_1)_{60}$ for SPT-3.

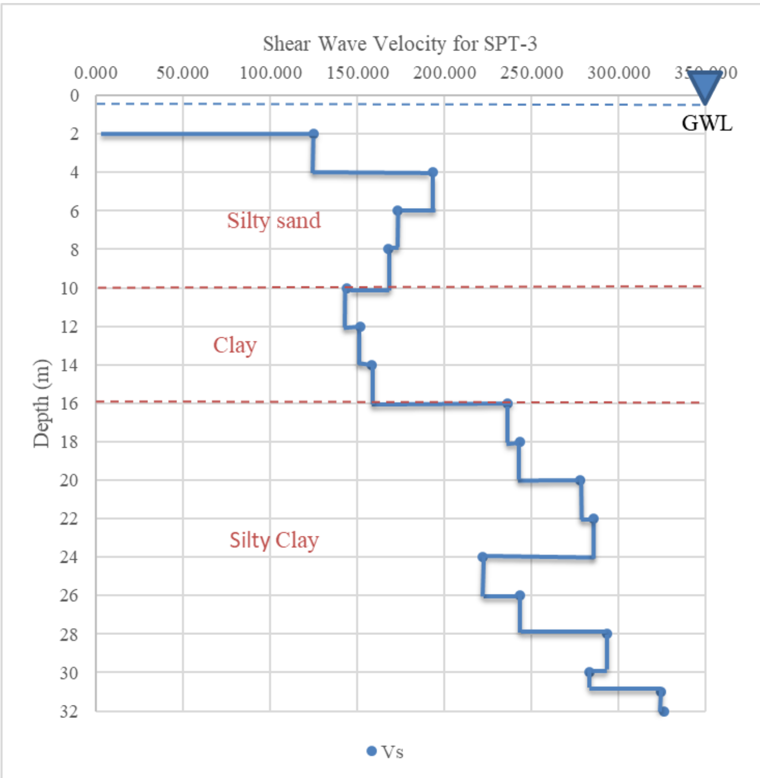

Figure A.25 : Shear wave velocity for SPT-3.

Equivalent Linear Site Response Analysis

<u>Response Spectra</u>

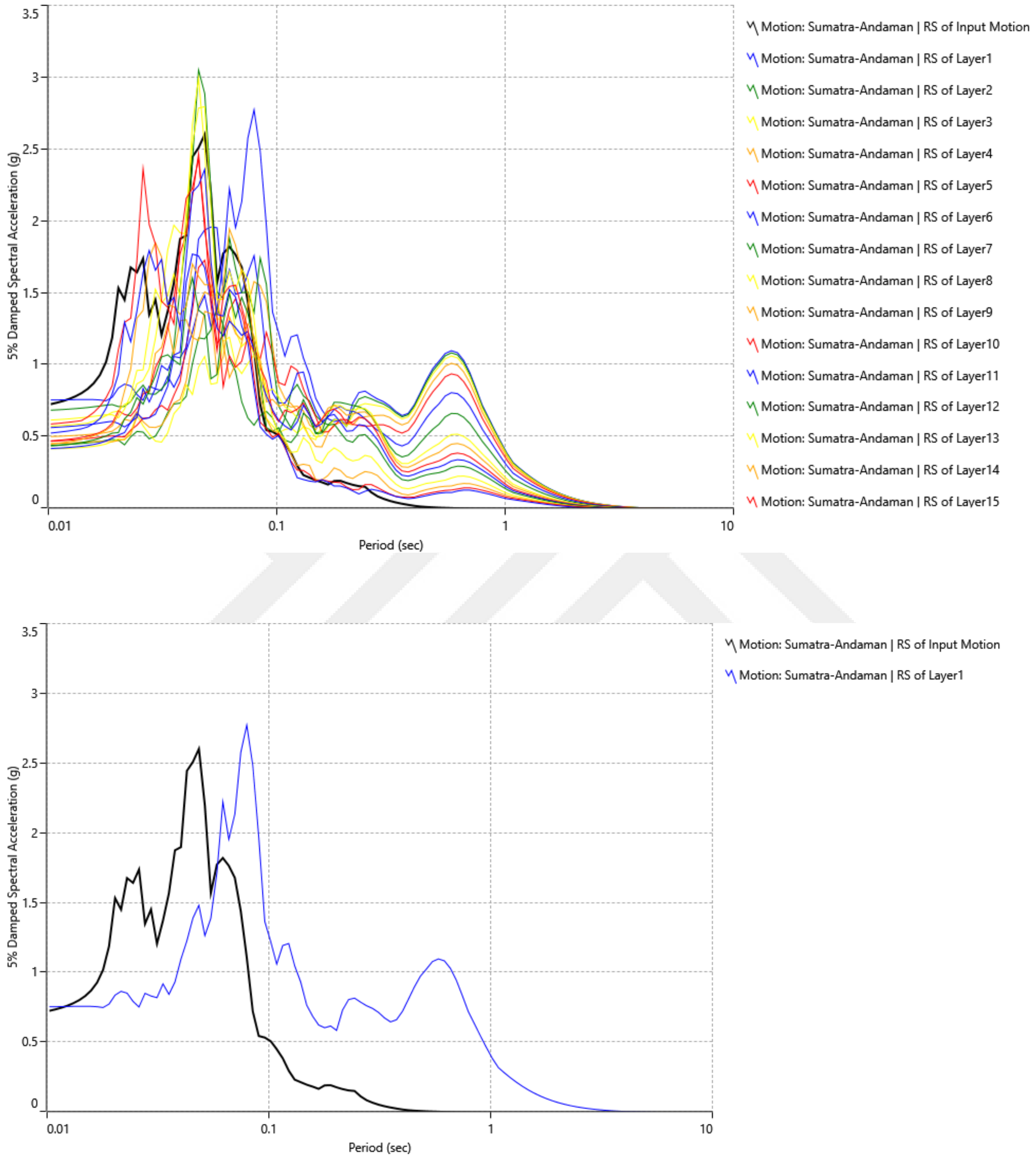

Figure A.26 : ELA Response Spectra for SPT-3.

Input motion = 2.64 g

Ground surface acceleration = 2.78 g

Earthquake motion was amplified by 5.30%

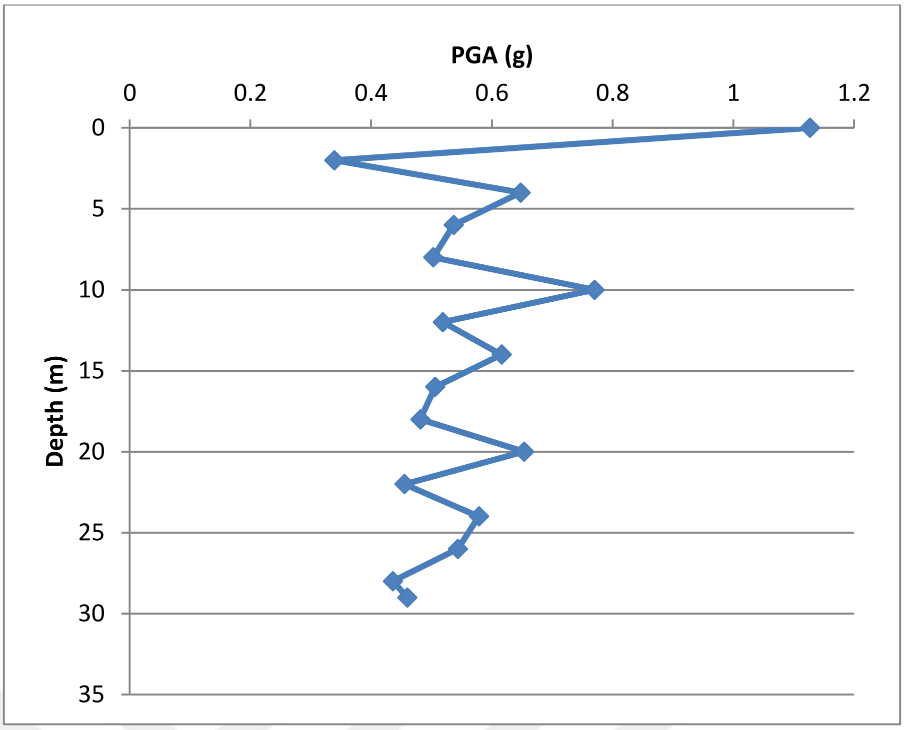

Figure A.27 : ELA Peak Ground Acceleration for SPT-3.

PGA at ground surface = 1.127 g

PGA at bedrocks = 0.459 g

PGA was amplıfied by 145.53%

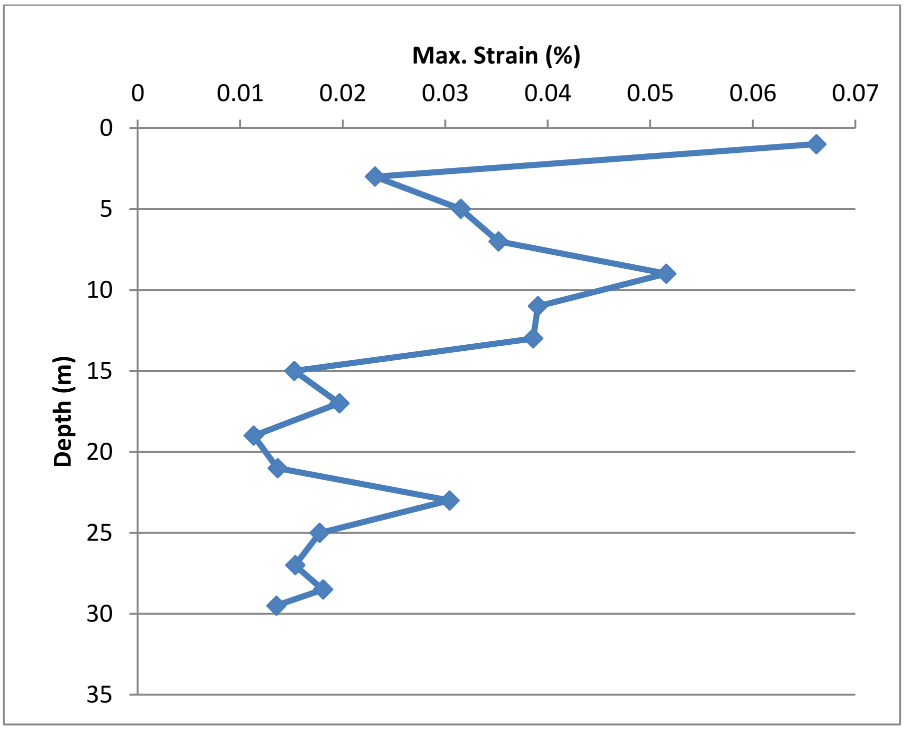

Figure A.28 : ELA Maximum Strain for SPT-3.

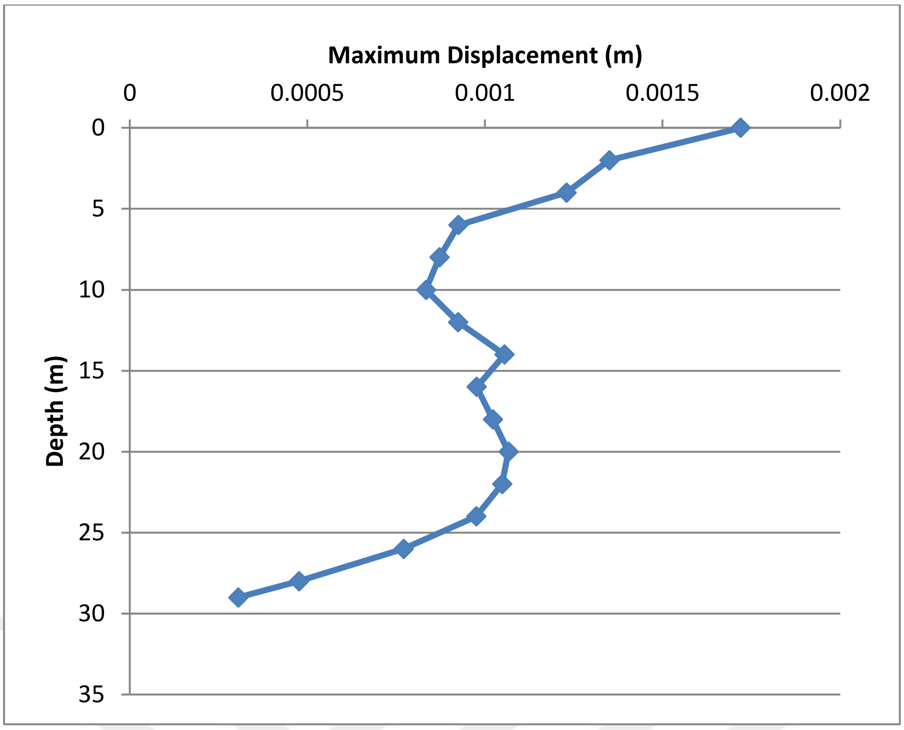

Figure A.29 : ELA Maximum Displacement for SPT-3.

Nonlinear Site Response Analysis

<u>Response Spectra</u>

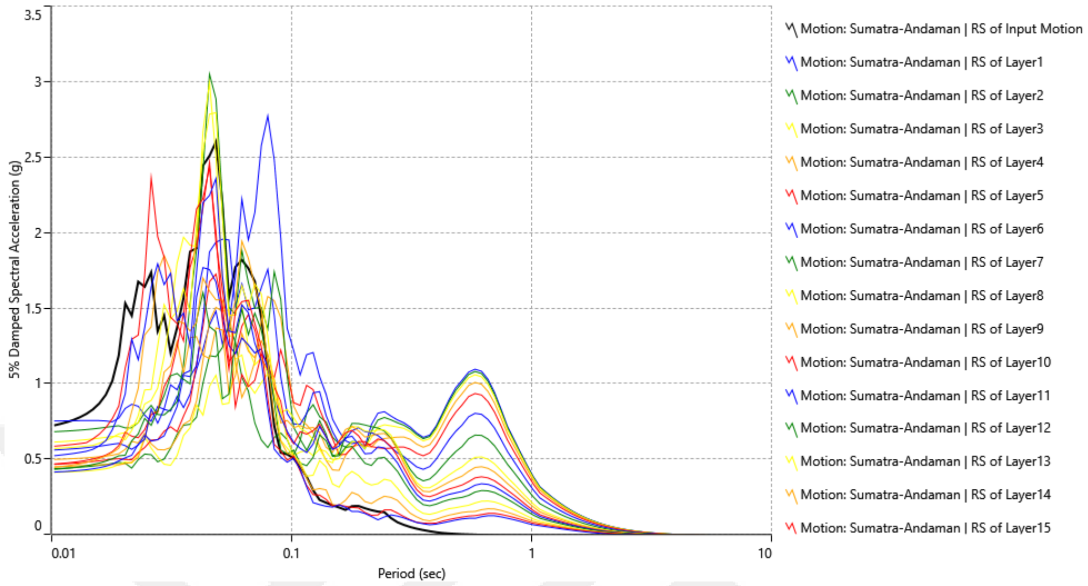

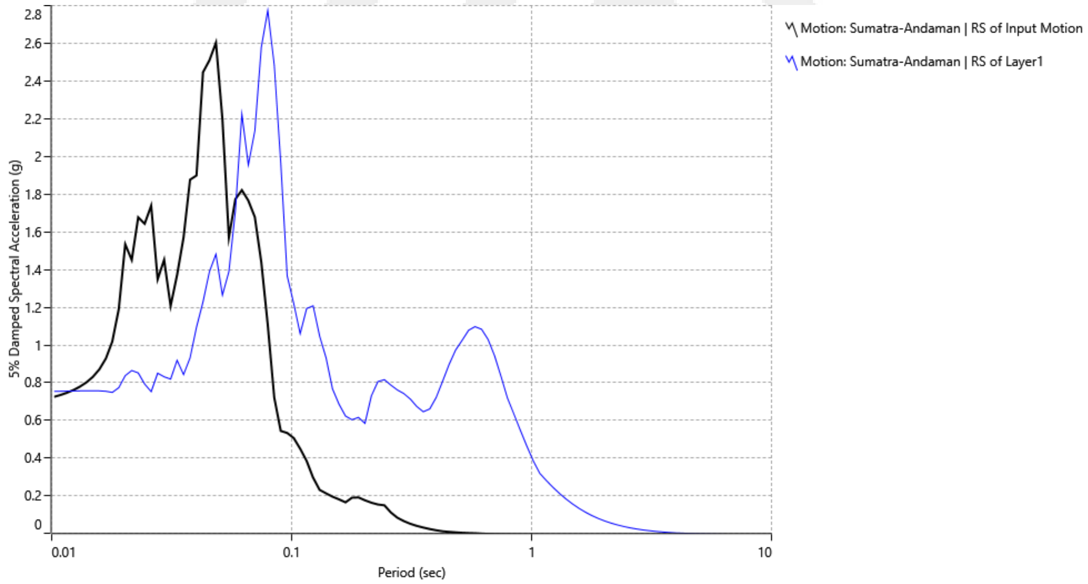

Figure A.30 : NLA Response Spectra for SPT-3.

Input motion = 2.62 g

Ground surface acceleration = 2.80 g

Earthquake motion was amplified by 6.87%

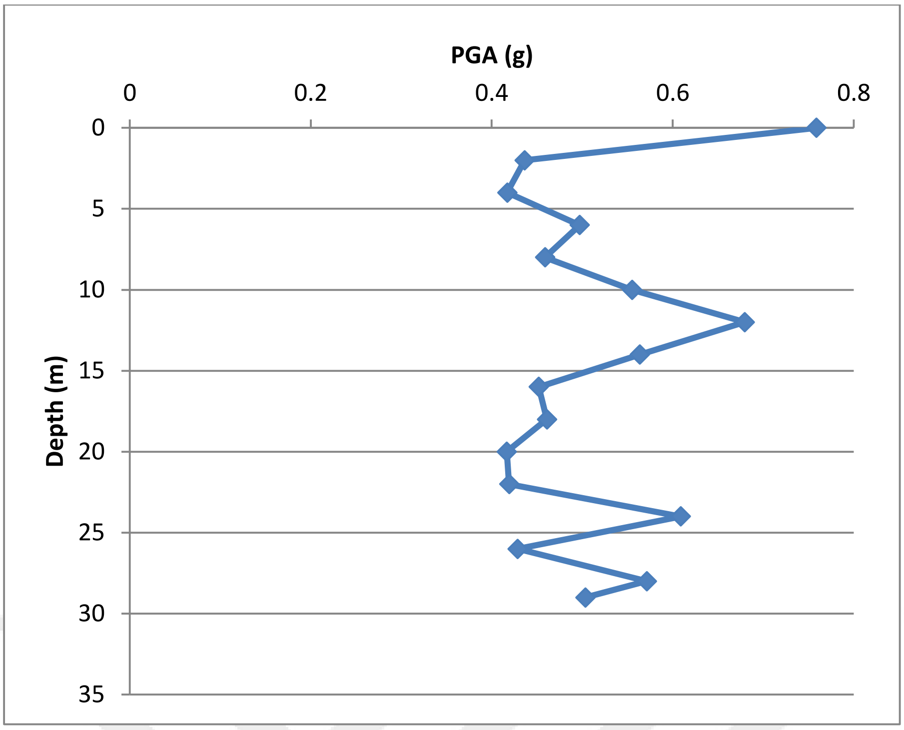

Figure A.31 : NLA Peak Ground Acceleration for SPT-3.

PGA at surface = 0.76 g

PGA at bedrocks = 0.50 g

PGA was increase by 52 %

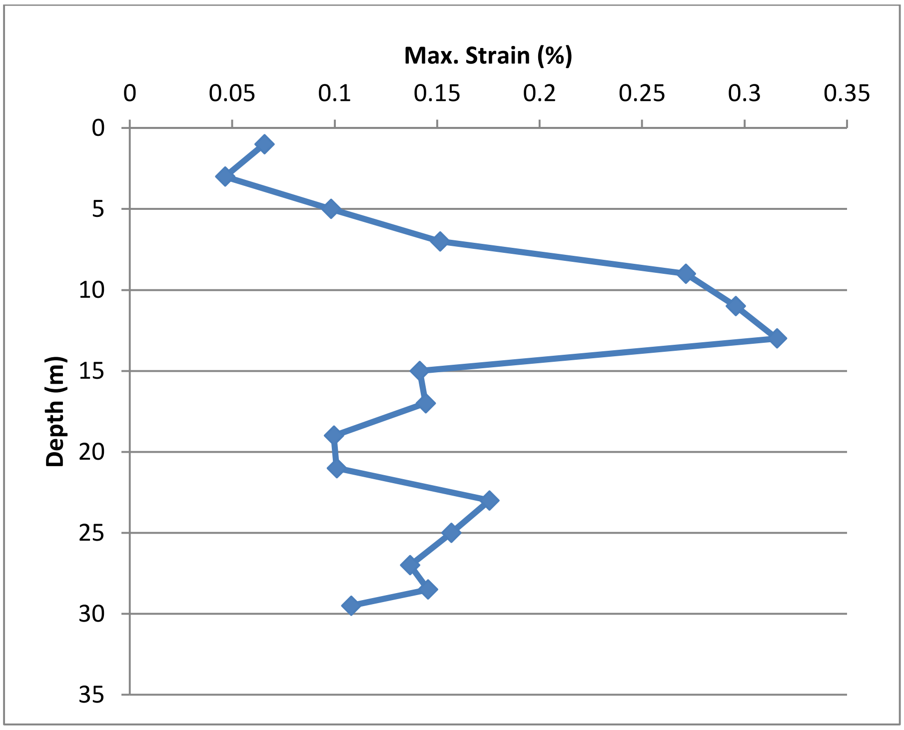

Figure A.32 : NLA Maximum Strain for SPT-3.

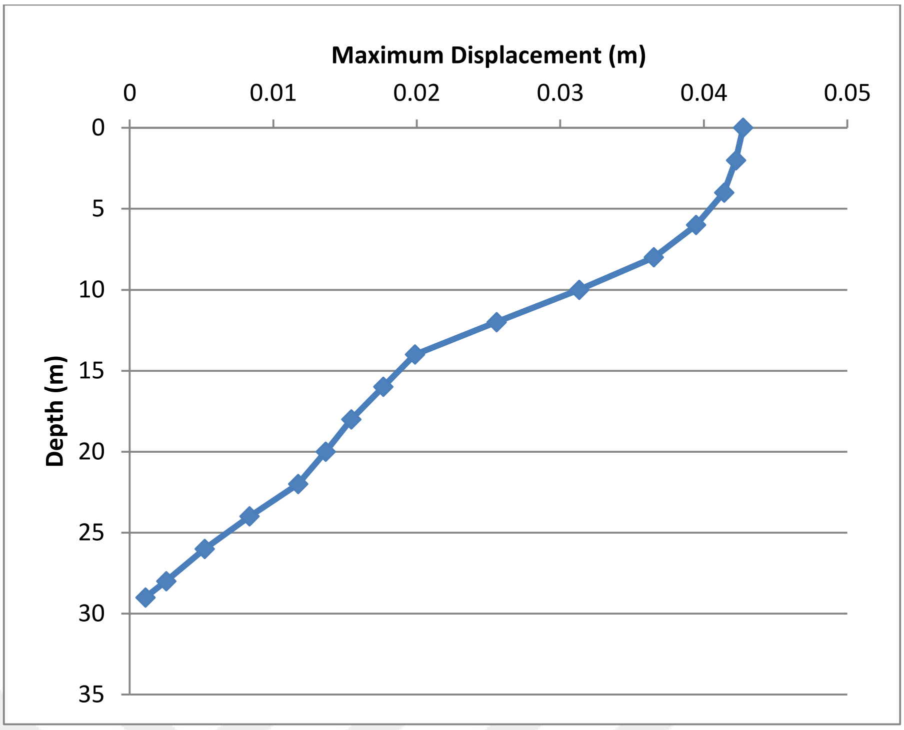

Figure A.33 : NLA Maximum Displacement for SPT-3.

Liquefaction Analysis

Table A.3 : Liquefaction evaluation of the SPT-3 soil profiles

Depth (m)	**N-SPT**	**Soil Type**	**Unit Weight (kN/m^3)**	**σ (kPa)**	**σ' (kPa)**	**C_E**	**C_B**	**C_R**	**C_S**	**C_N**	**$(N_1)_{60}$**
(1)	(2)	(3)	(4)	(5)	(6)	(7)	(8)	(9)	(10)	(11)	(12)
2	6	Silty Sand	16.360	32.72	13.12	0.75	1	0.8	1	1.00	3.60
4	18	Silty Sand	17.148	67.015	27.815	0.75	1	0.85	1	1.00	11.48
6	12	Silty Sand	16.855	100.725	41.925	0.75	1	0.95	1	1.00	8.55
8	11	Silty Sand	16.784	134.2925	55.8925	0.75	1	0.95	1	1.00	7.84
10	7	Silty Sand	16.525	167.3425	69.3425	0.75	1	1	1	1.00	5.25
12	8	Clay	17.700	202.7425	85.1425	0.75	1	1	1	1.00	6.00
14	9	Clay	17.813	238.3675	101.1675	0.75	1	1	1	1.00	6.75
16	26	Silty Clay	19.725	277.8175	121.0175	0.75	1	1	1	1.00	19.50
18	28	Silty Clay	19.950	317.7175	141.3175	0.75	1	1	1	1.00	21.00
20	40	Silty Clay	21.300	360.3175	164.3175	0.75	1	1	1	1.00	30.00
22	43	Silty Clay	21.638	403.5925	187.9925	0.75	1	1	1	1.00	32.25
24	22	Silty Clay	19.275	442.1425	206.9425	0.75	1	1	1	1.00	16.50
26	28	Silty Clay	19.950	482.0425	227.2425	0.75	1	1	1	1.00	21.00
28	46	Silty clay	21.975	525.9925	251.5925	0.75	1	1	1	1.00	34.50
30	42	Silty clay	21.525	569.0425	275.0425	0.75	1	1	1	1.00	31.50
31	60	Silty clay	23.550	592.5925	288.7925	0.75	1	1	1	1.00	45.00
32	61	Silty clay	23.663	616.255	302.655	0.75	1	1	1	1.00	45.75

Table A.3 (continued) : Liquefaction evaluation of the SPT-3 soil profiles.

Depth (m)	**Finese Content**	**Δ $N_{1(60)}$**	**$N_{1(60)cs}$**	**r_d**	**CSR**	**MSF**	**K_σ**	**CRR for $M_{7.5}$**	**CRR for $M_{9.0}$**	**SF**
(1)	(13)	(14)	(15)	(16)	(17)	(18)	(19)	(20)	(21)	(22)
2	5.9	0.004	3.604	0.875	0.851	0.650	1.000	0.078	0.051	0.060
4	5.9	0.004	11.479	0.550	0.517	0.650	1.000	0.129	0.084	0.162
6	5.9	0.004	8.554	0.303	0.284	0.650	1.000	0.108	0.070	0.248
8	5.9	0.004	7.842	0.168	0.158	0.650	1.000	0.104	0.067	0.427
10	5.9	0.004	5.254	0.099	0.093	0.650	1.000	0.088	0.057	0.610
12	5.6	0.002	6.002	0.064	0.059	0.650	1.000	0.092	0.060	Clay
14	5.6	0.002	6.752	0.045	0.041	0.650	1.000	0.097	0.063	Clay
16	5.6	0.002	19.502	0.035	0.031	0.650	1.000	0.200	0.130	Silty Clay
18	5.6	0.002	21.002	0.030	0.026	0.650	1.000	0.219	0.142	Silty Clay
20	5.6	0.002	30.002	0.027	0.023	0.650	1.000	0.485	0.315	Silty Clay
22	5.6	0.002	32.252	0.026	0.022	0.650	1.000	0.670	0.436	Silty Clay
24	5.6	0.002	16.502	0.026	0.021	0.650	1.000	0.169	0.110	Silty Clay
26	5.6	0.002	21.002	0.026	0.021	0.650	1.000	0.219	0.142	Silty Clay
28	5.6	0.002	34.502	0.026	0.022	0.650	1.000	1.002	0.651	Silty Clay
30	5.6	0.002	31.502	0.027	0.022	0.650	1.000	0.597	0.388	Silty Clay
31	5.6	0.002	45.002	0.028	0.022	0.650	1.000	31.158	20.253	Silty Clay
32	5.6	0.002	45.752	0.028	0.022	0.650	1.000	45.493	29.570	Silty Clay

CURRICULUM VITAE

Name Surname **:** Amelia FITRI

EDUCATION **:**

B.Sc. : 2015, Syiah Kuala University, Engineering Faculty, Civil Engineering Department